
Theses and Dissertations

Fall 2012

Modeling and optimization of industrial systems: data mining and computational intelligence approach

Yaohui Zeng
University of Iowa

Follow this and additional works at: <https://ir.uiowa.edu/etd>



Part of the [Industrial Engineering Commons](#)

Copyright 2012 Yaohui Zeng

This thesis is available at Iowa Research Online: <https://ir.uiowa.edu/etd/3557>

Recommended Citation

Zeng, Yaohui. "Modeling and optimization of industrial systems: data mining and computational intelligence approach." MS (Master of Science) thesis, University of Iowa, 2012.

<https://doi.org/10.17077/etd.qpxmhlgj>

Follow this and additional works at: <https://ir.uiowa.edu/etd>



Part of the [Industrial Engineering Commons](#)

MODELING AND OPTIMIZATION OF INDUSTRIAL SYSTEMS: DATA
MINING AND COMPUTATIONAL INTELLIGENCE APPROACH

by
Yaohui Zeng

A thesis submitted in partial fulfillment
of the requirements for the Master of Science
degree in Industrial Engineering
in the Graduate College of
The University of Iowa

December 2012

Thesis Supervisor: Professor Andrew Kusiak

Copyright by
YAOHUI ZENG
2012
All Rights Reserved

Graduate College
The University of Iowa
Iowa City, Iowa

CERTIFICATE OF APPROVAL

MASTER'S THESIS

This is to certify that the Master's thesis of

Yaohui Zeng

has been approved by the Examining Committee
for the thesis requirement for the Master of Science degree
in Industrial Engineering at the December 2012 graduation.

Thesis Committee: _____
Andrew Kusiak, Thesis Supervisor

Yong Chen

Pavlo A. Krokhmal

To My Family and Friends

Success is not final, failure is not fatal; it is the courage to continue that counts.

Winston Churchill

ACKNOWLEDGMENTS

I would like to express my sincere gratitude to my advisor Professor Andrew Kusiak for his devotion to this research. He has been the most instrumental person for my academic and research achievements. He provided the motivation, encouragement, guidance and advice which have prepared me for the challenges of future life. Working in the Intelligent Systems Laboratory exposed me to industrial applications in real world. This invaluable experience has allowed me to maintain a balance between theory and practice leading to realistic solutions.

I would like to thank Professor Yong Chen and Professor Pavlo A. Krokhmal for serving on my Thesis Committee and providing valuable suggestions and feedback on my research.

I am also grateful for the financial support from Iowa Energy Center. Discussions with energy experts, Xiaohui Zhou (Iowa Energy Center) and George Paterson (Facilities Management, The University of Iowa), have provided me invaluable information for this research.

I thank all the members of the Intelligent Systems Laboratory who have worked with me and provided me helpful suggestions and supports. Special thanks to my colleagues: Dr. Zijun Zhang, who worked with me on wastewater project and provided me valuable ideas and suggestion; Guanglin Xu, who worked with me on HVAC project and helped me a lot in both research and daily life. Dr. Anoop Verma and Xiupeng Wei, who shared their unique research experience with me and motivated me in research. I would also like to thank Xiaofei He, the new talented member, for discussing the problems and cooperated with me on HVAC implementation.

Finally, and most importantly, I would like to express my sincere gratitude to my family and my friends. They have given me their unyielding support for my academic journey and their deep love for my life.

ABSTRACT

Recent years have marked growing interest in energy conservation. Energy consumption by industrial systems has received attention of academic and industrial communities.

The research reported in this Thesis considers energy efficiency of two industrial systems, the heating, ventilating and air-conditioning (HVAC) system, and the wastewater pumping system. The dynamic, nonlinear, and multivariate nature of these systems offer challenges in modeling and performance optimization.

Traditional modeling approaches usually use physics-based equations and mathematical programming, with limitations in modeling complex systems and their optimization. As an emerging science with an abundance of successful applications in industrial, business, medical areas, data mining has proven powerful in modeling nonlinear systems. Successful applications of data mining algorithms, such as multilayer perceptron neural network, support vector machine, and boosting tree have been reported in the literature of complex system modeling.

Computational intelligence is an emerging and promising area applicable to solving difficult optimization problems, for instance, mixed integer nonlinear programming problems. Computational intelligence algorithms provide optimal or near-optimal solutions in limited computation time. This Thesis focuses on employing computational intelligence algorithms to generate optimal control strategies for industrial systems. The main contribution of this research is in utilizing computational intelligence to solve mixed integer nonlinear programming optimization models built by data mining algorithms. The research reported in the Thesis offers a unified framework of applying data mining and computational intelligence to real-world system control and optimization.

TABLE OF CONTENTS

LIST OF TABLES	viii
LIST OF FIGURES	x
CHAPTER 1 INTRODUCTION	1
1.1. Review of methodologies of modeling and optimization HVAC systems.....	2
1.2. Review of methodologies of modeling and optimizing pumping systems.....	3
1.3. Review of data mining and computational intelligence in system modeling and optimization	4
1.4. Thesis structure.....	5
CHAPTER 2 DATA-DRIVEN PERFORMANCE OPTIMIZATION OF A WASTEWATER PUMP SYSTEM.....	7
2.1. Introduction.....	7
2.2. Pump System Description.....	7
2.3. Model Development and Validation.....	9
2.3.1. Data description and model formulation	9
2.3.2. Model validation.....	11
2.4. Overall Energy Optimization Model	16
2.5. Proposed Greedy Electromagnetism-like Algorithm.....	18
2.5.1. Theory of electromagnetism-like algorithm	18
2.5.2 Proposed greedy electromagnetism-like algorithm	21
2.6. Computational Results and Analysis	22
2.7. Summary.....	28
2.7. Appendix.....	29
CHAPTER 3 MINIMIZING ENERGY CONSUMPTION OF AN AIR HANDLING UNIT WITH A COMPUTATIONAL INTELLIGENCE APPROACH.....	32
3.1. Introduction.....	32
3.2. Model Formulation	32
3.3. Model Development and Validation.....	35
3.3.1. Experiment Description and Data Preprocessing	35
3.3.2. Parameter Selection	36
3.3.3 Energy consumption modeling and validation	40
3.3.4 Modeling and Validation of the Temperature and Static Pressure of the Supply Air.....	45
3.4. Optimization of the Energy Consumption of the AHU System	46
3.4.1. Overall optimization model	46
3.4.2. Dynamic penalty-based electromagnetism-like algorithm	47
3.4. Computational Results and Discussion	50
3.5. Summary.....	55
CHAPTER 4 MODEL-PREDICTIVE CONTROL OF A MULTI-ZONE HVAC SYSTEM.....	56

4.1. Introduction.....	56
4.2. System Description and Modeling.....	57
4.2.1 System description and data collection	57
4.2.2 Predictive modeling.....	59
4.3. Energy Optimization Modeling	65
4.3.1 Overall energy optimization model.....	65
4.3.2 Firefly algorithm.....	66
4.4. Computational Results and Analysis	69
4.5. Summary.....	75
CHAPTER 5 HVAC SYSTEM OPTIMIZATION VIA DATA MINING AND COMPUTATIONAL INTELLIGENCE: AN IMPLEMENTATION.....	77
5.1. Introduction.....	77
5.2. Building and System.....	79
5.3. Data Collection Experiment	81
5.4. Room Selection.....	85
5.5. Data Mining Modeling	88
5.6. Implementation	91
5.6. Summary.....	94
CHAPTER 6 CONCLUSION.....	95
REFERENCES	97

LIST OF TABLES

Table 2.1	Different pump configurations and corresponding dataset sizes	10
Table 2.2	Test results of energy consumption and the wastewater outflow rate models derived using MLP algorithm	12
Table 2.3	Summary of computational results for three cases	24
Table 2.4	The observed and optimized pump schedules for the medium flow rate.	29
Table 3.1	Description of the datasets	36
Table 3.2	Parameters selected based on the input-output analysis of the AHU system ..	38
Table 3.3	Parameters selected for developing models of the energy consumption of the chiller, temperature of the supply air, and static pressure of the supply air	39
Table 3.4	Parameters selected for developing the energy consumption model of the pump	39
Table 3.5	Parameters selected for developing the energy consumption model of the return fan.....	40
Table 3.6	Parameters selected for developing the energy consumption model of the supply fan.....	40
Table 3.7	Accuracy of the prediction of energy consumption by the chiller provided by different data-mining algorithms	41
Table 3.8	Prediction accuracy of different models by the MLP ensemble algorithm	42
Table 3.9	Energy optimization results for different components of the AHU system	51
Table 4.1	Parameters selected for building total energy consumption model	60
Table 4.2	Parameters selected for building temperature model in East Room (Temp-EA).....	61
Table 4.3	Parameters selected for building temperature model in Interior Room (Temp-IA).....	62
Table 4.4	Parameters selected for building temperature model in South Room (Temp-SA).....	62
Table 4.5	Parameters selected for building temperature model in West Room (Temp-WA)	63
Table 4.6	Detailed information of the neural networks	64
Table 4.7	Prediction accuracy of the data-mining models.....	64

Table 4.8	Energy consumption before and after optimization.....	70
Table 5.1	The room selected and the original control ratio	86
Table 5.2	The critical rooms selected for the implementation.....	88
Table 5.3	Parameters selected for building energy consumption model	89
Table 5.4	Parameters selected for building temperature model in Room 8.....	89
Table 5.5	Information about the neural network models.....	90
Table 5.6	Prediction accuracy of the data-mining models.....	91

LIST OF FIGURES

Figure 2.1	Schematic diagram of wastewater preliminary treatment process	8
Figure 2.2	Observed and MLP predicted energy for configuration (1, 3)	13
Figure 2.3	Observed and MLP predicted energy for configuration (1, 4, 5)	14
Figure 2.4	Observed and MLP predicted energy for configuration (1, 3, 4, 5)	14
Figure 2.5	Observed and MLP predicted outflow rate for configuration (1, 3).....	15
Figure 2.6	Observed and MLP predicted outflow rate for configuration (1, 4, 5).....	15
Figure 2.7	Observed and MLP predicted outflow rate for configuration (1, 3, 4, 5).....	15
Figure 2.8	Attraction-repulsion mechanism	20
Figure 2.9	Pseudo code of electromagnetism-like algorithm	20
Figure 2.10	Pseudo code of the proposed greedy electromagnetism-like algorithm.....	22
Figure 2.11	Observed and optimized energy consumptions for low inflow rate.....	24
Figure 2.12	Observed and optimized effluent flow rates for low inflow rate.....	24
Figure 2.13	Observed and optimized chamber levels for low inflow rate.....	25
Figure 2.14	Observed and optimized energy consumptions for medium inflow rate.....	25
Figure 2.15	Observed and optimized effluent flow rates for medium inflow rate	26
Figure 2.16	Observed and optimized chamber levels for low inflow rate.....	26
Figure 2.17	Observed and optimized energy consumptions for high inflow rate.....	27
Figure 2.18	Observed and optimized effluent flow rates for high inflow rate	27
Figure 2.19	Observed and optimized chamber levels for high inflow rate.....	28
Figure 3.1	Schematic diagram of a typical AHU system.....	33
Figure 3.2	Energy consumption of different components in a sample cooling session...33	
Figure 3.3	The observed and predicted chiller energy consumption by the MLP	43
Figure 3.4	The observed and predicted pump energy consumption by the MLP	43
Figure 3.5	The observed and predicted supply fan energy consumption by the MLP	44
Figure 3.6	The observed and predicted return fan energy consumption by the MLP	44
Figure 3.7	Comparison of the observed and predicted temperature of the supply air	45

Figure 3.8	Comparison of observed and predicted static pressure of the supply air	46
Figure 3.9	Total energy consumption before and after optimization.....	52
Figure 3.10	Temperature of the supply air before and after optimization	52
Figure 3.11	Static pressure of the supply air before and after optimization	53
Figure 3.12	Observed and optimized water flow rates for the 200 cases	53
Figure 3.13	Observed and optimized supply fan speeds for the 200 cases.....	54
Figure 3.14	Observed and optimized chilled water cooling coil VLV position for the 200 cases	54
Figure 3.15	Observed and optimized chilled water supply temperatures for 200 cases....	55
Figure 4.1	Schematic diagram of a typical HVAC system with multi-zones.....	58
Figure 4.2	Plane view of ERS facility	58
Figure 4.3	The comparison of the observed and predicted energy consumption	65
Figure 4.4	Pseudo code of the firefly algorithm	68
Figure 4.5	The iterations of the firefly algorithm in one case	70
Figure 4.6	The recorded and optimized total energy consumption in Experiment 1.....	71
Figure 4.7	The recorded and recommended supply air temperature setpoint settings in Experiment 1.....	71
Figure 4.8	The recorded and recommended supply air static pressure setpoint settings in Experiment 1.	72
Figure 4.9	The recorded and optimized total energy consumption in Experiment 2.....	72
Figure 4.10	The recorded and recommended supply air static pressure setpoint settings in Experiment 2	73
Figure 4.11	The recorded and recommended supply air temperature setpoint settings in Experiment 2.....	73
Figure 4.12	The recorded and optimized temperature of East Room in Experiment 1	74
Figure 4.13	The recorded and optimized temperature of Interior Room in Experiment 1.....	74
Figure 4.14	The recorded and optimized temperature of South Room in Experiment 1 ...	75
Figure 4.15	The recorded and optimized temperature of West Room in Experiment 1	75
Figure 5.1	Framework of the real time online implementation	78

Figure 5.2	The University Services Building	79
Figure 5.3	Johnson control system – parameters in the USB air handling unit.....	80
Figure 5.4	SQL server – store real time data	80
Figure 5.5	Data Command interface.....	81
Figure 5.6	MATLAB for data collection	82
Figure 5.7	The data collection experiment on a virtual machine.....	83
Figure 5.8	The first type of error during the data collection experiment.....	84
Figure 5.9	The second type of error during the data collection experiment.....	84
Figure 5.10	The comparison of the actual room temperature and setpoints in Room 4....	87
Figure 5.11	The comparison of the actual room temperature and setpoints in Room 7....	87
Figure 5.12	The comparison of the actual room temperature and setpoints in Room 8....	88
Figure 5.13	Comparison between the observed and predicted energy consumption.....	91
Figure 5.14	Software output for scenario where outside air temperature is below 60 °F	92
Figure 5.15	Software output for scenario where outside air temperature is above 60 °F	93
Figure 5.16	Network error forced the software to stop.....	93

CHAPTER 1

INTRODUCTION

Due to the increasingly growing energy use, energy savings are important. This research is aimed to apply data mining and computational intelligence to optimal control of high energy-consuming facilities. Among those facilities are HVAC systems in commercial buildings and pumping systems in wastewater treatment plants.

HVAC systems are designed to provide a comfortable thermal environment for occupants in buildings while meeting the requirements of indoor air qualities in all thermal zones. They are widely used in residential and commercial buildings all over the world. According to [1, 2], HVAC systems use as much as 60% of the energy consumed in buildings, and they account for approximately 30% of the total energy consumption in the United States. Therefore, the energy efficiency of HVAC systems is being considered as a vehicle for accomplishing energy savings. On the other hand, significant energy savings could be achieved in pumping systems in wastewater treatment plants (WWTPs). It has been reported that WWTPs are intensively energy-consuming facilities with 4% of the US electricity being used to move and treat water/wastewater [3], and more than 80% of the energy costs for WWTPs are consumed by pump and blowers systems [4, 5].

Optimizing both systems require trade-offs between seeking energy savings and maintaining system performance. The performance of the systems defines the constraints of optimization models. Solely minimizing energy consumption while ignoring the performance requirements is impractical and of little usefulness in system control. At this point, optimal control strategies in HVAC systems are those leading to energy savings while maintaining thermal comfort in buildings. While in pumping systems, optimal control settings are those provide system capacity to meeting workloads and reduce energy cost at the same time. This thesis emphasizes formulating comprehensive optimization framework for system modeling and optimization.

1.1. Review of methodologies of modeling and optimization HVAC systems

Traditional approaches for modeling HVAC systems involve mathematical models or simulation software. Mathematical models are often generated from fundamental laws of energy, mass flow, heat transfer, and so forth.

Lu *et al.* [6, 7] formulated a mixed-integer, non-linearly-constrained model for minimizing the energy consumption of HVAC systems. Wang *et al.* [8] used energy balance and heat transfer principles to develop a simple, yet accurate engineering cooling coil unit model for control and optimization of HVAC systems. Experiments showed that the model is robust and gave a better match to real performance over the operating range. Zhang *et al.* [9] developed a system model by incorporating solar air and water heating, a ventilated photovoltaic array, biomass boiler and active and passive thermal storage and utilized the proposed optimization algorithm to devise optimal or near-optimal supervisory control strategy for the system. Engdahl and Johansson [10] minimized the energy use of a system with variable air volumes by setting the supply air temperature optimally in response to load, fan power, coefficient of performance of the chiller, outdoor temperature, and outdoor relative humidity. They showed that the recommended control strategy was more energy-efficient than requiring a constant temperature for the supply air. Yao *et al.* [11] proposed specific energy models of the primary equipments in HVAC systems by using classic control theory. Energy savings of variable-air-volume system was compared to constant-air-volume system and fan-coil system by a simulation case. Yu *et al.* [12] discussed mathematical modeling with two different approaches, block-wise Simulink and bond graph for fault detection and diagnosis with objective of energy consumption reduction.

Mathematical modeling approaches are generalized for wide application once assumptions are met in real applications. However, those models are always complex and nonlinear, which makes them computationally expensive and difficult for real-time implementation [13]. Simulation models were built and simulation program and packages were widely studied in literature. Some widely used programs are TRNSYS [14], HVACSIM+ [15], SIMBAD [16], and EnergyPlus [17]. Zhou *et al.* [17] developed a new simulation module on the

basis of the building energy simulation program, EnergyPlus, to evaluate the energy performance of the VRV air-condition system. Crawley *et al.* [18] comprehensively reviewed over 20 major building energy simulation programs and compared their features and capabilities.

1.2. Review of methodologies of modeling and optimizing pumping systems

Modeling approaches for pumping systems developed to date are predominantly physics and mathematical programming based. Research on pumping systems has been reported in the literature. Ormsbee and Lansley [19] reviewed different models and approaches proposed for water-supply pumping systems. Bechwith and Wong [20] used a genetic algorithm to solve the pump scheduling problem in a multi-source water supply system with multiple tanks. Barán *et al.* [21] utilized a mass balance model and evolutionary computational algorithms to solve a multi-objective, pump-scheduling problem by minimizing four types of costs while satisfying the water demand and other constraints. More recently, Yang and Børsing [22] developed a mixed-integer, non-linear, programming model for a simple, multi-pump, boosting system that included three variable speed pumps, a simple water circular loop, and a storage tank. Wang *et al.* [23] modeled pump scheduling in a water distribution system as a bi-objective optimization problem by taking into account pump operational costs and the land subsidence issue to reduce costs and address environmental concerns. The results obtained by the proposed genetic algorithm-based method have resulted in a wide range of schedules.

Kevin *et al.* [24] presented a methodology to generate pump schedules for small or midsize systems that produces the minimum energy cost while limiting the number of pump switches. Magatao *et al.* [25] studied scheduling for real-world pipeline applications. They proposed a mixed-integer linear programming model with uniform time discretization to optimize the pipeline operations and minimize the operational cost. Farmani *et al.* [26] developed a multi-objective optimization model that included cost, water quality, and reliability objectives in a water distribution network. The pipe network, pipe sizes, and pump operation

schedules were optimized. Although the results reported in Wang *et al.* [23] showed significant potential to improve the efficiency of multi-pump systems, the implementation horizon was limited by the static model of the pumps.

1.3. Review of data mining and computational intelligence in system modeling and optimization

Data mining approaches have gained attention in recent years. It enables establishing accurate underlying patterns of complex systems and processes from complicated, noisy, and imprecise data sets. It has proven to be a promising approach for modeling complex, dynamic, and non-linear systems. Rygielski *et al.* [27] reviewed the evolution and applications of data mining, and compared neural networks and chi-square automated interaction detection (CHAID) in dealing with customer relationship management problems. Harding *et al.* [28] reviewed applications of data mining in manufacturing engineering, customer relationship management, information integration, and standardization. Zhang *et al.* [29] proposed a modified *k*-means clustering algorithm to develop one vibration monitoring model based on SCADA data for the wind turbine monitoring. Kusiak *et al.* [30] presented a data-driven approach to optimize the HVAC system. A neural network algorithm was used to build predictive model and a multi-objective PSO algorithm was utilized to optimize overall energy optimization model. Moreover, data mining has widely applied in wind energy [31-33], HVAC systems [34, 35], and other areas [36-38].

On the other hand, computational intelligence have rapidly developed and been widely applied in tackling optimization problems in business, economics, industry, and manufacturing, engineering after first introduced by Bezdek [39]. The increasing complexity of nowadays real problems poses great challenges in solving these problems for optimal solutions, which makes traditional exact algorithms , like branch-and-bound, often perform poorly to obtain a satisfactory solution within a reasonable amount of time. Computational intelligence mainly

includes paradigms [40], like neural network [41, 42], evolutionary computing [43, 44], swarm intelligence [45], fuzzy system [46] and so forth [47].

Classical intelligent algorithms, such as genetic algorithms (GAs), particle swarm optimization (PSO), simulated annealing (SA), tabu search (TS), have shown great potential and remarkable successes in energy optimization domain [48-51]. At the same time, new intelligent algorithms, like harmony search (HS) [52], firefly algorithm (FA) [53], bat-inspired algorithm (BA) [54], are continuously developed for optimization.

In this research, a framework of applying data mining and computational intelligence to system modeling and optimization is discussed. Data-driven models are first built by data mining algorithms. Then optimization model is established by combining data-driven models and related constraints. Computational intelligence algorithms are designed to solve overall optimization model for optimal system settings or operational strategies.

1.4. Thesis structure

The structure of this thesis is organized as follows. Chapter 1 gives reviews on traditional methodologies in modeling HVAC system and wastewater pumping systems, and the proposed data mining and computation intelligence for system modeling and optimization. In Chapter 2, energy optimization of a wastewater pumping system is studied. A neural network algorithm is proposed to model the performance of the system, and a greedy electromagnetism-like algorithm is designed to solve the mixed integer nonlinear programming model. Chapter 3 applies a data mining approach to model the energy consumption of an air handling unit in a HVAC system. Then a dynamic, penalty-based, electromagnetism-like algorithm is proposed to solve the energy optimization model to generate optimal settings for two set points of the system. In Chapter 4, the multi-layer perceptron neural network is to model a multi-zone HVAC system. The Firefly Algorithm is then utilized to solve the model with respect to energy savings as well as thermal comfort. Chapter 5 summarizes a practical implementation to demonstrate how data mining and

computational intelligence are combined in HVAC system optimization. Chapter 6 concludes the thesis and discusses future research directions.

CHAPTER 2

DATA-DRIVEN PERFORMANCE OPTIMIZATION OF A WASTEWATER PUMP SYSTEM

2.1. Introduction

In this chapter, performance of a pumping system in the preliminary treatment process of a municipal wastewater treatment plant is optimized by improving the control strategies. Energy consumption and outflow rate of the pumping system are used to assess the performance and are modeled by a data mining approach. A mixed-integer nonlinear programming (MINLP) problem composed of data-driven models and related constraints is developed to produce strategies for improving performance of the pump system. The objective of the proposed MINLP model is minimizing energy consumption of the system while maintaining its pumping performance. Since data driven models are nonlinear and nonparametric, solving the MINLP by conventional optimization tools is challenging. In this research, a greedy electromagnetism-like (GEM) algorithm is proposed to solve the model. Three cases are studied to demonstrate the improvement of the pump system performance. The computational results show that the energy consumption of the pumping system can be significantly reduced by the proposed control strategies.

2.2. Pump System Description

The pumping system studied in this research operates at the Wastewater Reclamation Facility (WRF) located in Des Moines, Iowa. The pumping station includes six 55 MGD-class variable-speed wastewater pumps, five mechanical bar screens, and six aerated grit chambers, as illustrated in Figure 2.1. The preliminary treatment process involves collecting wastewater from sewers and removing debris and large particles from the wastewater. The bar screens in Figure 2.1 remove paper, sticks, and other solids that could damage the plant equipment. Then, the pumping system conveys the influent into aerated grit chambers for grit removal. The pumping

system is the major energy consumer in the wastewater treatment process. Improving performance of the pump system by optimizing its energy consumption is desired and beneficial.

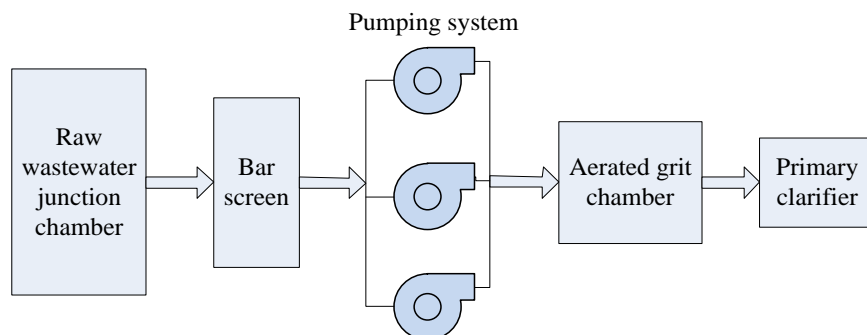


Figure 2.1 Schematic diagram of wastewater preliminary treatment process

Six pumps can be operated under different configurations to meet the workload demand. Currently used control rules recommended by the pump supplier are based on the variation of the chamber level, denoted as L . Different rules are used to response to different chamber level, which is aimed to be controlled within a required range. Two issues pertaining to the optimization of the pumps will be investigated. First, the energy consumption should be taken into consideration while controlling the pumps. The second issue is related to the performance of each pump. When initially installed, the six pumps were identical and thus had the same mechanical and hydraulic performances. However, the different workload assigned to the pumps and their maintenance has led to differentiation in the pump dynamics. Therefore, each pump has acquired its own performance curve. Moreover, the head phenomenon [21-23] differentiates the performance of the pumping system for different pump configurations (sets of pumps operating at the same time). The original rules for selecting the pump configurations neglect these facts, and thus energy saving opportunity is missed.

The selection of a pump configuration and its timing calls for the optimization of the pump schedules. The pump schedules should consider the best pump configuration and the optimal speeds for the workload to minimize the energy consumption. To achieve this goal, accurate pump models are needed. Because of the complex, dynamic, and highly nonlinear nature of the pumping system, establishing accurate pump models to optimize the performance of the pumping system is a challenge. It is accomplished with a data-driven approach in this research.

2.3. Model Development and Validation

2.3.1. Data description and model formulation

The performance of a pumping system can be evaluated using two metrics: the energy it consumes and the flow rate it provides. Two types of models, the energy consumption model and wastewater outflow rate model, are built based on the available datasets. The datasets used in this paper were collected from July 20, 2010, to January 31, 2012. The parameters used in this research are the speed of each pump, energy consumption of the pumping system, wastewater outflow rate, and junction chamber level. The values of these parameters are recorded every 5 min and averaged over 15-min time intervals. Models developed based on 15-min data are more meaningful in the study of investigating the operational schedules. The pump speed is measured as a percentage of the nominal speed (500 RPM). The maximum pump output is around 50 MGD, and it could be increased to 55 MGD at a high wet well elevation.

In total, there are 63 (2^6-1) different configurations for the 6 pumps. Because the pumps are controlled using variable frequency drives (VFDs), pumping begins only if the pump achieves at least 80% of its nominal speed to overcome the head pressure of the system. The pump is thus considered not in work when its speed is lower than 80% of the nominal speed, i.e., a speed value below 80% is disregarded. To ensure a dataset of sufficient size for the data mining, pump configurations with more than 300 data points are considered in this research. The raw

data are preprocessed for abnormal, noisy, erroneous, missing, and irrelevant data. The preprocessed dataset for each pump configuration is then divided into training (75%) and test (25%) sets. The training data sets are used to build the energy consumption and wastewater outflow rate models using data-mining algorithms. The test data sets are then utilized to evaluate the accuracy and robustness of the developed models. Table 2.1 summarizes all the 24 pump configurations considered in this research.

Table 2.1 Different pump configurations and corresponding dataset sizes

Pump Configuration	Number of Data Points		
	Overall Set	Training Set	Test Set
1	800	600	200
2	800	600	200
3	800	600	200
4	800	600	200
5	800	600	200
6	800	600	200
1, 3	786	590	196
1, 4	695	522	173
1, 5	620	465	155
1, 6	478	359	119
2, 4	447	336	111
2, 6	1080	810	270
3, 6	872	654	218
4, 6	3451	2589	862
5, 6	1602	1202	400
1, 4, 5	407	306	101
2, 4, 5	354	266	88
2, 4, 6	584	438	146
2, 5, 6	1078	809	269
3, 4, 5	485	364	121
3, 4, 6	347	261	86
3, 5, 6	479	360	119
1, 3, 4, 5	329	247	82
2, 3, 4, 5, 6	729	547	182

The energy consumption model and outflow rate model use the pump speeds as inputs. The respective outputs are the energy consumption of the pumping system and the wastewater outflow rate of the system. The two models are presented in (2.1) and (2.2).

$$E_{\pi(i)}(t) = f(\bar{\omega}_{\pi(i)}(t)) \quad (2.1)$$

$$Q_{\pi(i)}(t) = f(\bar{\omega}_{\pi(i)}(t)) \quad (2.2)$$

where $\pi(i)$ is i -th pump configuration, e.g., $\pi(1)=[1]$, $\pi(7)=[1,3]$, $\pi(24)=[2,3,4,5,6]$, and so on; $\bar{\omega}_{\pi(i)}(t)$ is the pump speed vector for the i -th configuration, e.g., $\bar{\omega}_{\pi(16)}(t)=[\omega_1(t), \omega_4(t), \omega_5(t)]$; $E_{\pi(i)}(t)$ is the energy consumption; and $Q_{\pi(i)}(t)$ is the outflow rate of the pumping system.

Although the chamber level impacts the head pressure of the pumps, and thus impacts the pump efficiency, it is not considered as an input for the data mining models. This is mainly because the level changes over a fairly small range and sometimes remains constant in 15-min data, which implies that this parameter would provide limited information to the models.

2.3.2. Model validation

In this research, a multi-layer perceptron (MLP) neural network is utilized to extract models of the energy consumption and flow rate for each pump configuration. MLP models are powerful tools with applications to classification, regression analysis, time series prediction, and other science and engineering areas [55-57]. The following four metrics ((2.3)–(2.6)) are used to assess the performance of the MLP derived models: the mean absolute error (*MAE*), standard deviation of the absolute error (*SdAE*), mean relative percentage error (*MRPE*), and standard deviation of the relative percentage error (*SdPE*).

$$MAE = \frac{1}{n} \sum_{i=1}^n |y_i - \hat{y}_i| \quad (2.3)$$

$$SdAE = \sqrt{\frac{\sum_{i=1}^n (|y_i - \hat{y}_i| - MAE)^2}{n-1}} \quad (2.4)$$

$$MRPE = \frac{1}{n} \sum_{i=1}^n \left| \frac{y_i - \hat{y}_i}{y_i} \right| \times 100\% \quad (2.5)$$

$$SdPE = \sqrt{\frac{\sum_{i=1}^n \left(\left| \frac{y_i - \hat{y}_i}{y_i} - MAPE \right| \right)^2}{n-1}} \quad (2.6)$$

where y_i is the value observed by the model, \hat{y}_i is the predicted value, and n is the size of the training or test data set.

Table 2.2 summarizes the accuracy of the models. With the exception of configuration (2, 4), the accuracies of the energy consumption models are above 95%. Meanwhile, the outflow rate models achieve accuracies of at least 95%, except for configurations (2, 4), (3, 6), and (2, 3, 4, 5, 6). The accuracies of all of the MLP models are higher than 90%. Configurations (1, 3), (1, 4, 5), and (1, 3, 4, 5) are used to demonstrate the performance of the energy consumption and outflow rate models. Figures 2.2–2.4 depict the test results of the energy consumption models and Figures. 2.5–2.7 demonstrate the test results of the outflow rate models for the three pump configurations. Based on the comparisons, the predicted values closely follow the patterns of the observed values for the energy consumption and outflow rate models. The models are accurate enough to be used in the optimization discussed in the next section.

Table 2.2 Test results of energy consumption and the wastewater outflow rate models derived using MLP algorithm

Pump Configuration	Energy Consumption Model				Wastewater Outflow Rate Model			
	MAE	SdAE	MRPE	SdPE	MAE	SdAE	MRPE	SdPE
1	8.27	6.60	0.02	0.01	0.98	0.82	0.02	0.02
2	7.44	5.85	0.02	0.02	0.77	0.46	0.02	0.01
3	7.44	10.60	0.02	0.02	0.86	1.17	0.02	0.03
4	9.00	5.10	0.02	0.01	1.35	0.84	0.02	0.02
5	5.34	6.17	0.01	0.01	0.95	0.81	0.02	0.02
6	9.97	12.09	0.02	0.03	1.39	1.30	0.03	0.02
1, 3	8.96	11.02	0.01	0.01	2.29	5.64	0.03	0.09
1, 4	5.48	4.76	0.01	0.01	1.20	0.83	0.01	0.01
1, 5	16.66	19.69	0.02	0.02	1.84	3.71	0.02	0.05
1, 6	14.25	10.35	0.03	0.02	1.36	1.25	0.02	0.02
2, 4	50.90	19.67	0.09	0.04	4.50	1.81	0.07	0.03

Table 2.2-continued

2, 6	16.65	18.43	0.03	0.03	2.28	2.26	0.04	0.03
3, 6	14.90	11.52	0.03	0.02	4.25	6.89	0.07	0.12
4, 6	14.64	11.25	0.02	0.02	3.28	6.64	0.04	0.11
5, 6	15.16	14.18	0.03	0.03	3.27	4.51	0.05	0.08
1, 4, 5	11.22	10.81	0.01	0.01	4.98	8.64	0.03	0.05
2, 4, 5	8.79	6.69	0.01	0.01	1.37	1.33	0.01	0.01
2, 4, 6	12.02	9.85	0.01	0.01	2.64	2.30	0.02	0.02
2, 5, 6	16.37	14.34	0.02	0.02	2.08	2.05	0.02	0.02
3, 4, 5	13.01	21.45	0.01	0.02	4.13	2.97	0.04	0.03
3, 4, 6	17.14	10.98	0.02	0.01	2.43	1.52	0.02	0.01
3, 5, 6	16.89	13.31	0.02	0.01	2.99	1.61	0.03	0.02
1, 3, 4, 5	15.44	9.90	0.01	0.01	2.10	1.62	0.01	0.01
2, 3, 4, 5, 6	77.39	123.80	0.04	0.06	13.67	11.25	0.06	0.05

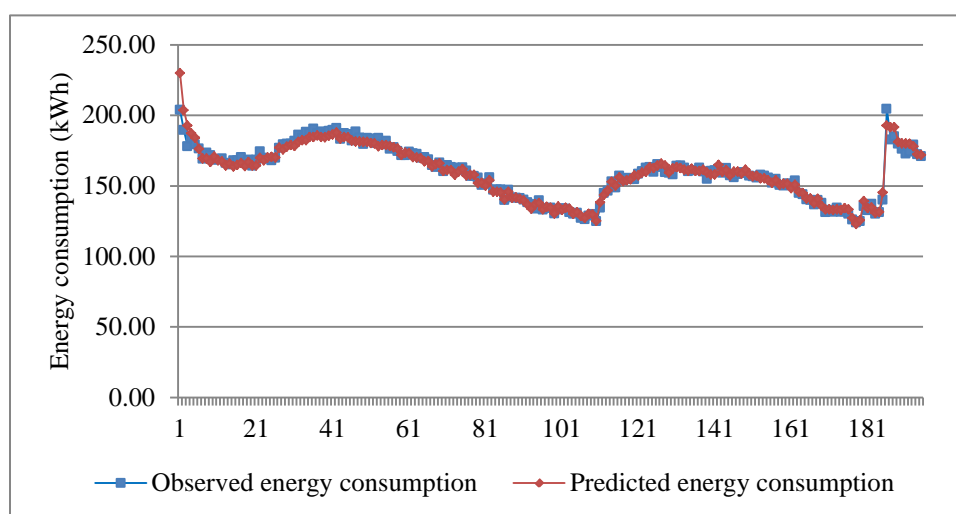


Figure 2.2 Observed and MLP predicted energy for configuration (1, 3)

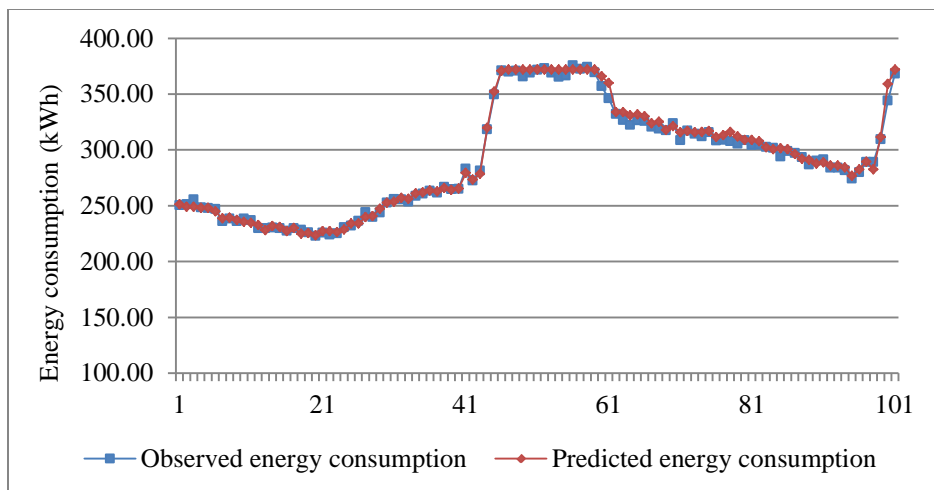


Figure 2.3 Observed and MLP predicted energy for configuration (1, 4, 5)

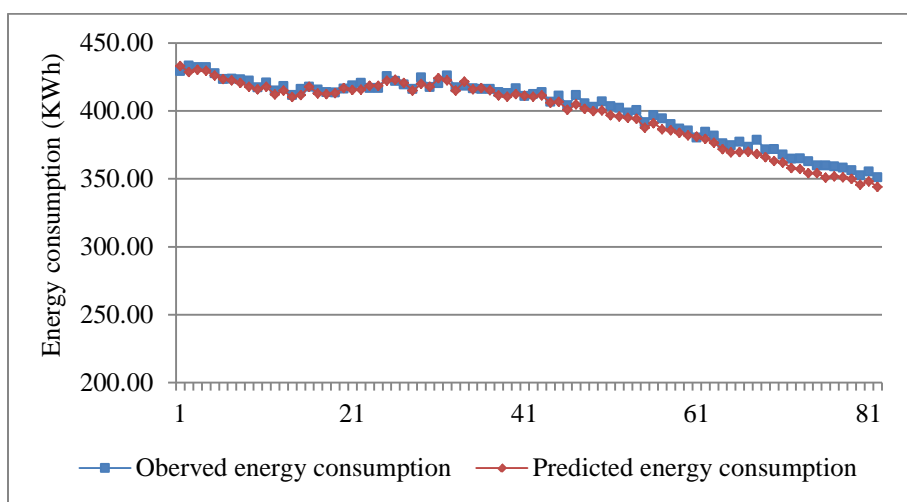


Figure 2.4 Observed and MLP predicted energy for configuration (1, 3, 4, 5)

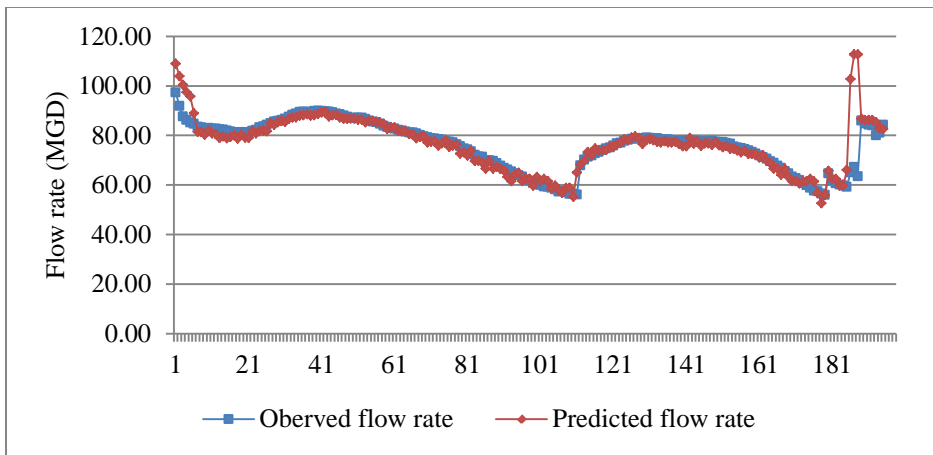


Figure 2.5 Observed and MLP predicted outflow rate for configuration (1, 3)

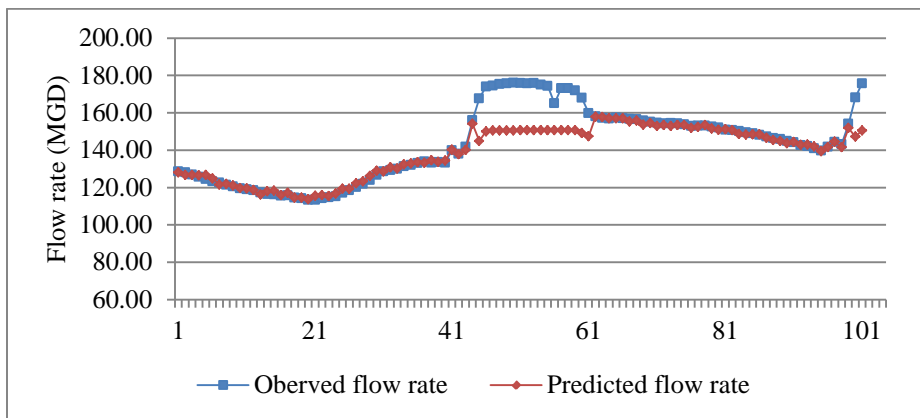


Figure 2.6 Observed and MLP predicted outflow rate for configuration (1, 4, 5)

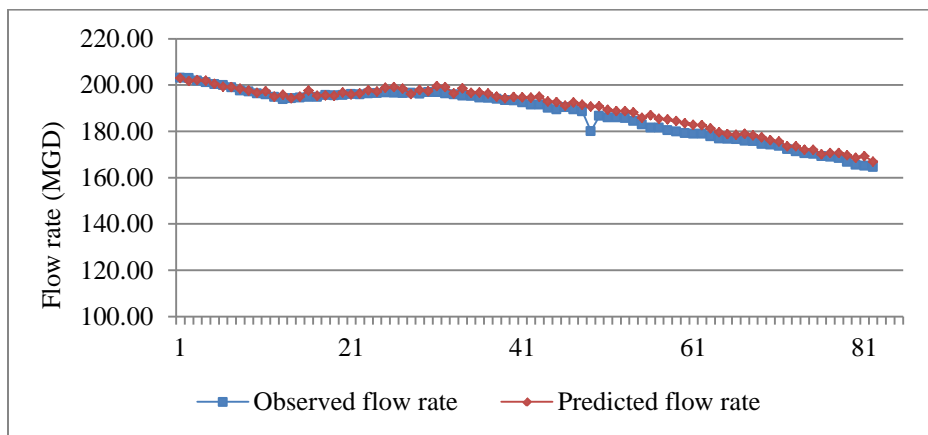


Figure 2.7 Observed and MLP predicted outflow rate for configuration (1, 3, 4, 5)

2.4. Overall Energy Optimization Model

The energy consumed by the pumping system is impacted by the system operations, *i.e.*, pump configuration and the pump speeds. An optimal pump schedule includes the best pump configurations and the best pump speeds over time horizon T . In this research, $T = 100$ time increments, each 15 min long representing an optimization stage ($\Delta t=15$). At the beginning of each optimization stage, the pump configuration and pump speeds are determined based on the wastewater inflow rate. In practice, the inflow rate is difficult to measure. However, it can be computed according to the mass balance equation (2.7).

$$A(L(t) - L(t - \Delta t)) = \Delta t(q(t) - Q_{\pi(i)}(t)) \quad (2.7)$$

where A is the bottom area of the chamber (here assuming $A = 10000 \text{ ft}^2$), $L(t)$ is the junction chamber level corresponding to the current time increment, $L(t - \Delta t)$ is the junction chamber level at the previous time increment (15 min ago), $q(t)$ is the inflow rate, and $Q_{\pi(i)}(t)$ is the outflow rate of the pumping system. Because the junction chamber level and outflow rate of the pumping system are measured, the inflow rate can be calculated. Therefore, in this paper it is assumed that the inflow rate is known at each time increment.

The objective of the model is to minimize the energy consumed by the pumping system in the planning horizon T (see (2.8)).

$$\min \sum_{t \in T} \sum_{i \in I} x_i E_{\pi(i)}(t) \quad (2.8)$$

Two decision variables are introduced. The first is a binary variable, denoted as x_i , that is used to select a pump configuration. If pump configuration $\pi(i)$ is employed, $x_i = 1$; otherwise $x_i = 0$. The second decision variable is the pump speed vector, $\vec{\omega}_{\pi(i)}(t)$, for the i -th pump configuration.

Several constraints are considered in the model. First, at each time increment, only one pump configuration can be chosen, as expressed in (2.9).

$$\sum_{i \in I} x_i = 1 \quad (2.9)$$

Second, during the planning horizon T , the chamber level should be kept within an acceptable range, as expressed in (2.10).

$$L_{lb} \leq L(t) \leq L_{ub} \quad (2.10)$$

where L_{lb} and L_{ub} are the lower and upper bounds of the level, respectively. The chamber level is defined by transforming mass balance equation (2.7) to (2.11).

$$L(t) = \frac{\Delta t (q(t) - Q_{\pi(i)}(t))}{A} + L(t - \Delta t) \quad (2.11)$$

Another constraint is related to the pump speeds. A pump is considered as working when its speed is in the range [80%, 100%]. However, in the industrial dataset available for this research, the number of data points that included values near 80% and 100% was small. This may lead that it is hard to capture the patterns near these speeds. To ensure the accuracy of the models, the pump speed was restricted to the range in (2.12).

$$\omega \in [0.85, 0.95] \quad (2.12)$$

Last, two types of constraints learned by the data-mining algorithm are included in the model. One is the energy consumption constraint, and the other is the flow rate constraint, as shown in (2.13) and (2.14).

$$E_{\pi(i)}^{lb} \leq E_{\pi(i)}(t) \leq E_{\pi(i)}^{ub} \quad (2.13)$$

$$Q_{\pi(i)}^{lb} \leq Q_{\pi(i)}(t) \leq Q_{\pi(i)}^{ub} \quad (2.14)$$

where $E_{\pi(i)}^{lb}$ and $E_{\pi(i)}^{ub}$ are the minimum and maximum energy consumptions of the i -th pump configuration. Similarly, $Q_{\pi(i)}^{lb}$ and $Q_{\pi(i)}^{ub}$ are the lower and upper bounds of the flow rate for the i -th pump configuration.

By combining the energy consumption and outflow rate models with the related constraints, the overall mixed integer nonlinear model for optimizing the pump energy is established, expressed in (2.15).

$$\begin{aligned}
& \min \sum_{i \in I} \sum_{t \in T} x_i E_{\pi(i)}(t) \\
& E_{\pi(i)}(t) = f(\bar{\omega}_{\pi(i)}(t)) \\
& Q_{\pi(i)}(t) = f(\bar{\omega}_{\pi(i)}(t)) \\
& L(t) = \frac{\Delta t (q(t) - Q_{\pi(i)}(t))}{A} + L(t - \Delta t) \\
& L_{lb} \leq L(t) \leq L_{ub} \\
& E_{\pi(i)}^{lb} \leq E_{\pi(i)}(t) \leq E_{\pi(i)}^{ub} \\
& Q_{\pi(i)}^{lb} \leq Q_{\pi(i)}(t) \leq Q_{\pi(i)}^{ub} \\
& I = \{1, 2, \dots, 24\} \\
& x_i = \{0, 1\} \\
& \omega \in [0.85, 0.95]
\end{aligned} \tag{2.15}$$

2.5. Proposed Greedy Electromagnetism-like Algorithm

In this section, a greedy electromagnetism-like algorithm, on the strength of cardinal electromagnetism-like algorithm (EM) [58], is proposed to solve the MINLP model in this research. The EM algorithm was first introduced by Birbil and Fang. Research has demonstrated that the EM algorithm outperforms traditional intelligent algorithms algorithm in optimization [59], neural network training [60], production scheduling [61], and other applications [62, 63]. However, little progress, to the best of our knowledge, has been made in applying the EM algorithm to solve MINLP models. The basic concepts and procedure of the cardinal electromagnetism-like algorithm is first introduced. The proposed greedy EM algorithm is then designed for solving the model.

2.5.1. Theory of electromagnetism-like algorithm

The EM algorithm utilizes an attraction-repulsion mechanism to move sample points toward optimality. The algorithm starts with sample points (a population) selected from a feasible space and continues its iterative process until a stopping condition (e.g., the maximum number of iterations) is met. Two steps are performed at each iteration of the algorithm. In the first step, each point is assigned a charge related to the value of the objective function, according to (2.16). Points that improve the values of the objective function are assigned higher charges.

The charge determines the magnitude of attraction of the point relative to the other points in the population, with a better objective function value leading to a higher magnitude of attraction.

The force exerted on a point via other points is computed according to (2.17), and the total force vector is obtained by adding these attractive–repulsive forces (2.18).

$$q^i = \exp\left(\frac{-n(f(x^i) - f(x^{best}))}{\sum_{j=1}^m (f(x^j) - f(x^{best}))}\right), i = 1, 2, \dots, m \quad (2.16)$$

$$F_j^i = \begin{cases} (x^j - x^i) \frac{q^i q^j}{\|x^j - x^i\|} & \text{if } f(x^j) < f(x^i) \\ (x^i - x^j) \frac{q^i q^j}{\|x^j - x^i\|} & \text{if } f(x^j) \geq f(x^i) \end{cases}, j \neq i, \forall i \quad (2.17)$$

$$F^i = \sum_{j \neq i}^m F_j^i, i = 1, 2, \dots, m \quad (2.18)$$

$$x_k^i = \begin{cases} x_k^i + \lambda \frac{F_k^i}{\|F^i\|} (u_k - x_k^i) & \text{if } F_k^i > 0 \\ x_k^i + \lambda \frac{F_k^i}{\|F^i\|} (x_k^i - l_k) & \text{if } F_k^i \leq 0 \end{cases} \quad (2.19)$$

Then, each point moves to a new location in the direction of the total force vector (2.19).

In expressions (2.16)–(2.19), m is the population size; n is the dimension; and k is the dimension index of the model.

The attraction-repulsion mechanism is captured in (2.17), implying that between two points, the point with the more favorable objective function value attracts the other one. Conversely, the point with the less favorable objective function value repels the other one. For example, consider the three points (1, 2, and 3) in Figure 2.8. Point 1 denotes a less favorable solution than point 2, yet, a better one than point 3. According to (2.17), point 2 attracts point 1, represented by F_{21} , while point 3 repels point 1, represented by F_{31} . The total force, F_1 , exerted on point 1 is the sum of the two force vectors, and point 1 moves in the direction of F_1 .

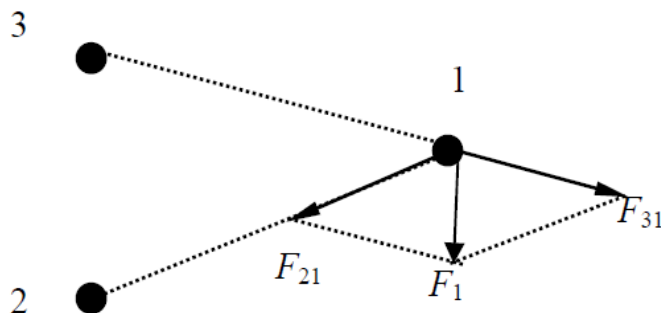


Figure 2.8 Attraction-repulsion mechanism

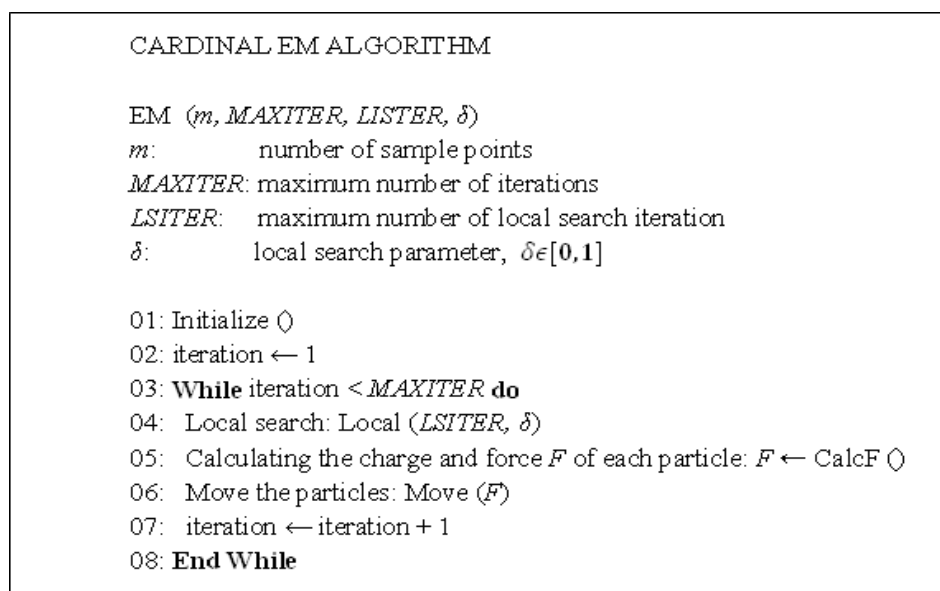


Figure 2.9 Pseudo code of electromagnetism-like algorithm

In the second step, a local search procedure is incorporated to improve the accuracy of the solution. A local refinement is applied, coordinate by coordinate, to the current best point in the population. Based on parameter δ , the maximum feasible step length, $S_{\max} = \delta(\max_k (u_k - l_k))$, is computed. Then, for each coordinate, a step length between 0 and 1 is randomly generated, and a new point is computed along that direction. If an improvement in the objective function is observed within the local search iterations ($LSITER$), the current best point is replaced, and the

search continues with the next coordinate. The pseudo code of the algorithm is illustrated in Figure 2.9.

2.5.2 Proposed greedy electromagnetism-like algorithm

The MINLP model (2.15) aims to select the optimal pump configurations and speeds, which is a two-level optimization. The upper level is to select the right pump configuration, and based on that the lower level optimization generates optimal pump speed settings. Considering that there are 100 optimization stages in model (2.15), it's hard to obtain global optimal solution of the pump schedules. Thus, a greedy electromagnetism-like algorithm (GEM) is proposed to solve model (2.15) for each stage. Basically, at the beginning of optimization procedure, the algorithm will enumerate all the available pump configurations, and find the optimal pump speed settings regarding to the minimum energy consumption for each pump configuration. After that, the best pump configuration and the corresponding speeds are selected from all the obtained pump configurations and speeds. The algorithm iteratively finds best pump configurations and speeds for every stage, which form the best pump schedule for the planning horizon. The pseudo code of the GEM is illustrated in Figure 2.10.

```

GREEDY EM ALGORITHM

GEM (STAGES, CONFIGLIST, m, MAXITER, LISTER,  $\delta$ )
STAGES:      number of optimization stages
CONFIGLIST:  list of pump configurations
m:          number of sample points
MAXITER:    maximum number of iterations
LISTER:    maximum number of local search iteration
 $\delta$ :      local search parameter,  $\delta \in [0,1]$ 

01: Initialize  $\emptyset$ 
02: iteration  $\leftarrow 1$ , stage  $\leftarrow 1$ , schedule  $\leftarrow \{\}$ , set up CONFIGLIST
03: While stage < STAGES Do
04:   Initialize CANDIDATELIST
05:   While CONFIGLIST not empty Do
06:     Select config from CONFIGLIST
07:     While iteration < MAXITER Do
08:       Local search: Local (LISTER,  $\delta$ )
09:       Calculating the charge and force F of each particle:  $F \leftarrow \text{CalcF}$   $\emptyset$ 
10:       Move the particles: Move (F)
11:       Check boundaries: Check  $\emptyset$ 
12:     End While
13:     newconfig  $\leftarrow \{\textit{config}, \textit{speeds}\}$ 
14:     If newconfig is feasible
15:       Remove config from CONFIGLIST
16:       Add newconfig to CANDIDATELIST
17:     End If
18:   End While
19:   Select optimalConfig from CANDIDATELIST, add to schedule
20: End While
21: Output schedule

```

Figure 2.10 Pseudo code of the proposed greedy electromagnetism-like algorithm

2.6. Computational Results and Analysis

Three cases corresponding to low, medium, and high inflow rates are considered. The parameters for the EM algorithm are set for all cases as $m = 50$, $MAXITER = 100$, $\delta = 0.01$, and $LISTER = 10$. The lower and upper bounds of the chamber level are $L_{lb} = 4$ and $L_{ub} = 8$ in all three cases. In each case, 100 data points (100 time increments) are considered, planning horizon $T = 25$ h since each data point represents 15 minutes long. In the low inflow rate case, the flow

rate ranges from 46 MGD to 61 MGD. Only pump 1 is used in this case. The inflow rate in the second case varies from 114 MGD to 139 MGD for the recorded pump configuration (2, 4, and 6). For the high inflow rate case, the range of the inflow rate is between 155 MGD and 211 MGD for the pump configuration (1, 3, 4, 5).

The computational results are summarized in Table 2.3. Based on these results, the energy consumed by the pumping system can be reduced by 25%, 32%, and 17%, respectively, for the three different cases. Figures 2.11–2.13 compare the optimized and observed energy consumptions and chamber levels for the low inflow rate. Figures 2.14–2.16 compare the optimized and observed energy consumptions and chamber levels for the medium inflow rate. Finally, Figures 2.17–2.19 illustrate the optimized and observed energy consumptions and the chamber levels for the high inflow rate. As shown in Figures 2.13 and 2.16, the optimized low and medium inflow rate cases, the chamber is used to store wastewater until the upper bound of the chamber level is reached. Then, the wastewater is pumped out according the optimal pump schedule until the chamber level reaches the lower bound. Thus, the chamber becomes available for water storage. Accordingly, the wastewater outflow rate after the pumping system change fluctuates, as illustrated in Figures 2.12 and 2.15. In this way, the energy savings in the low inflow rate case comes from two parts, one is optimized pump speeds for each pump configuration, the other is the optimal pump schedules for the whole planning horizon. For the high inflow rate case, the flow rate behaves in a manner similar to the observed pattern (Figure 2.18). This is mainly because the workload for the pumping system is always high. All of the inflow needs to be pumped out, and thus there is no buffer to store wastewater. In addition, there are few pump configurations that meet the workload because of the high inflow rate, which indicates there is little room for optimizing pump schedules. The energy savings for the high inflow rate case are mainly the result of the optimized pump speeds.

The optimized pump schedule for the medium inflow rate case is listed in Table 2.4 in the Appendix. The optimized pump schedules for the other two cases are not included because of space limitations.

Table 2.3 Summary of computational results for three cases

Case	Low	Medium	High
No. of Time Increments	100	100	100
Observed Pump Configuration	Pump 1 only	Pumps 2, 4, 6	Pumps 1, 3, 4, 5
Inflow Rate Range (MGD)	46–61	114–139	155–211
Observed Total Energy Consumption (kWh)	11148.26	27461.49	37214.32
Optimized Total Energy Consumption (kWh)	8324.50	18776.66	30972.69
Energy Saving Amount (kWh)	2823.76	8684.83	6241.63
Energy Saving Percentage (%)	25	32	17

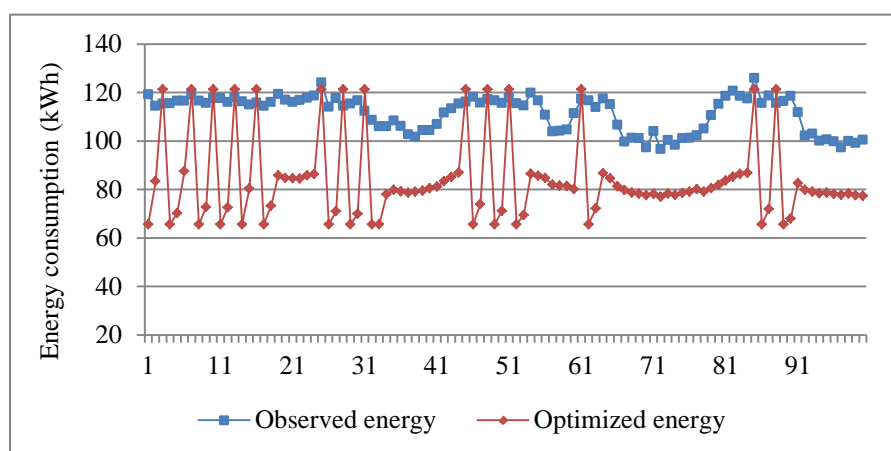


Figure 2.11 Observed and optimized energy consumptions for low inflow rate

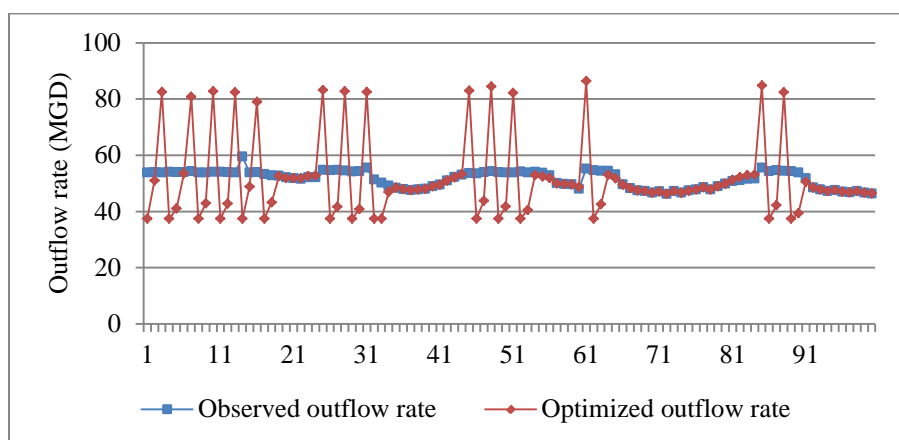


Figure 2.12 Observed and optimized effluent flow rates for low inflow rate

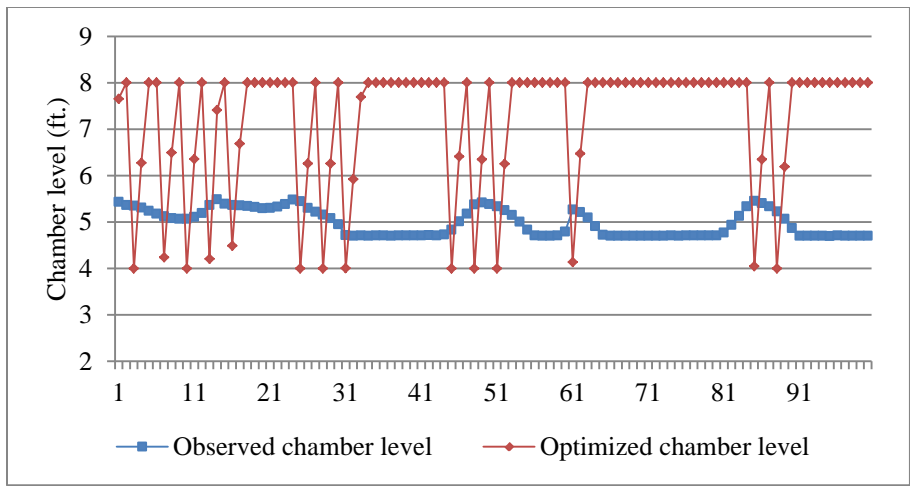


Figure 2.13 Observed and optimized chamber levels for low inflow rate

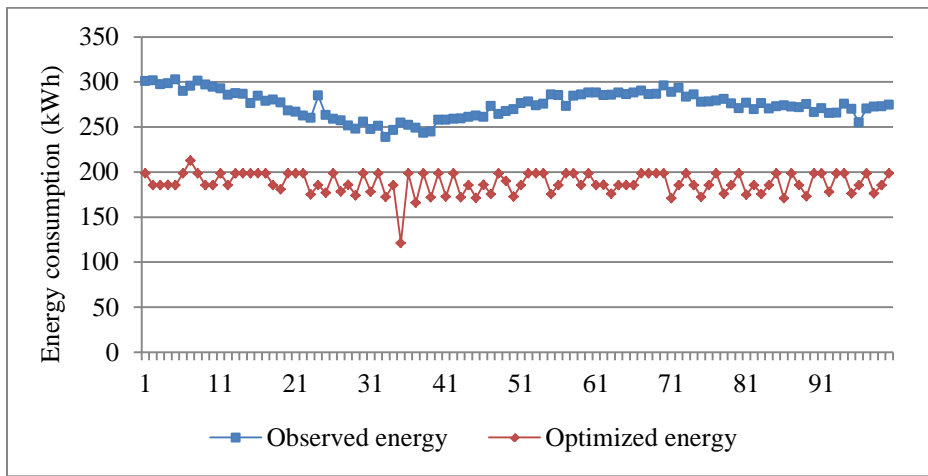


Figure 2.14 Observed and optimized energy consumptions for medium inflow rate

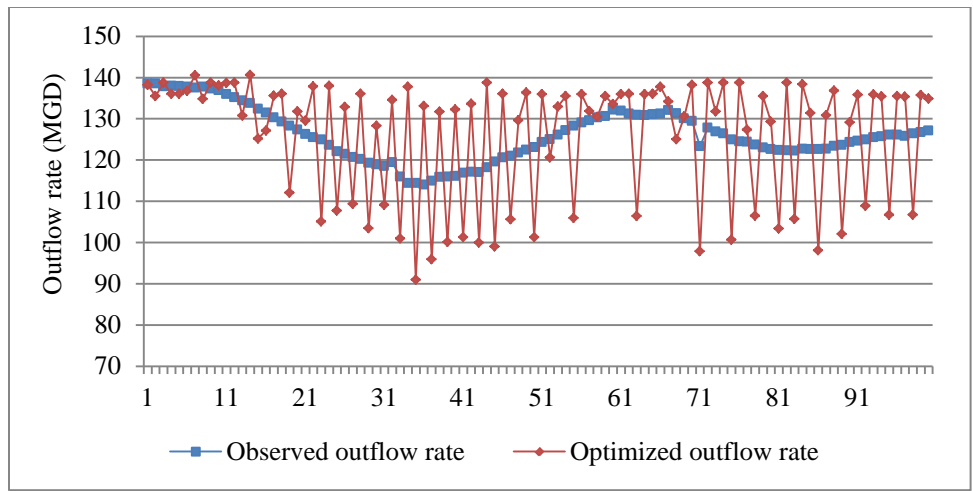


Figure 2.15 Observed and optimized effluent flow rates for medium inflow rate

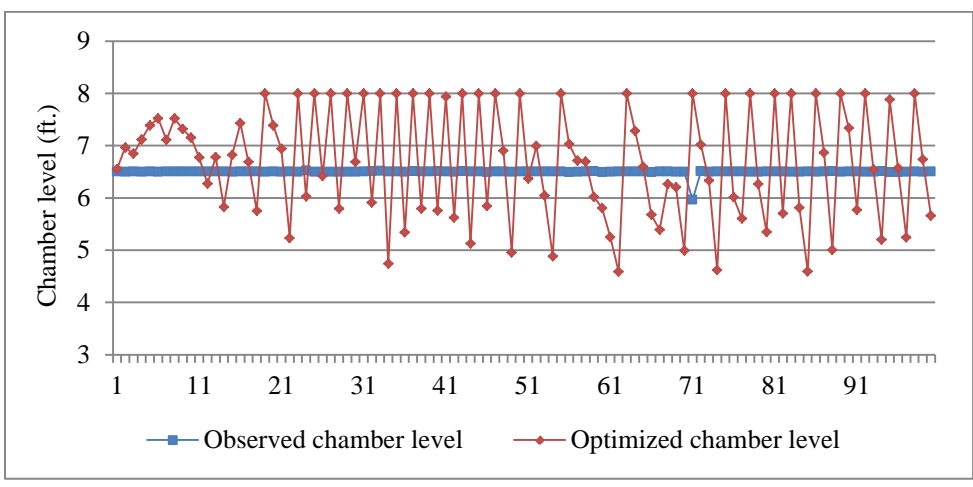


Figure 2.16 Observed and optimized chamber levels for low inflow rate

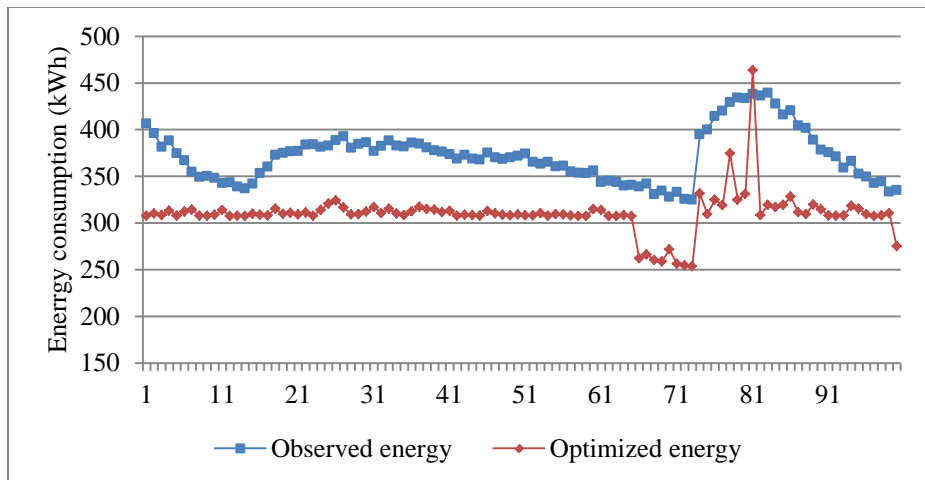


Figure 2.17 Observed and optimized energy consumptions for high inflow rate

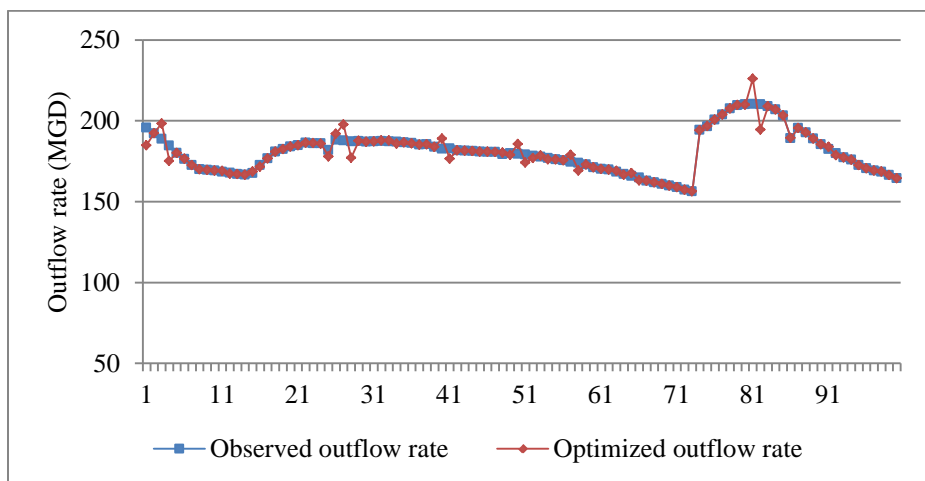


Figure 2.18 Observed and optimized effluent flow rates for high inflow rate

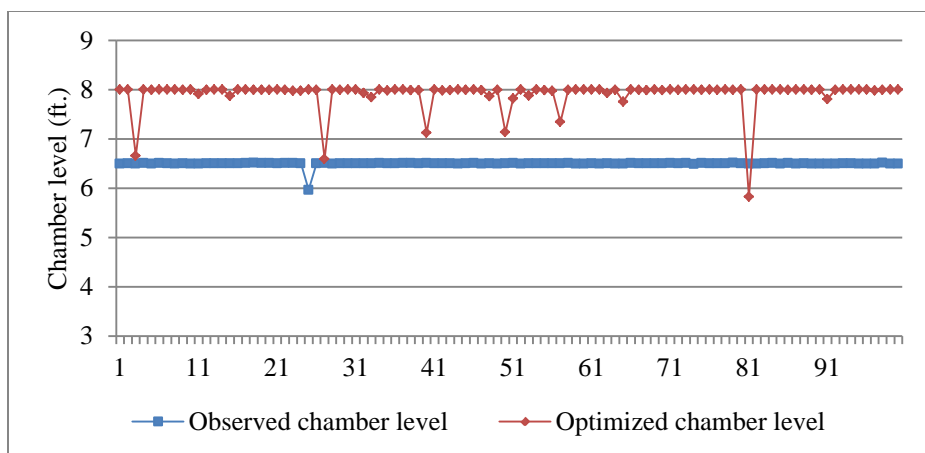


Figure 2.19 Observed and optimized chamber levels for high inflow rate

2.7. Summary

Performance optimization of a pumping system in a wastewater treatment process for energy savings was presented. A neural network algorithm was utilized to extract two types of models, energy consumption and outflow rate, of each pumping system configuration. Accuracy of extracted models was validated by a test dataset. These two types of models were used to evaluate the performance of the pumping system.

A mixed integer nonlinear programming model was then developed by incorporating the extracted data driven models and constraints. The objective was to optimize the energy consumption of the pumping system. The electromagnetism-like algorithm was applied to solve the MINLP model. The energy savings were demonstrated by solving the optimization model for three cases: low, medium, and high inflow rates. In each case, the optimization horizon of 100 time increments (25 h) was considered. The computational experiments demonstrated that significant energy savings can be achieved by the modeling approach presented in this chapter.

2.7. Appendix

Table 2.4 The observed and optimized pump schedules for the medium flow rate.

Observed Pump Schedule						Optimized Pump Schedule					
Pump 1	Pump 2	Pump 3	Pump 4	Pump 5	Pump 6	Pump 1	Pump 2	Pump 3	Pump 4	Pump 5	Pump 6
-	90.74	-	93.49	-	94.32	-	89.31	-	86.26	94.72	-
-	90.92	-	93.82	-	94.50	-	-	85.00	94.37	94.99	-
-	90.89	-	93.82	-	94.64	-	-	85.80	94.99	95.00	-
-	90.39	-	93.48	-	93.97	-	-	85.00	95.00	94.55	-
-	90.74	-	93.81	-	94.49	-	-	85.00	95.00	94.55	-
-	90.23	-	93.31	-	93.81	-	88.08	-	87.58	94.95	-
-	90.41	-	93.32	-	94.32	-	92.14	-	85.00	95.00	-
-	90.21	-	93.33	-	93.78	-	87.05	-	88.13	94.41	-
-	90.22	-	93.32	-	93.97	-	-	85.81	95.00	95.00	-
-	90.23	-	92.97	-	93.98	-	-	85.63	94.85	95.00	-
-	90.24	-	92.99	-	93.82	-	90.04	-	85.09	94.07	-
-	90.04	-	92.82	-	93.62	-	-	85.81	95.00	95.00	-
-	89.71	-	92.46	-	93.30	-	85.87	-	87.69	92.57	-
-	89.02	-	92.12	-	92.97	-	90.87	-	85.00	95.00	-
-	89.19	-	92.12	-	92.96	-	85.00	-	87.46	91.44	-
-	89.36	-	92.10	-	92.97	-	85.43	-	87.28	91.68	-
-	89.03	-	91.95	-	92.64	-	87.74	-	87.33	94.20	-
-	88.84	-	91.78	-	92.60	-	-	85.00	95.00	94.55	-
-	88.68	-	91.28	-	92.29	-	-	85.00	-	-	93.62
-	88.00	-	90.96	-	91.77	-	85.18	-	89.58	94.02	-
-	87.81	-	90.76	-	91.40	-	85.72	-	87.47	92.17	-
-	87.67	-	90.43	-	91.23	-	89.55	-	85.37	93.84	-
-	87.28	-	90.26	-	90.87	-	-	85.00	-	-	92.20
-	89.19	-	92.12	-	92.97	-	-	85.56	95.00	94.86	-
-	87.11	-	89.94	-	90.88	-	-	85.00	-	-	92.66
-	87.13	-	90.09	-	90.72	-	88.08	-	85.24	92.12	-
-	86.95	-	89.76	-	90.53	-	-	85.00	-	-	92.98
-	86.26	-	89.42	-	89.87	-	-	85.00	94.99	94.55	-
-	86.43	-	89.08	-	90.02	-	-	85.00	-	-	91.95
-	86.26	-	89.08	-	89.53	-	85.46	-	87.49	91.93	-
-	86.25	-	89.43	-	90.01	-	-	85.00	-	-	92.93
-	86.79	-	89.73	-	90.40	-	86.88	-	88.29	94.41	-
-	84.72	-	87.53	-	88.33	-	-	85.00	-	-	91.59
-	85.74	-	88.81	-	89.36	-	-	85.49	95.00	94.83	-
-	86.04	-	88.91	-	89.46	-	95.00	-	-	-	87.37

Table 2.4-continued

-	86.06	-	89.24	-	89.68	-	86.87	-	87.23	93.09	-
-	86.09	-	89.25	-	89.69	90.02	-	-	-	93.36	-
-	86.43	-	89.43	-	90.03	-	85.21	-	89.41	93.86	-
-	86.26	-	89.26	-	89.86	-	-	85.00	-	-	91.47
-	86.61	-	89.42	-	90.19	-	87.39	-	86.02	92.27	-
-	86.59	-	89.59	-	90.18	-	-	85.00	-	-	91.63
-	86.95	-	89.92	-	90.72	-	87.68	-	86.13	92.70	-
-	87.48	-	90.44	-	91.06	-	-	85.00	-	-	91.46
-	87.46	-	90.26	-	91.04	-	-	85.80	95.00	95.00	-
-	87.66	-	90.42	-	91.41	-	-	85.00	-	-	91.32
-	87.48	-	90.08	-	91.05	-	-	85.00	95.00	94.55	-
-	88.16	-	90.79	-	91.76	-	-	85.00	-	-	92.29
-	88.00	-	90.79	-	91.59	-	85.00	-	88.54	92.62	-
-	87.83	-	90.79	-	91.41	-	-	85.00	95.00	94.40	-
-	88.34	-	91.13	-	91.94	-	-	85.00	-	-	91.63
-	88.32	-	91.28	-	92.26	-	-	85.00	94.90	94.61	-
-	88.85	-	91.79	-	92.27	-	86.33	-	85.46	90.64	-
-	88.34	-	91.28	-	92.11	-	85.88	-	89.09	94.23	-
-	89.03	-	91.97	-	92.79	-	87.59	-	87.57	94.33	-
-	89.38	-	91.95	-	92.80	-	-	85.00	-	-	92.34
-	89.03	-	91.79	-	92.63	-	-	85.00	94.83	94.65	-
-	88.85	-	91.62	-	92.48	-	85.77	-	88.45	93.33	-
-	89.21	-	92.13	-	92.80	-	85.60	-	87.98	92.61	-
-	89.38	-	92.30	-	93.31	-	-	85.00	94.36	95.00	-
-	90.06	-	92.99	-	93.64	-	86.29	-	88.72	94.25	-
-	89.72	-	92.64	-	93.47	-	-	85.00	94.87	94.64	-
-	89.37	-	92.30	-	93.14	-	-	85.00	95.00	94.55	-
-	90.06	-	92.81	-	93.65	-	-	85.00	-	-	92.42
-	90.06	-	92.63	-	93.48	-	-	85.00	94.84	94.65	-
-	89.89	-	92.63	-	93.48	-	-	85.02	94.94	94.60	-
-	89.71	-	92.80	-	93.48	-	-	85.49	95.00	94.83	-
-	89.89	-	92.64	-	93.48	-	86.27	-	89.30	95.00	-
-	89.54	-	92.65	-	93.13	-	86.07	-	86.21	91.16	-
-	89.54	-	92.48	-	92.97	-	85.82	-	87.67	92.49	-
-	89.89	-	92.98	-	93.47	-	89.50	-	85.79	94.34	-
-	89.54	-	92.47	-	93.14	-	-	85.00	-	-	91.17
-	90.06	-	92.81	-	93.47	-	-	85.80	95.00	95.00	-
-	89.37	-	92.29	-	92.97	-	85.00	-	89.96	94.30	-
-	89.19	-	91.78	-	92.80	-	-	85.81	95.00	95.00	-
-	88.86	-	91.96	-	92.63	-	-	85.00	-	-	91.54
-	88.69	-	91.64	-	92.47	-	-	85.79	94.99	95.00	-

Table 2.4-continued

-	89.20	-	91.95	-	92.81	-	86.74	-	85.77	91.36	-
-	89.03	-	91.79	-	92.47	-	-	85.00	-	-	92.43
-	88.69	-	91.46	-	92.47	-	-	85.00	94.36	95.00	-
-	88.01	-	91.12	-	91.95	-	85.28	-	88.01	92.31	-
-	88.50	-	91.63	-	92.08	-	-	85.17	-	-	92.00
-	87.99	-	91.12	-	91.76	-	-	85.81	95.00	95.00	-
-	88.51	-	91.11	-	92.11	-	-	85.00	-	-	92.30
-	88.52	-	91.46	-	92.30	-	-	85.71	94.93	94.99	-
-	88.35	-	91.29	-	92.13	-	86.87	-	86.47	92.24	-
-	88.34	-	91.16	-	91.91	-	-	85.00	-	-	91.20
-	88.16	-	91.12	-	91.92	-	85.63	-	88.12	92.79	-
-	88.14	-	91.11	-	91.93	-	-	85.28	94.71	94.90	-
-	88.01	-	91.13	-	91.78	-	-	85.00	-	-	91.74
-	87.63	-	90.61	-	91.21	-	87.24	-	85.47	91.54	-
-	87.81	-	90.77	-	91.76	-	88.51	-	85.93	93.37	-
-	87.82	-	90.94	-	91.60	-	-	85.00	-	-	92.88
-	88.00	-	91.13	-	91.74	-	87.89	-	87.29	94.33	-
-	88.33	-	91.28	-	91.93	-	87.53	-	87.66	94.38	-
-	88.17	-	91.12	-	91.78	-	-	85.00	-	-	92.48
-	86.94	-	89.74	-	90.55	-	-	85.00	94.36	95.00	-
-	88.67	-	91.45	-	92.27	-	88.65	-	85.40	92.89	-
-	88.33	-	91.11	-	92.12	-	-	85.00	-	-	92.47
-	88.33	-	91.45	-	92.27	-	-	85.00	94.56	94.85	-
-	88.50	-	91.28	-	92.29	-	86.91	-	88.55	94.78	-

CHAPTER 3

MINIMIZING ENERGY CONSUMPTION OF AN AIR HANDLING UNIT WITH A COMPUTATIONAL INTELLIGENCE APPROACH

3.1. Introduction

The air handling unit (AHU) in an HVAC system impacts its overall performance. In this chapter, a data-mining approach is applied to optimize the energy consumption of an air handling unit. The goal of this research is to minimize the total energy consumption of an AHU system while maintaining the temperature and static pressure of the supply air at an acceptable level. Four controllable parameters, i.e., the flow rate of the chilled water supply, the position of the chilled-water coil valve, the temperature of the chilled water supply, and the speed of the supply fan speed were taken into consideration for optimal control.

Considering the multi-dimensional, non-linear, mixed-variable, and constrained nature of HVAC systems, a data-mining approach was used to build separate energy consumption models for the chiller, the pump, and the supply and return fans. A non-linear model was developed to minimize the total energy consumption of the air-handling unit while maintaining the temperature of the supply air and the static pressure in a predetermined range. To obtain optimal setting for the AHU system, a dynamic, penalty-based, electromagnetism-like algorithm was designed to solve the proposed model. In all, 200 test data points were used to validate the proposed algorithm. The computational results showed that the total energy consumed by the air-handling unit was reduced by almost 23%.

3.2. Model Formulation

A typical air handling unit (AHU) of an HVAC system supplies conditioned air to building zones. Figure 3.1 illustrates schematic diagram of an AHU. The supply air is at a specific temperature and flows at a specific rate to meet the heating or cooling load and ensure thermal comfort. Outdoor air mixes with the return air, and the mixed air passes through cooling

coils, heating coils, and the supply fan. Chilled water in the cooling coils cools the mixed air, and hot water or steam in the heating coils heats the mixed air to maintain the desired temperature of the supply.

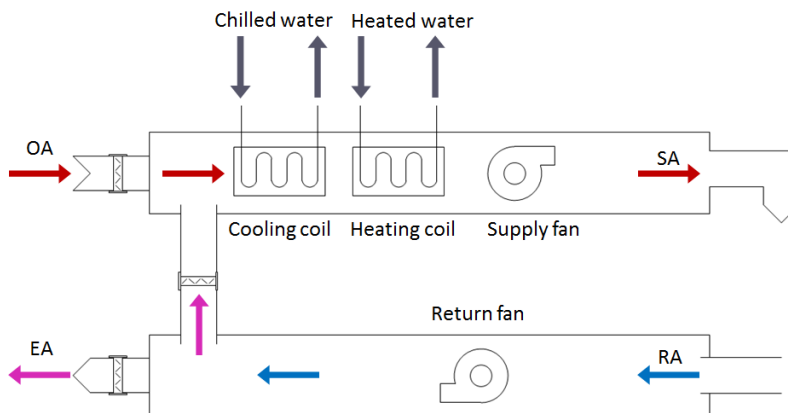


Figure 3.1 Schematic diagram of a typical AHU system

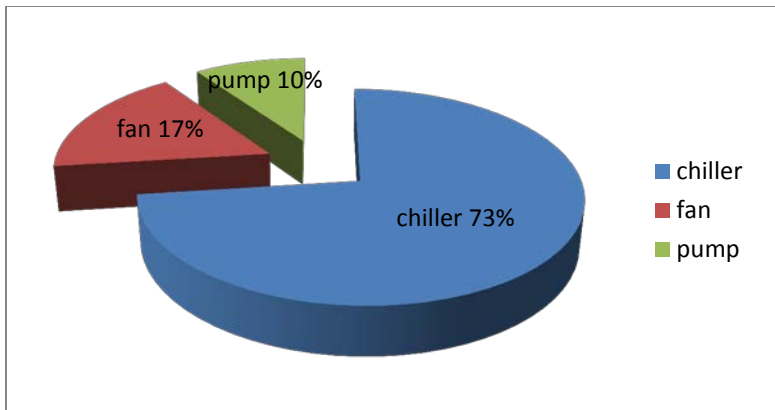


Figure 3.2 Energy consumption of different components in a sample cooling session

The supply and return fans assist in moving the air for heat exchange as well as circulating it in the HVAC system at the required flow rate. Several components, i.e., the chiller, the boiler, the supply and return fans, and the water pump, consume energy. Since the

experiment for this research was conducted between June 22, 2011 and July 5, 2011, the energy used for heating was insignificant and, thus, was not taken into consideration.

Figure 3.2 shows the energy consumption of different components of the HVAC system. Because our two-week experiment was performed in the summer, the chiller accounted for most of the energy consumed by the AHU system. The amount of energy consumed by a chiller is highly dependent on the heat transfer efficiency of the cooling coils. The greater the efficiency is, the less the energy consumption is. Turbulent air and water flows result in greater heat transfer efficiency than laminar flows [64]. A trade-off of the energy consumption between the chiller, the pump, and the fans can be accomplished by controlling the temperature of the chilled water supply, the flow rate of the water, and the flow rate of the air flow at optimal conditions. Thus, four controllable parameters, *i.e.*, the flow rate of the chilled water, the temperature of the chilled water, the position of the valve on the chilled water coil, and the speed of the supply fan, were considered to optimize the total energy consumed by the chiller, the pump, and the fans while maintaining the temperature and static pressure of the supply air at the required levels.

A data-mining approach was used to establish dynamic predictive models of the energy consumption of different components of the AHU system. Based on large datasets, the data-mining algorithms captured the dynamic operating patterns of the system. After the learning process, data-driven predictive models were developed. Once the current values of the inputs are determined, the output of the system at some chosen future time can be predicted by the models. Eq. (3.1), below, is a typical, multi-input, single-output predictive model derived by the data-mining algorithms:

$$y(t+d) = f(x(t), x(t-1), \dots, u(t), u(t-1), \dots,) \quad (3.1)$$

where $x \in R^m$ is a vector of m controllable parameters, $u \in R^n$ is a vector of n uncontrollable parameters, and $y(t+d)$ is the predicted values of the outputs at time stamp $(t+d)$.

Note that the terms $y_1(t+d)$, $y_2(t+d)$, $y_3(t+d)$ are the energy consumed by the chiller, the fans, and the pump, respectively.

The AHU energy optimization model is presented in (3.2).

$$\begin{aligned}
& \min E_{total} \\
& E_{total} = E_{fans} + E_{pump} + E_{chiller} \\
& E_{fans}(t+d) = f(\bar{x}_1(t+d), \dots, \bar{x}_1(t), \bar{x}_1(t-1), \dots, \bar{u}_1(t), \bar{u}_1(t-1), \dots) \\
& E_{pump}(t+d) = f(\bar{x}_2(t+d), \dots, \bar{x}_2(t), \bar{x}_2(t-1), \dots, \bar{u}_2(t), \bar{u}_2(t-1), \dots) \\
& E_{chiller}(t+d) = f(\bar{x}_3(t+d), \dots, \bar{x}_3(t), \bar{x}_3(t-1), \dots, \bar{u}_3(t), \bar{u}_3(t-1), \dots) \\
& T(t+d) = f(\bar{x}_4(t+d), \dots, \bar{x}_4(t), \bar{x}_4(t-1), \dots, \bar{u}_4(t), \bar{u}_4(t-1), \dots) \\
& P(t+d) = f(\bar{x}_5(t+d), \dots, \bar{x}_5(t), \bar{x}_5(t-1), \dots, \bar{u}_5(t), \bar{u}_5(t-1), \dots)
\end{aligned} \tag{3.2}$$

subject to:

$$\begin{aligned}
& \bar{x}_i \in S_i \quad (i = 1, 2, \dots, 5) \\
& T \in S_T \\
& P \in S_P
\end{aligned}$$

where each \bar{x}_i and \bar{u}_i ($i = 1, 2, \dots, 5$) represent the controllable and uncontrollable parameters used for each predictive model, respectively. $T(t+d)$ and $P(t+d)$ are the temperature and static pressure of the supply air, respectively, at time stamp $(t+d)$ after passing through the AHU system. S refers to the constraints imposed by each parameter.

3.3. Model Development and Validation

3.3.1. Experiment Description and Data Preprocessing

The HVAC system discussed in this paper is operated by the Energy Resource Station (ERS) of the Iowa Energy Center in Ankeny, Iowa. The ERS is equipped with two identical air-handling units, each with identical, dedicated chillers. One air handling unit supplies four test rooms designated as the “A” rooms, and the other unit serves the four test rooms designated as the “B” rooms. In this research, the experiment setups for the four rooms are the same, and thus the system is regarded as one AHU serving a single zone. The designed total cooling capacity of the AHU is 122,100 BTU/H. The designed total supply air flow is 3200 CFM. The maximum supply fan static pressure is 3.2 in. WG and the supply fan speed is 1834 RPM. Sensors have

been installed to collect over 300 parameters for the AHU, heating and chilling plants, and various testing zones. The experiment was conducted from 12:00 A.M. on June 22, 2011, to 23:59 P.M. on July 5, 2011. The sampling time interval for the original data set was one minute. The 1-min data were averaged over 15-minute intervals (15-min data) for model training and testing. The transformed dataset included 1344 observations. This dataset was partitioned into training (85%) and test (15%) sets. The training set was used for selecting the desired features, selecting the algorithm to be used, and training the model. The test set was used to assess the predictive accuracy of the model. The datasets used for our research are described in Table 3.1.

Table 3.1 Description of the datasets

Data Set	Description	Number of Observations
1	Model training: 85% of the preprocessed data	1142
2	Model test: the remaining 15% of the data	202

3.3.2. Parameter Selection

The selection of parameters is an important step in data mining. It allows the removal of parameters that make insignificant contributions to the ability of the models to provide accurate predictions. The appropriate selection of parameters usually improves the scalability and accuracy of the resulting models, as well as the ability of users to understand and interpret the results [65].

Numerous algorithms for selecting parameters have been proposed in the literature. Wrapper algorithms [66] and boosting-tree algorithms [67-69] are commonly applied to reduce the dimensionality of the parameter space. Wrapper approaches use an introduction algorithm to search the space of all possible parameters and evaluate each subset of parameters. Models are built and their prediction performances are computed as regression scores to quantify the relevance of those subsets. Greedy forward-selection algorithms are frequently used as

introduction algorithms. They progressively integrate new parameters, thereby optimizing the regression score. The Wrapper approach is time consuming when the introduction algorithm is too complex.

The boosting-tree algorithm computes a sequence of trees in which each successive tree is built for the prediction residuals of the preceding tree [70]. At each step of the boosting algorithm, the data are partitioned into two samples at every split node. The best partitioning is determined, and the regression errors are computed. Then, the successive tree is fitted to reduce the error. In the process of generating successive trees, the statistical importance of each parameter at each split of every tree is accumulated and normalized. Predictors with a higher-importance rank indicate a larger contribution to the predicted output.

In this chapter, the input parameters are the parameters that impact the operation of the system, including controllable parameters, such as temperature of the chilled water, and uncontrollable parameters, such as the temperature of the outside air. The outputs of the AHU system are the required quality of the air (supply air temperature, humidity, and CO₂ concentration), the static pressure of supply air, and the flow rate of the supply air. The levels of energy consumption of different AHU components are considered as outputs since they are indicative of the performance of the AHU system. The parameters considered for this research are summarized in Table 3.2.

The properties of the pump and the fan are represented by Eqs. (3.3) and (4) [71], which suggest that variations of the pump/fan speed impact the water/air flow rate and the efficiency of the variable-frequency driver (VFD) and, ultimately, the energy consumption. Thus, the energy consumptions of the fan and the pump are modeled using the pump/fan VFD speed and the water/air flow rate as inputs.

The power of the constant-speed pump or fan is provided in Eq. (3.3):

$$N_{p/f} = \frac{\gamma_{w/a} H_{p/f} G_{p/f}}{\eta_{trans} \eta_{motor,p/f}} \quad (3.3)$$

Table 3.2 Parameters selected based on the input-output analysis of the AHU system

Type	Parameter Name	Description	Unit
Input	SAT-SPT	AHU supply air temperature set point (constant at 55 °F)	°F
	SASP-SPT	Supply air duct static pressure set point (constant at 1.4 in. WG)	In. WG
	ACCA-EWT	Chiller entering water temperature	°F
	CHWC-EAT	Chilled water coil entering air temperature	°F
	CHWC-EWT	Chilled water coil entering water (supply) temperature	°F
	CHWC-VLV	Chilled water coil valve position	%Open
	CHWPASPD	Pump % speed (constant at 75%)	%Speed
	CHWPAGPM	Chilled water pump water flow rate	GPM
	SA-SPD	Supply fan VFD speed	%Speed
	RA-SPD	Return fan VFD speed	%Speed
	RF%SFSPD	Return fan % of supply fan speed (constant at 90%)	%
	OA-TEMP	Outside air temperature	°F
	OA-HUMD	Outside air humidity	%RH
	IR-RADIA	Infrared radiation	B/HFt ²
	SOL-HORZ	Solar normal flux	B/HFt ²
	SOL-BEAM	Solar beam	B/HFt ²
	Output	SA-CFM	Supply air flow rate
SA-HUMD		Supply air humidity	%RH
SA-TEMP		AHU supply air temperature	°F
SA-SP		AHU Supply air duct static pressure	In. WG
CHILLER-ENERGY		Energy consumption of the chiller	KJ
FANS-ENERGY		Energy consumption of supply and return fans	KJ
PUMP-ENERGY		Energy consumption of the pump	KJ

The power of the variable-speed pump or fan is provided in Eq. (3.4):

$$N_{p/f, var} = \frac{\gamma_{w/a} H_{p/f} G_{p/f}}{\eta_{trans} \eta_{motor, p/f}(n) \eta_{vfd}(n)} \quad (3.4)$$

where N is the power, H is the head of the pump/fan, G is the mass flow rate, γ is the specific weight, η is the efficiency, n is speed of the motor, and p/f refers to the pump or fan.

In our experiment, the temperature and static pressure of the supply air were maintained constant at 55 °F (12.8 °C) and 1.4 in. WG (0.35 kPa), respectively. The speed of the return fan speed was set at 90%, and the speed of the chilled water pump was fixed at 75%. The models for the pump and fans were developed as follows:

1. The fan speed was the input of the return fan model.

2. The energy consumption of the pump was predicted by using the chilled water supply water flow rate.

3. The flow rates of the supply and return air also were introduced to the models of the supply and return fans.

The boosting-tree algorithm was used to select additional parameters for modeling the energy consumption of the chiller and the output of the temperature and the static pressure of the supply air. The time delay is also considered. Since the time interval of the data was 15 minutes, considering parameter values at the previous state of the system was enough to eliminate the system delay. Table 3.3 -3.6 list the parameters for developing the predictive models.

Table 3.3 Parameters selected for developing models of the energy consumption of the chiller, temperature of the supply air, and static pressure of the supply air

Parameter	Point Name	Description
$x_1(t+1)$	CHWPAGPM($t + 1$)	Chilled water flow rate at time stamp $t + 1$
$x_2(t+1)$	SF-SPD($t + 1$)	Supply Fan VFD speed at time stamp $t + 1$
$x_3(t+1)$	CHWC-VLV($t + 1$)	Chilled water coil valve position at time stamp $t + 1$
$x_4(t+1)$	CHWC-EWT($t + 1$)	Chilled water coil supply temperature at time stamp $t + 1$
$x_4(t)$	CHWC-EWT	Chilled water coil supply temperature at time stamp t
$u_1(t)$	ACCA-EWT	Chiller entering water temperature at time stamp t
$u_2(t)$	CHWC-EAT	Chilled water coil entering air temperature at time stamp t
$u_3(t)$	OA-TEMP	Outside air temperature at time stamp t

Table 3.4 Parameters selected for developing the energy consumption model of the pump

Parameter	Point Name	Description
$x_1(t+1)$	CHWPAGPM($t + 1$)	Chilled water flow rate at time stamp $t + 1$
$x_1(t)$	CHWPAGPM	Chilled water flow rate at time stamp t

Table 3.5 Parameters selected for developing the energy consumption model of the return fan

Parameter	Point Name	Description
$x_2(t+1)$	SF-SPD($t + 1$)	Supply fan VFD speed at time stamp $t + 1$
$x_2(t)$	SF-SPD	Supply fan VFD speed at time stamp t
$u_4(t)$	RA-CFM	Return air flow rate at time stamp t

Table 3.6 Parameters selected for developing the energy consumption model of the supply fan

Parameter	Point Name	Description
$x_2(t+1)$	SF-SPD($t + 1$)	Supply Fan VFD Speed at time stamp $t + 1$
$x_2(t)$	SF-SPD	Supply Fan VFD Speed at time stamp t
$u_5(t)$	SA-CFM	supply air flow rate at time stamp t

3.3.3 Energy consumption modeling and validation

Four energy consumption models for different components were established by data-mining algorithms. Since the chiller accounts for most of the energy consumed, the accuracy of the model used for estimating the energy consumption of the chiller will have a significant effect on the optimization of the overall system. The model of energy consumption by the chiller is shown in Eq. (3.5):

$$y_1(t+1) = f(x_1(t+1), x_2(t+1), x_3(t+1), x_4(t+1), x_4(t), u_1(t), u_2(t), u_3(t)) \quad (3.5)$$

where the input parameters are described in Table 3.3. In Eq. (5), t is the current time, and $t + 1$ is the next time period. Function $f(\cdot)$ describes the energy consumption model learned by the data mining algorithms.

In this research, the following data-mining algorithms have been considered: the multi-layer perceptron (MLP) ensemble algorithm, boosting-tree (regression) algorithm, the random-forest algorithm [72], the support vector machine [73], and the classification and regression tree (CART) algorithm [74]. To evaluate performance of the predictive models, four metrics, i.e., (3.6)

- (3.9) in the following, were used: the mean absolute error (*MAE*), the standard deviation of absolute error (*Sd_AE*), the mean absolute percentage error (*MAPE*), and the standard deviation of absolute percentage error (*Sd_PE*).

$$MAE = \frac{1}{n} \sum_{i=1}^n |y_i - \hat{y}_i| \quad (3.6)$$

$$Sd_AE = \sqrt{\frac{\sum_{i=1}^n (|y_i - \hat{y}_i| - MAE)^2}{n-1}} \quad (3.7)$$

$$MAPE = \frac{1}{n} \sum_{i=1}^n \left| \frac{y_i - \hat{y}_i}{y_i} \right| \times 100\% \quad (3.8)$$

$$Sd_APE = \sqrt{\frac{\sum_{i=1}^n \left(\left| \frac{y_i - \hat{y}_i}{y_i} \right| - MAPE \right)^2}{n-1}} \quad (3.9)$$

where y_i is the observed value, \hat{y}_i is the predicted value, and n is the size of the training or test data set.

Table 3.7 summarizes the performance of the models developed by the data-mining algorithms. The model derived by the MLP ensemble algorithm outperformed all other models in terms of the accuracy and stability. The corresponding values of *MAPE* (0.0599) and *Sd_PE* (0.0521) were the lowest obtained with any of the algorithms. Thus, the MLP ensemble was selected as the candidate algorithm to construct other predictive models.

Table 3.7 Accuracy of the prediction of energy consumption by the chiller provided by different data-mining algorithms

Algorithm	MAE	Sd_AE	MAPE	Sd_PE
MLP ensemble	160.971	7.772	0.060	0.052
Boosting-tree	231.665	13.788	0.080	0.073
Random forest	231.063	3.676	0.074	0.066
Support vector machine	244.425	11.815	0.085	0.067
CART	283.984	18.501	0.092	0.082

The energy consumption models for the pump, the supply fan, and the return fan are expressed as Eqs. (3.10), (3.11), and (3.12).

$$y_2(t+1) = f(x_1(t+1), x_1(t)) \quad (3.10)$$

$$y_3(t+1) = f(x_2(t+1), x_2(t), u_4(t)) \quad (3.11)$$

$$y_4(t+1) = f(x_2(t+1), x_2(t), u_5(t)) \quad (3.12)$$

To validate the accuracy of the models, 200 data points were considered. The comparison between the observed and the predicted values for energy consumption for the different models is provided in Figures 3.3-3.6. Table 3.8 shows the performance of the six models.

Table 3.8 Prediction accuracy of different models by the MLP ensemble algorithm

Model	Data set	MAE	Sd_AE	MAPE	Sd_PE
Chiller energy	Training	160.971	7.772	0.060	0.052
	Test	209.792	11.457	0.059	0.046
Supply fan energy	Training	7.613	0.543	0.015	0.017
	Test	9.914	0.940	0.017	0.026
Return fan energy	Training	1.839	0.149	0.009	0.012
	Test	2.455	0.164	0.011	0.013
Pump energy	Training	0.821	0.044	0.002	0.002
	Test	0.521	0.024	0.001	0.000
Supply air temperature	Training	0.046	0.044	0.001	0.001
	Test	0.076	0.080	0.001	0.001
Supply air static pressure	Training	0.007	0.006	0.005	0.004
	Test	0.006	0.007	0.005	0.005

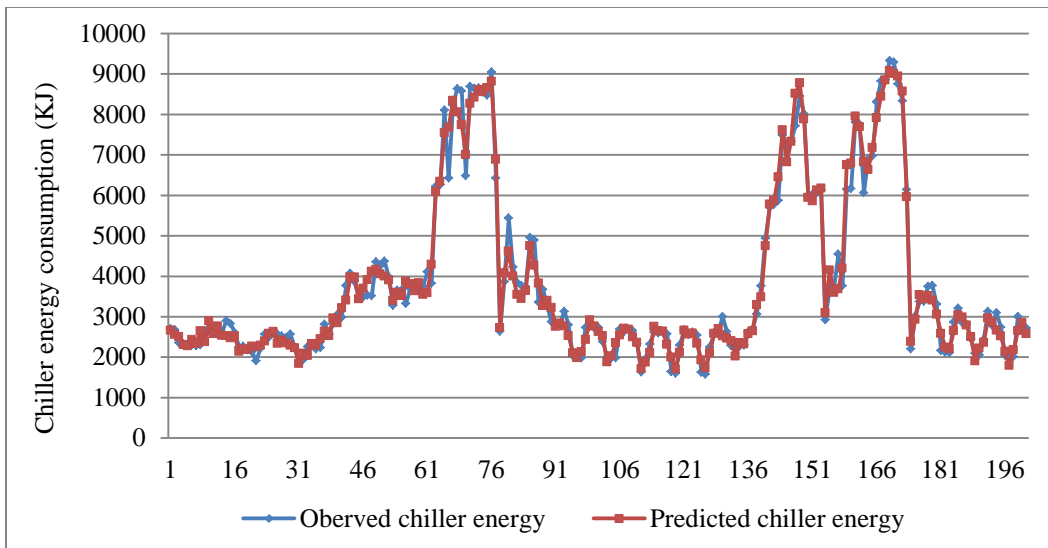


Figure 3.3 The observed and predicted chiller energy consumption by the MLP

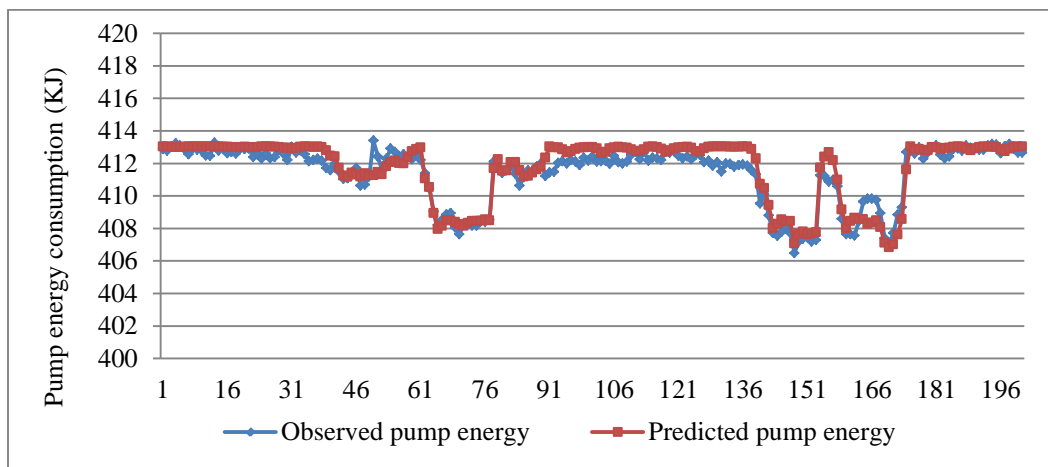


Figure 3.4 The observed and predicted pump energy consumption by the MLP

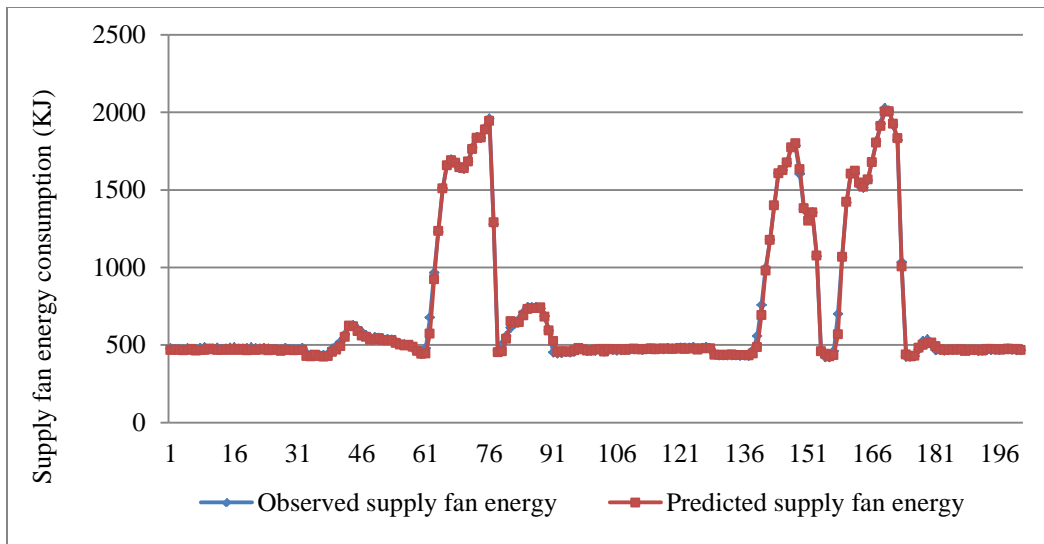


Figure 3.5 The observed and predicted supply fan energy consumption by the MLP

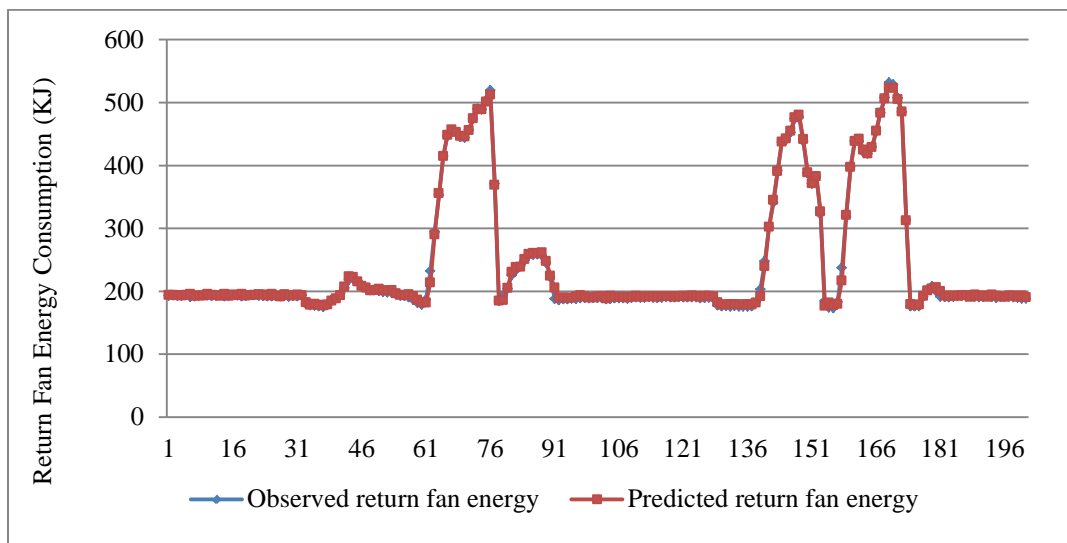


Figure 3.6 The observed and predicted return fan energy consumption by the MLP

3.3.4 Modeling and Validation of the Temperature and Static Pressure of the Supply Air

In the experiment reported in this paper, the set points of the temperature and static pressure of the supply air were kept constant at 55 °F (12.8 °C) and 1.4 in. WG (0.35 kPa), respectively. Some differences between the desired and the set values were observed in the experiment that involved the industrial-grade system. The predictive models of the temperature and static pressure of the supply air, shown in (3.13) and (3.14), respectively, were used to make sure the two parameters were in the acceptable range, given the optimal control settings. The inputs of the models, described in Table 3.3, were the same as those used in the model of the energy consumption of the chiller.

$$y_{temp}(t+1) = f(x_1(t+1), x_2(t+1), x_3(t+1), x_4(t+1), x_4(t), u_1(t), u_2(t), u_3(t)) \quad (3.13)$$

$$y_{pressure}(t+1) = f(x_1(t+1), x_2(t+1), x_3(t+1), x_4(t+1), x_4(t), u_1(t), u_2(t), u_3(t)) \quad (3.14)$$

Validation with 200 data points from the test set showed that the predicted values follow are in good agreement with the observed values (Figures 3.7 and 3.8). The statistics of the results are summarized in Table 3.8.

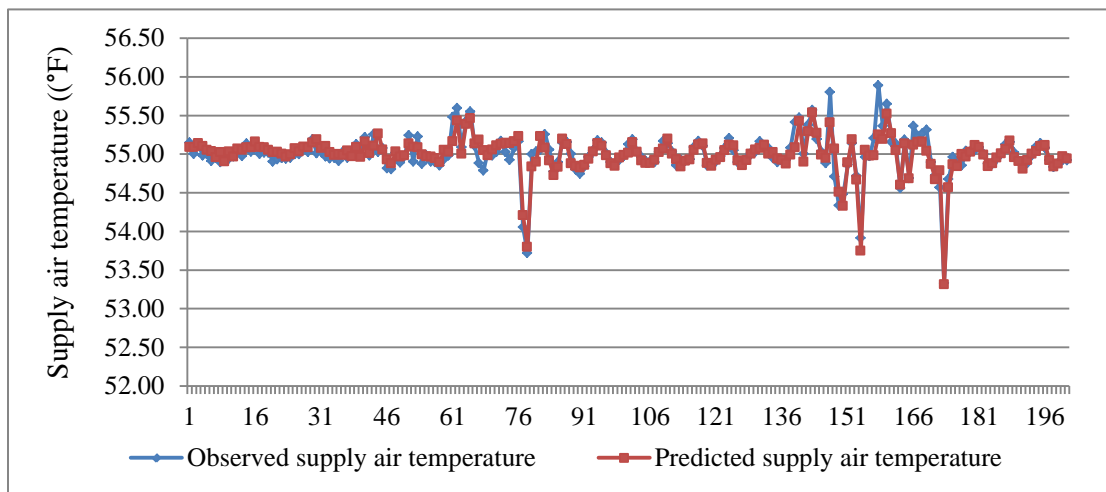


Figure 3.7 Comparison of the observed and predicted temperature of the supply air

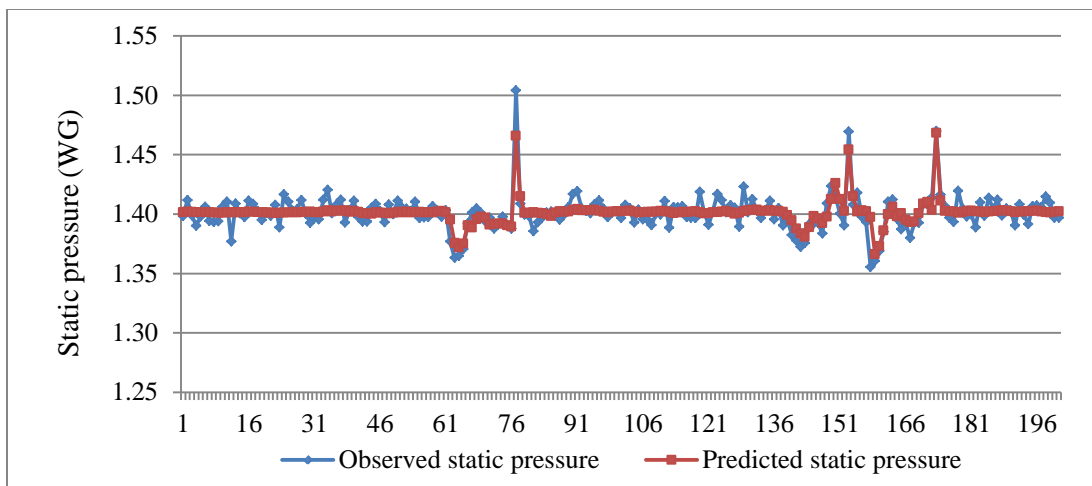


Figure 3.8 Comparison of observed and predicted static pressure of the supply air

3.4. Optimization of the Energy Consumption of the AHU System

In this section, we describe the development of an optimization model for use in for minimizing the overall energy consumption of the AHU. Due to the nonlinearity of the model, a novel, dynamic-penalty electromagnetism-like algorithm (DPEM) was used. The computational results show that a substantial amount of energy can be saved by using the settings of the controllable parameters computed by the DPEM algorithm.

3.4.1. Overall optimization model

The aim of the research reported in this paper was to minimize the overall energy consumption of the AHU while maintaining the predefined values of the temperature and static pressure of the supply air. Since the temperature and static pressure of the supply air change in response to the corresponding set points (constant at 55 °F (12.8 °C) and 1.4 in. WG (0.35 kPa, respectively), small deviations of the two parameters are captured as constraints. The upper and lower bounds of the controllable parameters are identified as constraints based on the ranges learned by the MLP ensemble algorithm. The constraints of the optimization model are as follows: (1) The acceptable ranges for the temperature and static pressure of the supply air are 53 to 56 °F (11.7 to 13.3 °C) and 1.3 to 1.5 in. WG (0.32 to 0.37 kPa); (2) The flow rate of the

chilled water provided by the pump can vary between 20 and 22 GPM; (3) The speed of the supply fan VFD can range from 58% to 70% of the design speed (1834 RPM); (4) The extent to which the valve position on the chilled water coil can open can vary from 17% to 67%; and (5) The temperature of the chilled water supply is controlled between 38 and 44 °F (3.3 °C and 6.7 °C).

The optimization model is presented in (3.15). An approach for solving model (15) is presented in the next section.

$$\min_{(x_1, x_2, x_3, x_4)} E_{total} = y_1 + y_2 + y_3 + y_4$$

subject to:

$$\begin{aligned} y_1(t+1) &= f(x_1(t+1), x_2(t+1), x_3(t+1), x_4(t+1), x_4(t), u_1(t), u_2(t), u_3(t)) \\ y_2(t+1) &= f(x_1(t+1), x_1(t)) \\ y_3(t+1) &= f(x_2(t+1), x_2(t), u_4(t)) \\ y_4(t+1) &= f(x_2(t+1), x_2(t), u_5(t)) \\ y_{temp}(t+1) &= f(x_1(t+1), x_2(t+1), x_3(t+1), x_4(t+1), x_4(t), u_1(t), u_2(t), u_3(t)) \\ y_{pressure}(t+1) &= f(x_1(t+1), x_2(t+1), x_3(t+1), x_4(t+1), x_4(t), u_1(t), u_2(t), u_3(t)) \\ 53 &\leq y_{temp} \leq 56 \\ 1.3 &\leq y_{pressure} \leq 1.5 \\ 20 &\leq x_1 \leq 22 \\ 58 &\leq x_2 \leq 70 \\ 17 &\leq x_3 \leq 67 \\ 38 &\leq x_4 \leq 44 \end{aligned} \tag{3.15}$$

3.4.2. Dynamic penalty-based electromagnetism-like algorithm

In the last two decades, significant progress has been made in the development and application of approximation optimization techniques, also known as intelligent algorithms. In this paper, a novel, dynamic penalty-based electromagnetism-like algorithm (DPEM) is proposed to optimize model (3.15).

The electromagnetism-like algorithm (EM) was introduced by Birbil and Fang [58]. The literature has shown that the EM algorithm outperforms many traditional algorithms in solving optimization problems [59], neural network training [60], production scheduling [61], and other

areas [62, 63]. The efficiency attribute of the EM algorithm has led to its application in optimization of HVAC systems.

The EM algorithm utilizes an attraction-repulsion mechanism to move sample points towards optimality. The algorithm starts with sample points (a population) selected from a feasible space and continues its iterative process until a stopping condition (e.g., the maximum number of iterations) is met.

$$q^i = \exp\left(\frac{-n(f(x^i) - f(x^{best}))}{\sum_{j=1}^m (f(x^j) - f(x^{best}))}\right), i = 1, 2, \dots, m \quad (3.16)$$

$$F_j^i = \begin{cases} (x^j - x^i) \frac{q^i q^j}{\|x^j - x^i\|} & \text{if } f(x^j) < f(x^i) \\ (x^i - x^j) \frac{q^i q^j}{\|x^j - x^i\|} & \text{if } f(x^j) \geq f(x^i) \end{cases}, j \neq i, \forall i \quad (3.17)$$

There are two steps at every iteration of the algorithm. In the first step, each point is assigned a charge related to the value of the objective function according to (3.16). Points that improve the values of the objective function are assigned higher charges. A charge determines the magnitude of attraction of the point relative to the other points in the population. The better the objective function value, the higher the magnitude of attraction. The force exerted on a point via other points is computed according to (3.17), and the total force vector is obtained by adding these attractive–repulsive forces (3.18). Then, each point moves to a new location in the direction of the total force vector (3.19). In Eqs. (3.16) - (3.19), m is the population size; n is the dimension; and k is the dimension index of the model.

$$F^i = \sum_{j \neq i}^m F_j^i, i = 1, 2, \dots, m \quad (3.18)$$

$$x_k^i = \begin{cases} x_k^i + \lambda \frac{F_k^i}{\|F^i\|} (u_k - x_k^i) & \text{if } F_k^i > 0 \\ x_k^i + \lambda \frac{F_k^i}{\|F^i\|} (x_k^i - l_k) & \text{if } F_k^i \leq 0 \end{cases} \quad (3.19)$$

In the second step, a local search procedure is incorporated to improve the accuracy of the solution. A local refinement is applied, coordinate by coordinate, to the current best point in the population. Using parameter δ , the maximum feasible step length $s_{\max} = \delta(\max_k (u_k - l_k))$ is computed. Then, for each coordinate, a step length between 0 and 1 is generated randomly, and a new point is computed along that direction. If an improvement of the objective function is observed within the local search iterations (*LSITER*), the current best point is replaced, and the search continues with the next coordinate.

To simplify the solution procedure of the non-linear, constrained model (3.15) presented in Section 4.1, a dynamic-penalty approach is employed [75]. The constraints of the temperature y_{temp} and static pressure $y_{pressure}$ of the supply air (model (3.15)) are transformed into penalty functions, as shown in Eqs. (3.20) and (3.21). The values of the two penalty functions are normalized to [0, 1] to eliminate their relative importance. The final objective function $f(x)$ is expressed as Eq. (3.21) after the penalty functions have been incorporated.

$$v_1(x) = \left\{ \max\{0, 53 - y_{temp}(t+1)\} + \max\{0, y_{temp}(t+1) - 56\} \right\} / (56 - 53) \quad (3.20)$$

$$v_2(x) = \left\{ \max\{0, 1.3 - y_{pressure}(t+1)\} + \max\{0, y_{pressure}(t+1) - 1.5\} \right\} / (1.5 - 1.3) \quad (3.21)$$

$$f(x) = E_{total} + (c \times gen)^\alpha \sum_{j=1}^2 v_j^\beta(x), \quad (3.22)$$

where c , α , and β are control parameters, gen is the iteration number of the DPEM algorithm, x is the solution vector that represents the values of the four controllable parameters at time stamp $t + 1$.

In the early stages of the DPEM, the penalty is small, which leads to the exploration of both the feasible and the infeasible regions. As the solution evolves, the penalty increases to guide the population toward a feasible region. In this research, a point in the population has four dimensions, each representing one of the four controllable parameters. Each dimension of the particles is initialized uniformly within the upper and lower bounds of the corresponding control parameter. Other uncontrollable inputs are read from the data set.

The steps of DPEM are shown below:

Step 0: Define EM parameters, population size m , maximum number of iterations $MAXITER$, local search parameter δ , and local search iterations $LSITER$. Initialize penalty control parameters c , α , and β .

Step 1: Initialize solution points with uniform distribution within the upper and lower bounds of the controllable parameters, and Set $i = 1$.

Step 2: Evaluate the points according to the objective function and compare them to select the current best point x^{best} .

Step 3: If iteration number is greater than $MAXITER$, stop; otherwise, go to Step 4.

Step 4: Compute the charges of all points from Eq. (3.16).

Step 5: Compute the forces of all points and select their directions according to Eq. (3.17).

Step 6: Compute the total force vector for each point and move all points, except the current best point, according to Eqs. (3.18) and (3.19).

Step 7: Evaluate the points and update the current best point x^{best} .

Step 8: Perform a local search about each coordinate of the current best point $LSITER$ times.

Step 9: Set $i = i + 1$ and go to Step 3.

3.4. Computational Results and Discussion

To demonstrate the optimization process, 200 test data points were used for simulation. The DPEM algorithm was applied to solve model (3.15) for each of the 200 cases. The parameters in the algorithm were set as $\alpha = 2$, $\beta = 1$, $m = 50$, $MAXITER = 100$, $\delta = 1$, and $LSITER = 10$. The value of the penalty parameter, $c = 10$, was due to the small values of the two penalty functions (normalized between 0 and 1). It should also be noted that the temperature and flow rate of the chilled water supply were adjusted in increments of 0.1°F and 0.1 GPM, respectively, in the local search process. The simulation results for all 200 cases are shown in Figs.3. 9 – 3.15. Fig. 3.9 shows the total energy consumption before and after optimization. Model (3.15) reduced the total energy consumption of the AHU system by almost 23% (Table

3.9). Figure 3.10 demonstrates that, in one case, the temperature of the supply air was less than 53 °F (11.7 °C), i.e., it was out of range, while the static pressure of the supply air remained in the required range for all cases (Figure 3.11). The optimal settings of the four controllable parameters, i.e., the flow rate of the chilled water, the speed of the supply fan, the position of VLV on the chilled water cooling coil, and the temperature of the chilled water, are illustrated in Figures 3.12 – 3.15 for all 200 simulation cases. In most cases, the flow rate of the chilled water and the speed of the supply fan were set higher than the original settings. The position of the chilled water cooling coil VLV had smaller values and the temperature of the chilled water supply changed within the controllable ranges. Table 3.9 summarizes the energy consumption results before and after optimization. Greater flow rates of chilled water and fan speeds allowed more efficient heat transfer between the air and the chilled water in the cooling coil. Small values of the VLV position decreased the amount of water supplied by the chiller, ultimately reducing the energy consumption of the chiller. The energy consumed by the pump and fans increased due to the high flow rate of water and the greater speed of the supply fan. The optimized control settings reduced the energy consumed by the chiller significantly, while the energy consumed by the fans and pumps was increased by a slight amount, thus decreasing the overall energy consumption of the AHU. The optimized control has resulted in energy savings while increasing variability of the controllable parameters. This is due to imperfect selection of the data sampling interval. This variability can be reduced by performing additional experiments.

Table 3.9 Energy optimization results for different components of the AHU system

	Chiller	Pump	Supply Fan	Return Fan	Total Energy
Observed (KJ)	606102.7	82629.7	96564.5	38397.4	823694.3
Optimized (KJ)	400715.5	86207.6	106426.9	41930.9	635280.9
Reduced (KJ)	205387.2	-3577.9	-9862.4	-3533.5	188413.4
Reduced Rate (%)	33.9	-4.3	-10.2	-9.2	22.9

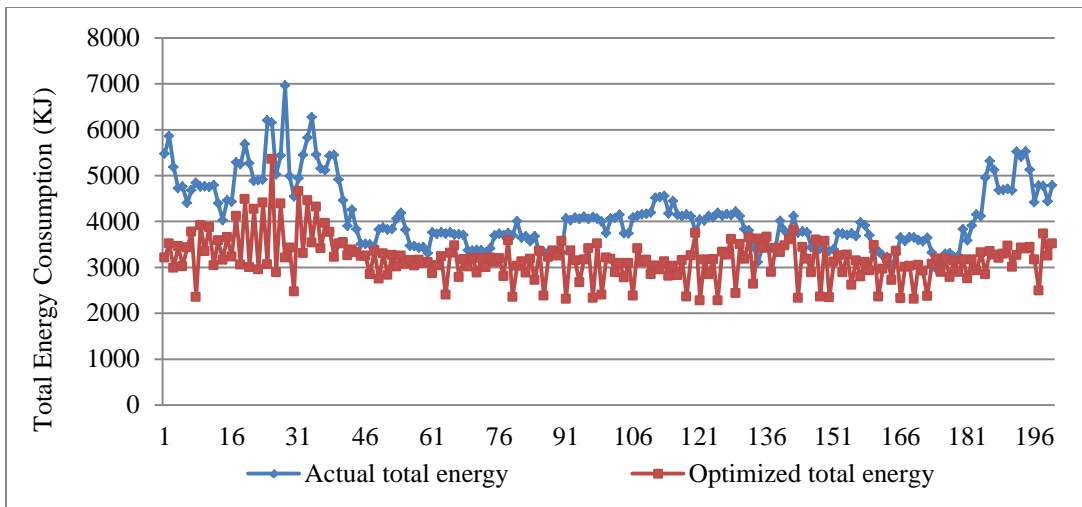


Figure 3.9 Total energy consumption before and after optimization

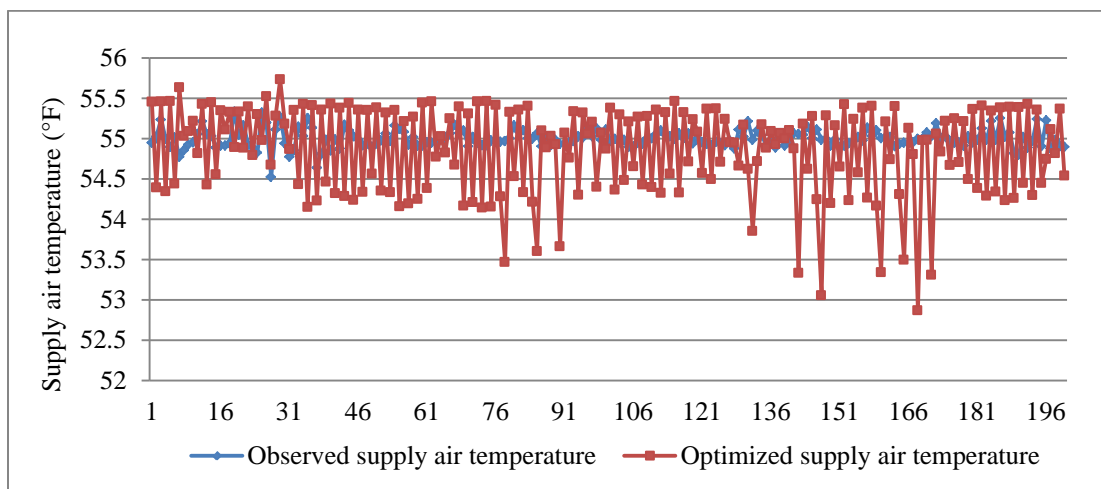


Figure 3.10 Temperature of the supply air before and after optimization

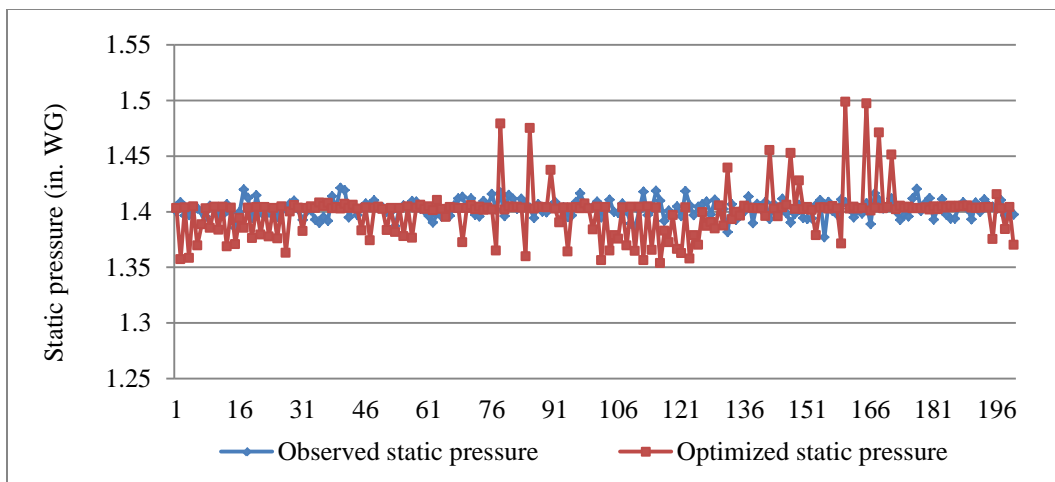


Figure 3.11 Static pressure of the supply air before and after optimization

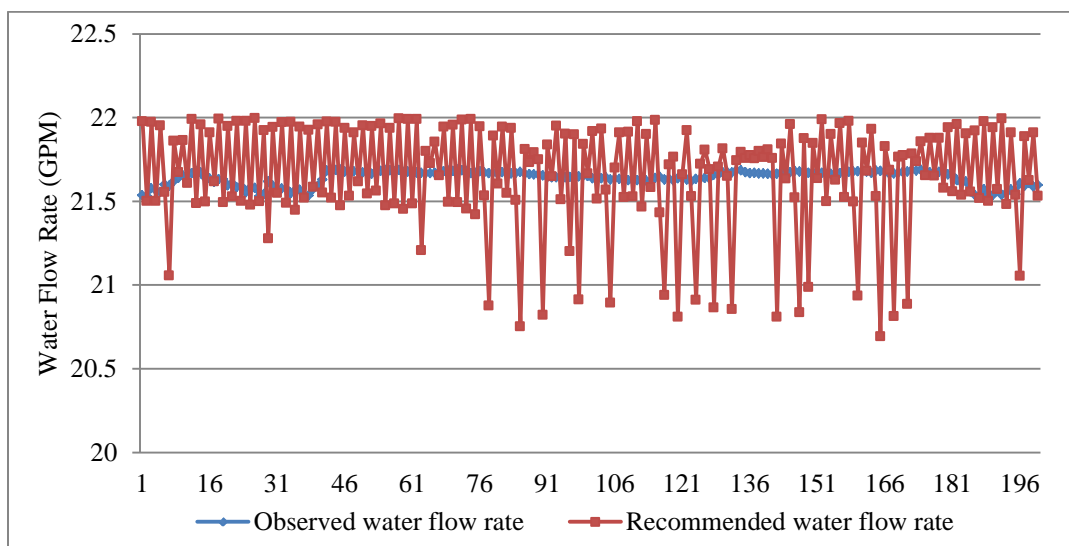


Figure 3.12 Observed and optimized water flow rates for the 200 cases

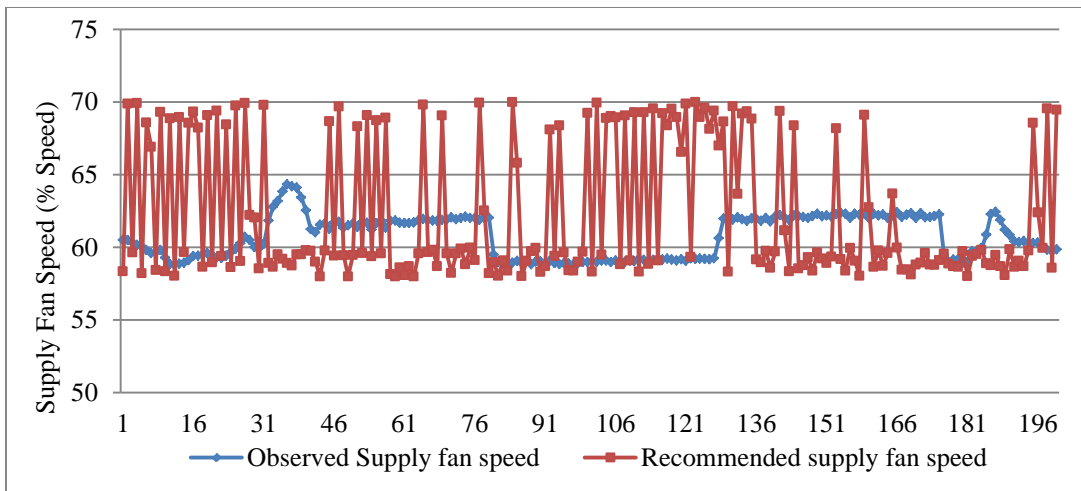


Figure 3.13 Observed and optimized supply fan speeds for the 200 cases

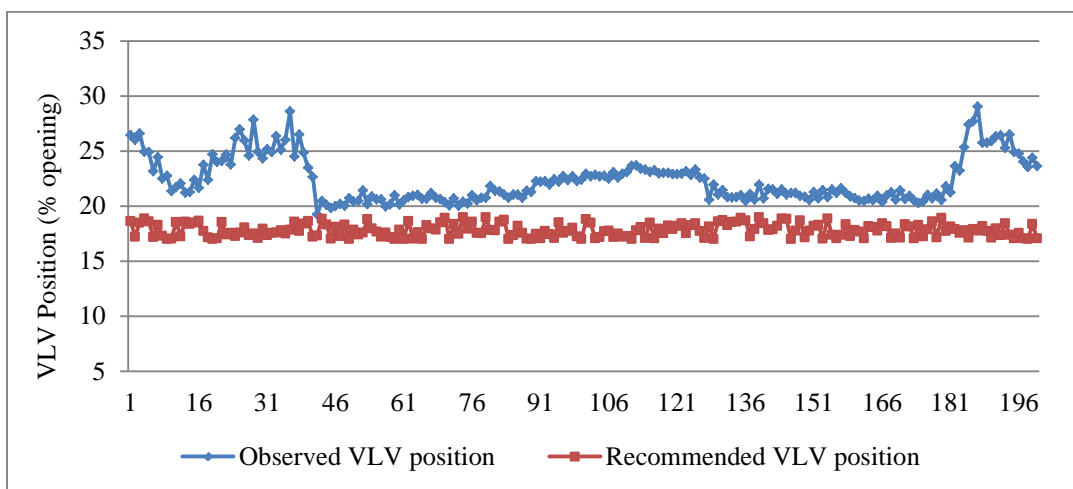


Figure 3.14 Observed and optimized chilled water cooling coil VLV position for the 200 cases

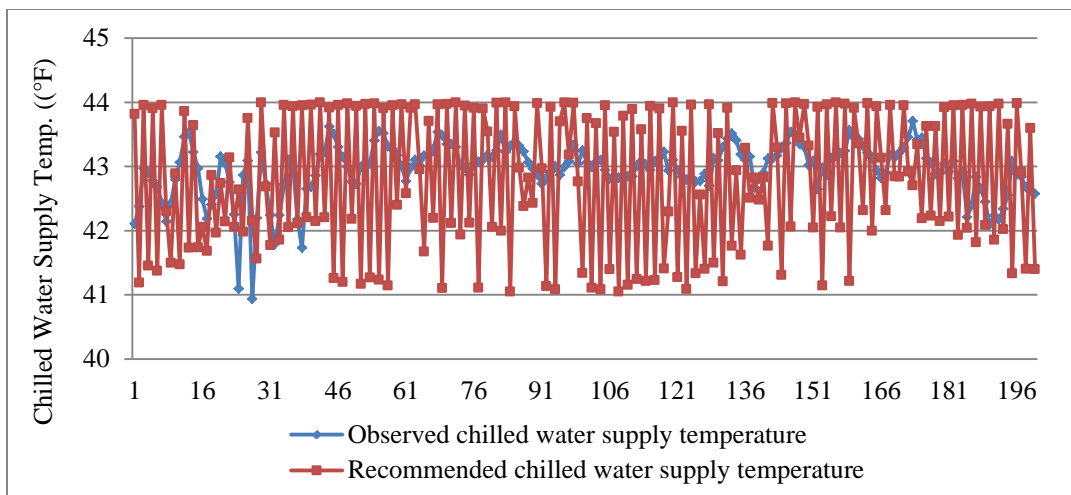


Figure 3.15 Observed and optimized chilled water supply temperatures for 200 cases

3.5. Summary

In this chapter, the energy consumed by an air handling unit was minimized by combining data-mining with computational intelligence. The multi-layer perceptron ensemble algorithm was applied to develop predictive models of the energy consumption the chiller, the pump, and the supply and return fans. To minimize the energy consumption while maintaining the temperature and static pressure of the supply air at predetermined levels, a non-linear, constrained optimization model was developed. A dynamic penalty function-based electromagnetism-like algorithm was proposed to solve the model. Computational results showed that the energy consumed by the chiller could be reduced significantly by slightly increasing the energy consumption of the pump and fans. The total energy consumption of the AHU system was reduced by almost 23%.

Future research involving optimization criteria is needed to accommodate different supply air requirements (e.g., humidity and CO₂ concentration). The research presented in the paper has focused on single zone modeling. Modeling different zones calls for new experiments and data which were not available in this research. The single-zone approach presented in this chapter is generalizable to a multi-zone optimization provided that the suitable data is available.

CHAPTER 4

MODEL-PREDICTIVE CONTROL OF A MULTI-ZONE HVAC SYSTEM

4.1. Introduction

In the research presented in Chapter 3, the HVAC system was regarded single AHU serving single zone. This assumption simplifies the relationship between the AHU and its terminal, and leads to a simple case of the HVAC system. However, cases in which one AHU serves several rooms to achieve thermal comfort for all rooms are more popular and widely seen in the real world. Thus, this research, aiming at further promoting the applicability and enhancing the validity of the HVAC research, is conducted to model the energy and thermal comfort of a multi-zone HVAC system and optimize the control strategy of the system with respect to the minimization of the energy consumption while maintain thermal comfort of all zones. The control strategy in a planning horizon involves the sequence settings of two setpoints, the supply air temperature setpoint and the supply air static pressure setpoint. The thermal comfort investigated in this research is solely measured by the temperature of each room.

A data-mining approach is applied to establish the total energy consumption model and temperature models corresponding to each zone. Afterwards, an overall optimization model with the objective of minimizing the total energy consumption is formulated. A new intelligent algorithm, called firefly algorithm, is introduced to solve the model and generate optimal settings of the two setpoints. The proposed approach has been validated with the computational experiments. Two experiments with different constraints on the controlled temperature deviations are used to demonstrate the proposed approach. 100 cases are computed in each experiment. In the first experiment, the controlled room temperature deviations are restricted within 1 °F ($\pm 0.5^\circ\text{F}$) compared with the room temperature generated from the original control strategy. In the second experiment, the deviations are set within 2°F ($\pm 1^\circ\text{F}$). Computational results show that more than 6% and 12% energy savings have been respectively observed.

4.2. System Description and Modeling

4.2.1 System description and data collection

A typical HVAC system includes an air handling unit (AHU) and one or several thermal zones. Figure 4.1 illustrates the schematic diagram of such an HVAC system. The supply air is at a specific temperature and flows at a specific rate to meet the heating or cooling load and ensure thermal comfort. Outdoor air mixes with the return air, and the mixed air passes through cooling coils, heating coils, and the supply fan. Chilled water in the cooling coils cools the mixed air, and hot water or steam in the heating coils heats the mixed air to maintain the desired temperature of the supply. The supply and return fans assist in moving the air for heat exchange as well as circulating it in the HVAC system at the required flow rate.

The HVAC system investigated in this research is operated by the ERS (Energy Resource Station) in Ankeny, Iowa. It is equipped with two identical air-handling units, each with identical, dedicated chillers. One air handling unit supplies four test rooms designated as the “A” rooms, and the other unit serves the four test rooms designated as the “B” rooms, shown as Figure 4.2. Each room as a thermal zone has a Viable-air-volume (VAV) box connected to the air handling unit. The VAV box could be adjusted by the thermostat to control the volume of the entering air and maintain the comfort of the room. To simulate the impact of people and thermal activities, the android systems and lighting in each room are used produce internal loads. In this research, we only take the AHU-A and its serving zones into account.

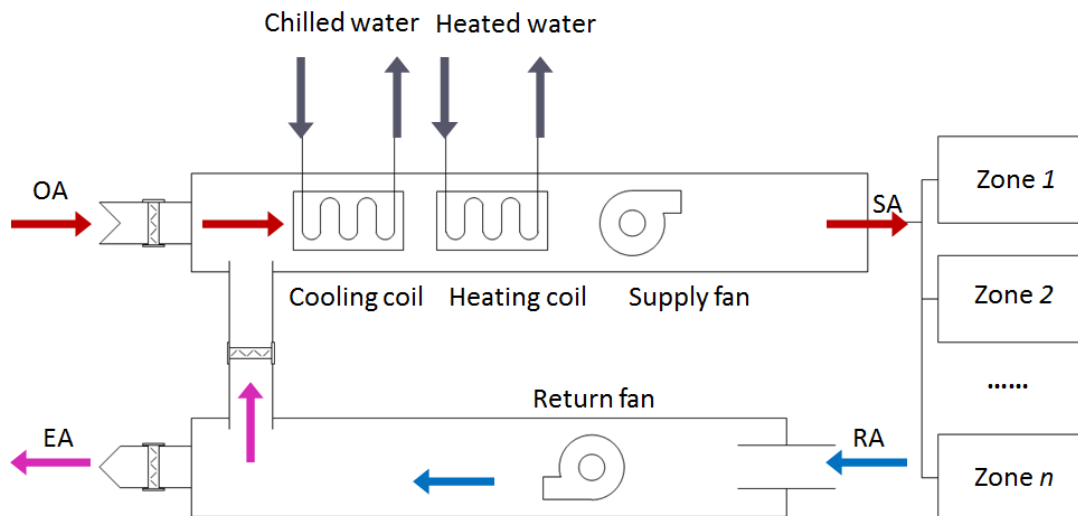


Figure 4.1 Schematic diagram of a typical HVAC system with multi-zones

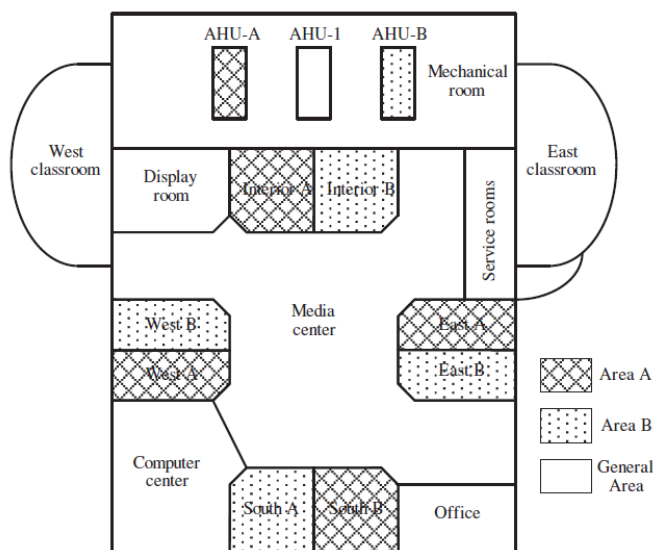


Figure 4.2 Plane view of ERS facility

The data for AHU-A was collected from 12:00 A.M. on February 15, 2011, to 23:59 P.M. on March 4, 2011. Over 300 parameters measuring the different the air handling unit, the chiller and heating plant, and the different test zones, as well as outside weather conditions are recorded every 1 minute. The sampling time interval is transformed into 30 minutes by averaging the 1-

min data. After preprocessing the data set, there are 911 data points in total. The first 85% data points are used for parameter selection and model training, while the remaining part is for the test procedure. In the recorded dataset, the supply air temperature setpoint varies from 55°F to 65 °F, the supply air static pressure changes from 0.5 In. WG to 1.8 In. WG. Since the experiment was conducted in heating session, the total energy consumed by the HVAC system includes several components, the chiller, the chilled water pump, the heating water boiler, the supply and return fans, and the loop A pump for circulating heating water. The energy consumption is measured by kW sine the time interval used for the sampling is the same, *i.e.* 30mins.

4.2.2 Predictive modeling

To build predictive data-mining models, proper parameter selection should be executed to decrease the data dimensions and reduce the information redundancy. Since that it's not easy to find relevant and significant parameters from the huge dataset, the process of parameter selection should always combines the domain knowledge obtained from understanding of the system and the insights gained by the efficient data-mining algorithms. The input parameters are those impact the operation of the system, including controllable parameters, the supply air temperature and the static pressure setpoints, and uncontrollable parameters such as the outside air temperature and the solar normal flux.

A boosted tree algorithm is applied to further select the more relevant parameters. Table 4.1 summarizes the final input parameters for the total energy consumption model. As for test rooms, the internal conditions of rooms should be taken into account. Parameters measuring the simulated loads are analyzed and relevant ones are added for the temperature model construction. Table 4.2-4.5 show the parameters for modeling the temperature of the four rooms. In these tables, the ranks and the importance values of parameters are computed by the boosted tree algorithm. It should be noted that the importance of the light levels on window #1 and #2 in the interior room are zero. This is because that in the recorded data set, the light levels on window #1

and #2 are zero all the time. Due to this fact, the temperature predictive model in the interior room doesn't include the two parameters. After identifying the input parameters and the output, the mathematical formulations for the five models could be expressed in the following Equations

$$E(t+1) = f(x_1(t+1), x_2(t+1), y_1(t), u_1(t), u_2(t), \dots, u_{10}(t), u_5(t-1), u_6(t-1), u_7(t-1), u_9(t-1))$$

$$T_{EA}(t+1) = f(x_1(t+1), x_2(t+1), u_1(t), u_2(t), \dots, u_9(t), v_{1,EA}(t) \dots, v_{7,EA}(t))$$

$$T_{IA}(t+1) = f(x_1(t+1), x_2(t+1), u_1(t), u_2(t), \dots, u_9(t), v_{1,IA}(t) \dots, v_{7,IA}(t))$$

$$T_{SA}(t+1) = f(x_1(t+1), x_2(t+1), u_1(t), u_2(t), \dots, u_9(t), v_{1,SA}(t) \dots, v_{7,SA}(t))$$

$$T_{WA}(t+1) = f(x_1(t+1), x_2(t+1), u_1(t), u_2(t), \dots, u_9(t), v_{1,WA}(t) \dots, v_{7,WA}(t))$$

where $E(t+1)$ is the total energy consumed by the HVAC system at time $t+1$, $T_{EA}(t+1)$, $T_{IA}(t+1)$, $T_{SA}(t+1)$, $T_{WA}(t+1)$, are respectively the room temperature in the east, interior, south, and west room at time $t+1$. $x_1(t+1)$ and $x_2(t+1)$ are the supply air static pressure setpoint and the supply air temperature setpoint values set for time $t+1$.

Table 4.1 Parameters selected for building total energy consumption model

Variable	Point Name	Rank	Importance	Description	Unit
$u_1(t)$	MA-TEMP	100	1.000000	Mixed air temperature	°F
$y_1(t)$	Total-WAT(t)	100	0.999407	Total energy consumption	KW
$u_2(t)$	SA-CFM	100	0.997013	Supply air flow rate	CFM
$u_3(t)$	CHWC-EAT	99	0.987172	Chilled water coil entering water temperature	°F
$u_4(t)$	HWC-DAT	99	0.987075	Heating water coiling departure air temperature	°F
$u_5(t)$	SF-SPD	80	0.798501	Supply fan VFD speed	% Speed
$u_8(t-1)$	SOL-HORZ(t-1)	79	0.793165	Solar normal flux	B/HFt2
$u_6(t)$	SOL-BEAM	78	0.776810	Solar beam	B/HFt2
$u_7(t)$	CHWC-VLV	75	0.751002	Chilled water coil valve position	%
$x_1(t+1)$	SA_SPSPT(t+1)	75	0.747956	Supply air static pressure setpoint	In. WG
$u_6(t-1)$	SOL-BEAM(t-1)	70	0.703182	Solar beam	B/HFt2
$u_8(t)$	SOL-HORZ	63	0.631291	Solar normal flux	B/HFt2
$u_9(t)$	ACCA-EWT	52	0.517922	Chiller entering water temperature	°F
$u_7(t-1)$	CHWC-VLV(t-1)	48	0.476723	Chilled water coil valve position	%Open

Table 4.1-continued

$u_{10}(t)$	OA-TEMP	45	0.451455	Outside air temperature	°F
$u_{11}(t)$	OA-HUMD	44	0.439442	Outside air humidity	%RH
$u_{10}(t-1)$	OA-TEMP(t-1)	43	0.430608	Outside air temperature	°F
$x_2(t+1)$	SAT_SPT(t+1)	43	0.427746	Supply air temperature setpoint	°F

Table 4.2 Parameters selected for building temperature model in East Room (Temp-EA)

Variable	Point Name	Rank	Importance	Description	Unit
$u_2(t)$	SA-CFM	100	1.000000	Supply air flow rate	CFM
$u_1(t)$	MA-TEMP	98	0.977668	Mixed air temperature	°F
$u_3(t)$	CHWC-EAT	94	0.935126	Chilled water coil entering water temperature	°F
$u_4(t)$	HWC-DAT	93	0.934324	Heating water coiling departure air temperature	°F
$v_{1,EA}(t)$	VAVHCGPM-EA	90	0.901850	VAV heating coil flow rate	GPM
$v_{2,EA}(t)$	VAV-DMPR-EA	81	0.805132	VAV damper position	%Open
$v_{3,EA}(t)$	VAV-DP-EA	79	0.791317	Velocity pressure differential	In. WG
$v_{4,EA}(t)$	RA-DMPR-EA	77	0.765095	Recirculated air damper	%Closed
$u_8(t)$	SOL-HORZ	74	0.743840	Solar normal flux	B/HFt2
$v_{5,EA}(t)$	RM-LITE2-EA	73	0.726915	Light level on window #2	FtC
$v_{6,EA}(t)$	RM-LITE1-EA	72	0.718760	Light level on window #1	FtC
$u_6(t)$	SOL-BEAM	71	0.714542	Solar beam	B/HFt2
$u_7(t)$	CHWC-VLV	71	0.713521	Chilled water coil valve position	%Open
$v_{7,EA}(t)$	LIGHTLVL-EA	70	0.695356	Light level from ceiling	FtC
$x_2(t+1)$	SAT_SPT(t+1)	69	0.687735	Supply air temperature setpoint	°F
$u_{10}(t)$	OA-TEMP	67	0.669883	Outside air temperature	°F
$u_5(t)$	SF-SPD	63	0.634715	Supply fan VFD speed	% Speed
$x_1(t+1)$	SA_SPSPT(t+1)	57	0.573135	Supply air static pressure setpoint	In. WG

Table 4.3 Parameters selected for building temperature model in Interior Room (Temp-IA)

Variable	Point Name	Rank	Importance	Description	Unit
$u_1(t)$	MA-TEMP	100	1.000000	Mixed air temperature	°F
$u_3(t)$	CHWC-EAT	97	0.966032	Chilled water coil entering water temperature	°F
$u_4(t)$	HWC-DAT	96	0.961214	Heating water coiling departure air temperature	°F
$v_{3,IA}(t)$	VAV-DP-IA	87	0.870300	Velocity pressure differential	In. WG
$u_2(t)$	SA-CFM	81	0.807753	Supply air flow rate	CFM
$v_{7,IA}(t)$	LIGHTLVL-IA	77	0.773773	Light level from ceiling	FtC
$x_2(t+1)$	SAT_SPT(t+1)	76	0.757145	Supply air temperature setpoint	°F
$v_{2,IA}(t)$	VAV-DMPR-IA	73	0.725705	VAV damper position	% Open
$u_8(t)$	SOL-HORZ	71	0.705119	Solar normal flux	B/HFt2
$v_{4,IA}(t)$	RA-DMPR-EA	68	0.681232	Recirculated air damper	% Closed
$u_6(t)$	SOL-BEAM	61	0.605456	Solar beam	B/HFt2
$u_7(t)$	CHWC-VLV	60	0.595037	Chilled water coil valve position	% Open
$u_{10}(t)$	OA-TEMP	58	0.580150	Outside air temperature	°F
$u_5(t)$	SF-SPD	57	0.568448	Supply fan VFD speed	% Speed
$x_1(t+1)$	SA_SPSPT(t+1)	43	0.433351	Supply air static pressure setpoint	In. WG
$v_{1,EA}(t)$	VAVHCGPM-IA	31	0.312092	VAV heating coil flow rate	GPM
$v_{5,IA}(t)$	RM-LITE2-IA	0	0.000000	Light level on window #2	FtC
$v_{6,IA}(t)$	RM-LITE1-IA	0	0.000000	Light level on window #1	FtC

Table 4.4 Parameters selected for building temperature model in South Room (Temp-SA)

Variable	Point Name	Rank	Importance	Description	Unit
$u_6(t)$	SOL-BEAM	100	1.000000	Solar beam	B/HFt2
$v_{2,SA}(t)$	VAV-DMPR-SA	98	0.982757	VAV damper position	% Open
$v_{6,SA}(t)$	RM-LITE1-SA	98	0.979662	Light level on window #1	FtC
$u_1(t)$	MA-TEMP	97	0.968453	Mixed air temperature	°F
$u_3(t)$	CHWC-EAT	95	0.952256	Chilled water coil entering water temperature	°F
$u_4(t)$	HWC-DAT	94	0.943306	Heating water coiling departure air temperature	°F
$v_{3,SA}(t)$	VAV-DP-SA	94	0.935909	Velocity pressure differential	In. WG
$u_8(t)$	SOL-HORZ	93	0.933969	Solar normal flux	B/HFt2

Table 4.4-continued

$v_{5,SA}(t)$	RM-LITE2-SA	93	0.931232	Light level on window #2	FtC
$v_{7,SA}(t)$	LIGHTLVL-SA	88	0.877913	Light level from ceiling	FtC
$u_2(t)$	SA-CFM	82	0.823981	Supply air flow rate	CFM
$v_{4,SA}(t)$	RA-DMPR-SA	74	0.744208	Recirculated air damper	%Closed
$v_{1,SA}(t)$	VAVHCGPM-SA	68	0.684999	VAV heating coil flow rate	GPM
$u_7(t)$	CHWC-VLV	65	0.645336	Chilled water coil valve position	%Open
$x_2(t+1)$	SAT_SPT(t+1)	62	0.619476	Supply air temperature setpoint	°F
$u_5(t)$	SF-SPD	55	0.552893	Supply fan VFD speed	% Speed
$x_1(t+1)$	SA_SPSPT(t+1)	49	0.485930	Supply air static pressure setpoint	In. WG
$u_{10}(t)$	OA-TEMP	37	0.372192	Outside air temperature	°F

Table 4.5 Parameters selected for building temperature model in West Room (Temp-WA)

Variable	Point Name	Rank	Importance	Description	Unit
$u_1(t)$	MA-TEMP	100	1.000000	Mixed air temperature	°F
$u_4(t)$	HWC-DAT	97	0.967260	Heating water coiling departure air temperature	°F
$u_3(t)$	CHWC-EAT	96	0.959010	Chilled water coil entering water temperature	°F
$v_{2,WA}(t)$	VAVHCGPM-WA	91	0.912558	VAV damper position	%Open
$v_{6,WA}(t)$	RM-LITE1-WA	85	0.852728	Light level on window #1	FtC
$v_{3,WA}(t)$	VAV-DP-WA	80	0.796603	Velocity pressure differential	In. WG
$v_{5,WA}(t)$	RM-LITE2-WA	77	0.768865	Light level on window #2	FtC
$v_{7,WA}(t)$	LIGHTLVL-WA	71	0.711310	Light level from ceiling	FtC
$v_{2,WA}(t)$	VAV-DMPR-WA	67	0.672981	VAV damper position	%Open
$u_7(t)$	CHWC-VLV	63	0.629861	Chilled water coil valve position	%Open
$u_6(t)$	SOL-BEAM	59	0.592312	Solar beam	B/HFt2
$u_2(t)$	SA-CFM	54	0.540244	Supply air flow rate	CFM
$u_8(t)$	SOL-HORZ	53	0.534687	Solar normal flux	B/HFt2
$u_5(t)$	SF-SPD	51	0.512276	Supply fan VFD speed	% Speed
$u_{10}(t)$	OA-TEMP	49	0.490121	Outside air temperature	°F
$v_{4,WA}(t)$	RA-DMPR-WA	41	0.406538	Recirculated air damper	%Closed
$x_2(t+1)$	SAT_SPT(t+1)	33	0.326308	Supply air temperature setpoint	°F
$x_1(t+1)$	SA_SPSPT(t+1)	31	0.308902	Supply air static pressure setpoint	In. WG

The multi-layer perceptron (MLP) neural network is employed to establish the models. To evaluate the performance of the predictive models, four metrics in the following are used: the mean absolute percentage error (*MAPE*), the standard deviation of absolute percentage error (*Sd_PE*), the maximum absolute error (*MAX*), and the minimum absolute error (*MIN*).

$$MAPE = \frac{1}{n} \sum_{i=1}^n \left| \frac{y_i - \hat{y}_i}{y_i} \right| \times 100\%$$

$$Sd_APE = \sqrt{\frac{\sum_{i=1}^n \left(\left| \frac{y_i - \hat{y}_i}{y_i} \right| - MAPE \right)^2}{n-1}}$$

$$MAX = \max \{ |y_1 - \hat{y}_1|, |y_2 - \hat{y}_2|, \dots, |y_n - \hat{y}_n| \}$$

$$MIN = \min \{ |y_1 - \hat{y}_1|, |y_2 - \hat{y}_2|, \dots, |y_n - \hat{y}_n| \}$$

Table 4.6 Detailed information of the neural networks

Model Output	No. of Hidden Units	Training Algorithm	Hidden Layer Activation Function	Output Activation Function
Total energy consumption	5	BFGS 99	Tanh	Identity
Temp-EA	5	BFGS 100	Tanh	Identity
Temp-IA	5	BFGS 57	Tanh	Logistic
Temp-SA	11	BFGS 118	Exponential	Exponential
Temp-WA	8	BFGS 129	Tanh	Exponential

Table 4.7 Prediction accuracy of the data-mining models

Model	Dataset	MAPE	Sd_PE	MAX	MIN
Total energy consumption	Training	0.1025	0.0925	1312.7	0.0752
	Test	0.1069	0.1038	2098.7	1.2475
Temp-EA	Training	0.0072	0.0068	2.9029	0.0009
	Test	0.0079	0.0072	2.7613	0.0001
Temp-IA	Training	0.0077	0.0067	2.9972	0.0032
	Test	0.0075	0.0067	2.7362	0.0021
Temp-SA	Training	0.0071	0.0069	2.7016	0.0022
	Test	0.0082	0.0083	2.9380	0.0014
Temp-WA	Training	0.0098	0.0090	4.0789	0.6307
	Test	0.0083	0.0064	2.2613	0.4492

Table 4.6 summaries the detailed information of the five neural network models. Table 4.7 presents the training and test accuracies measured by the four metrics. The total energy consumption model has accuracy nearly 90%, and the accuracies of all the temperature models achieve 99%. Figure 4.3 illustrates the observed and predicted energy consumption. The predictive models established by the MLP are then used for the optimization process discussed in the next section.

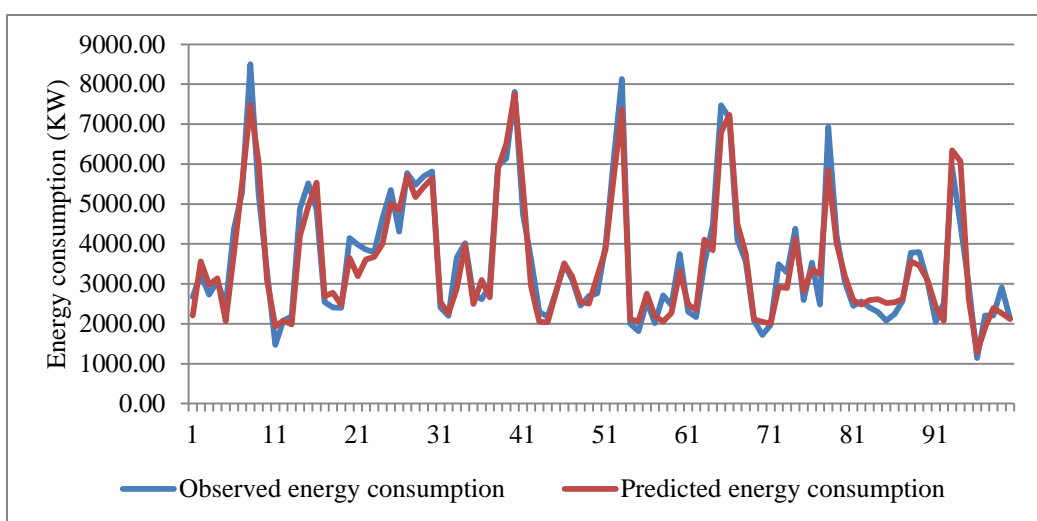


Figure 4.3 The comparison of the observed and predicted energy consumption

4.3. Energy Optimization Modeling

4.3.1 Overall energy optimization model

The objective is to optimize the settings of the two setpoints to achieve the minimum energy consumption of the HVAC system while maintaining the thermal comfort in all four rooms. $E(t+1)$, the total energy consumption at time $t+1$, is used as the objective function to be minimized in search of the optimal settings of the supply air temperature and static pressure setpoints. The varying ranges for the two setpoints recorded in the original dataset are [0.5 In. WG, 1.8 In. WG] and [55°F, 65°F], respectively. However, the data points near the bounds are

very rare, which makes it hard for the data mining algorithm to capture the pattern if the setpoint values are near the bounds. Considering this fact, the constraints for the two setpoints are restricted within [0.8 In. WG, 1.5 In. WG] and [56°F, 64°F]. The constraints of the temperature in four rooms are defined by the deviation from the recorded temperature generated by the original control strategies. In this research, two types of temperature constraints with deviation within 1 °F (+/- 0.5°F) and 2°F (+/-1°F) are considered. With the first type of controlled temperature constraints, the overall optimization model is shown as follows.

$$\min_{(x_1, x_2)} E(t+1)$$

subject to:

$$E(t+1) = f(x_1(t+1), x_2(t+1), y_1(t)u_1(t), u_2(t), \dots, u_{10}(t), u_5(t-1), u_6(t-1), u_7(t-1), u_9(t-1))$$

$$T_{EA}(t+1) = f(x_1(t+1), x_2(t+1), u_1(t), u_2(t), \dots, u_9(t), v_{1,EA}(t) \dots, v_{7,EA}(t))$$

$$T_{IA}(t+1) = f(x_1(t+1), x_2(t+1), u_1(t), u_2(t), \dots, u_9(t), v_{1,IA}(t) \dots, v_{7,IA}(t))$$

$$T_{SA}(t+1) = f(x_1(t+1), x_2(t+1), u_1(t), u_2(t), \dots, u_9(t), v_{1,SA}(t) \dots, v_{7,SA}(t))$$

$$T_{WA}(t+1) = f(x_1(t+1), x_2(t+1), u_1(t), u_2(t), \dots, u_9(t), v_{1,WA}(t) \dots, v_{7,WA}(t))$$

$$T_{EA}^*(t+1) - 0.5 \leq T_{EA}(t+1) \leq T_{EA}^*(t+1) + 0.5$$

$$T_{IA}^*(t+1) - 0.5 \leq T_{IA}(t+1) \leq T_{IA}^*(t+1) + 0.5$$

$$T_{SA}^*(t+1) - 0.5 \leq T_{SA}(t+1) \leq T_{SA}^*(t+1) + 0.5$$

$$T_{WA}^*(t+1) - 0.5 \leq T_{WA}(t+1) \leq T_{WA}^*(t+1) + 0.5$$

$$0.8 \leq x_1 \leq 1.5$$

$$56 \leq x_2 \leq 64$$

where T^* is the room temperature by implementing the original control strategies.

4.3.2 Firefly algorithm

Solving this nonlinear model pose a challenge for traditional optimization algorithm. Nature-inspired algorithms, like particle swarm optimization (PSO), simulated annealing (SA), are highly capable of finding optimal or near optimal solutions for complex optimization problems. In this paper, a new novel nature-inspired intelligent algorithm, called firefly algorithm (FA) is employed to tackle this problem.

Firefly algorithm is a novel nature-inspired algorithm inspired by social behavior of fireflies. Fireflies are one of the most special, captivating and fascinating creature in the nature. There are about two thousand firefly species, and most fireflies produce short and rhythmic flashes. The rate and the rhythmic flash, and the amount of time form part of the signal system which brings both sexes together. Therefore, the main part of a firefly's flash is to act as a signal system to attract other fireflies. By idealizing some of the flashing characteristics of fireflies, firefly-inspired algorithm was presented by Xin-She Yang [53, 54]. Firefly-inspired algorithms use the following three idealized rules: 1) All fireflies are unisex which means that they are attracted to other fireflies regardless of their sex; 2) The degree of the attractiveness of a firefly is proportion to its brightness, thus for any two flashing fireflies, the less brighter one will move towards the brighter one and the more brightness means the less distance between two fireflies. If there is no brighter one than a particular firefly, it will move randomly; 3) The brightness of a firefly is determined by the value of the objective function. For a maximization problem, the brightness can be proportional to the value of the objective function. Other forms of brightness can be defined in a similar way to the fitness function in genetic algorithms.

The research work done by Xin-She Yang shows that firefly algorithm is very efficient in finding the global optima with high success rates. This gives inspiration to introduce the algorithm for solving this complex optimization model. Based on the three rules stated before, the basic steps of the firefly algorithm can be summarized as the pseudo code shown in Figure 4.4.

```

FIREFLY ALGORITHM

01: Objective function  $f(x)$ ,  $x = (x_1, \dots, x_d)^T$ 
02: Generate initial population of fireflies  $x_i (i = 1, 2, \dots, n)$ 
03: Light intensity  $I_i$  at is determined by  $f(x_i)$ 
04: While ( $t < MaxGen$ )
05:   For  $i = 1 : n$  all  $n$  fireflies
06:     For  $j = 1 : i$  all  $n$  fireflies
07:       If ( $I_j > I_i$ ),
08:         Move firefly  $i$  towards  $j$  in  $d$ -dimension;
09:       End If
10:       Attractiveness varies with distance  $r$  via  $\exp[-\gamma r]$ 
11:       Evaluate new solutions and update light intensity
12:     End For
13:   End For
14: Rank the fireflies and find the current best
15: End While

```

Figure 4.4 Pseudo code of the firefly algorithm

Three components of the algorithm based on the three rules are explained here.

Attractiveness: In the firefly algorithm, the main form of attractiveness function $\beta(r)$ can be any monotonically decreasing functions such as the following generalized form:

$$\beta(r) = \beta_0 \exp(-\gamma r)$$

where r is the distance between two fireflies, β_0 is the attractiveness at $r = 0$ and γ is a fixed light absorption coefficient.

Distance: The distance between any two fireflies i and j at x_i and x_j is the Cartesian distance as follows,

$$r_{ij} = \|x_i - x_j\| = \sqrt{\sum_{k=1}^d (x_{i,k} - x_{j,k})^2}$$

where $x_{i,k}$ is the k -th component of the i -th firefly.

Movement: The movement of a firefly, i is attracted to another more attractive (brighter) firefly j , is determined by

$$x_i = x_i + \beta_0 \exp(-\gamma r)(x_j - x_i) + \alpha \left(\text{rand} - \frac{1}{2} \right)$$

where the second term is due to the attraction while the third term is randomization with α being the randomization parameter and “rand” is a random number generator uniformly distributed in $[0, 1]$.

The firefly algorithm is originally designed for the continuous global optimization problem. For the nonlinear constrained optimization model in this research, the constraints are integrated into the objective function by transforming into a penalty function. The penalized objective function is stated as following.

$$\min_{(x_1, x_2)} obj$$

$$obj = E(t+1) + w \sum_{k=1}^4 \left\{ \max \left\{ 0, T_k(t+1) - (T_k^*(t+1) + 0.5) \right\} + \max \left\{ 0, (T_k^*(t+1) - 0.5) - T_k(t+1) \right\} \right\}$$

where w is the penalty parameter (set as a large number in the computation, 1000000). $k=1, 2, 3, 4$, representing the four rooms.

4.4. Computational Results and Analysis

Two experiments are considered. Experiment 1 restricts the controlled temperature deviation in each room within 1 °F, which means the deviation falls in the range $[-0.5^\circ\text{F}, 0.5^\circ\text{F}]$. While in Experiment 2, the deviation of the controlled temperature in each room falls in the range $[-1^\circ\text{F}, 1^\circ\text{F}]$. In each of the experiments, 100 cases are computed to demonstrate the effectiveness of the proposed approach. Parameters for the firefly algorithm are set as $\beta_0 = \gamma = 1$, $\alpha = 0.2$, $MaxGen=50$, $popsiz=50$. Figure 4.5 demonstrates the iteration process of the firefly algorithm for one computing case. The algorithm finds the optimal solution at the 36-th iteration, which shows that the algorithm could escape from the local minimum during later iterations.

Table 4.8 presents the energy consumption before and after optimization in these two experiments. 6.38% and 12.85% energy saving are achieved by this optimization strategy.

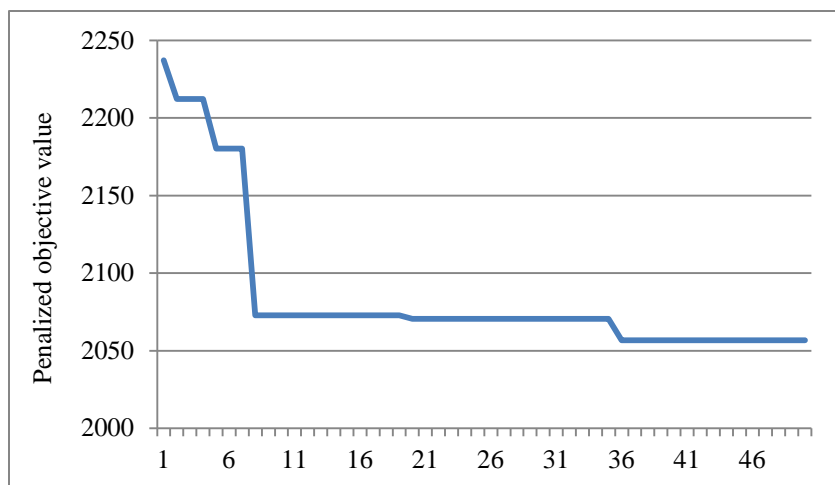


Figure 4.5 The iterations of the firefly algorithm in one case

Table 4.8 Energy consumption before and after optimization

	Scenario 1	Scenario 2
Recorded total energy consumption	360929.78	
Optimized total energy consumption	337887.08	317311.66
Total energy savings	23042.70	43618.12
Saving ratio	6.38%	12.85%

Figure 4.6 depicts the recorded and optimized total energy consumption in Experiment 1. Figures 4.7-4.8 compare the original and recommended settings of the supply air temperature and static pressure setpoints in Experiment 1. Similarly, Figure 4.9 demonstrates the recorded and optimized total energy consumption in Experiment 2. Figures 4.10-4.11 show the comparisons of the recorded and recommended two setpoints in Experiment 2. By comparing the two experiments, we can see that relaxing the temperature constraints can lead to more energy savings.

Figures 4.12-4.15 illustrate the controlled temperature in the four rooms in Experiment 1. The figures suggest that the room temperatures are under control. Illustrations of controlled room temperature in Experiment 2 are not included.

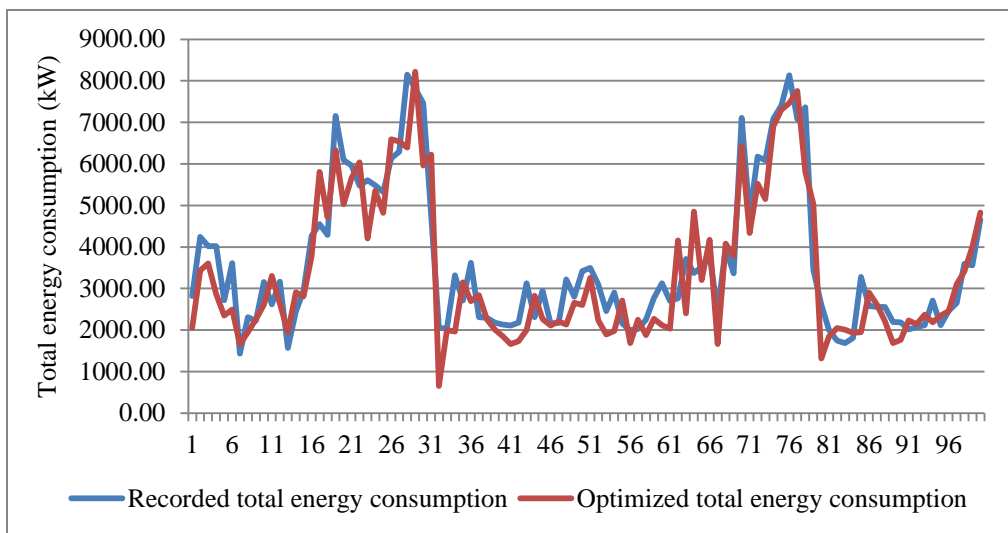


Figure 4.6 The recorded and optimized total energy consumption in Experiment 1

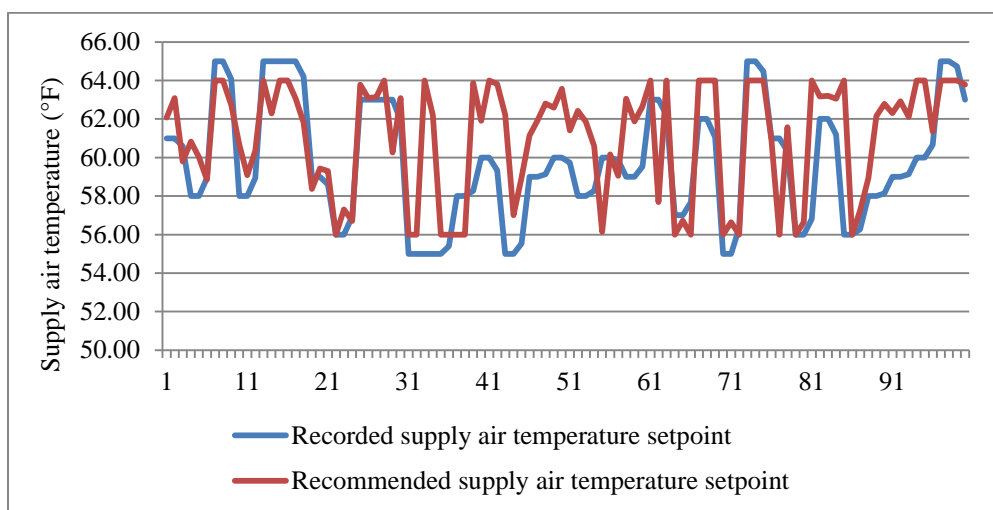


Figure 4.7 The recorded and recommended supply air temperature setpoint settings in Experiment 1.

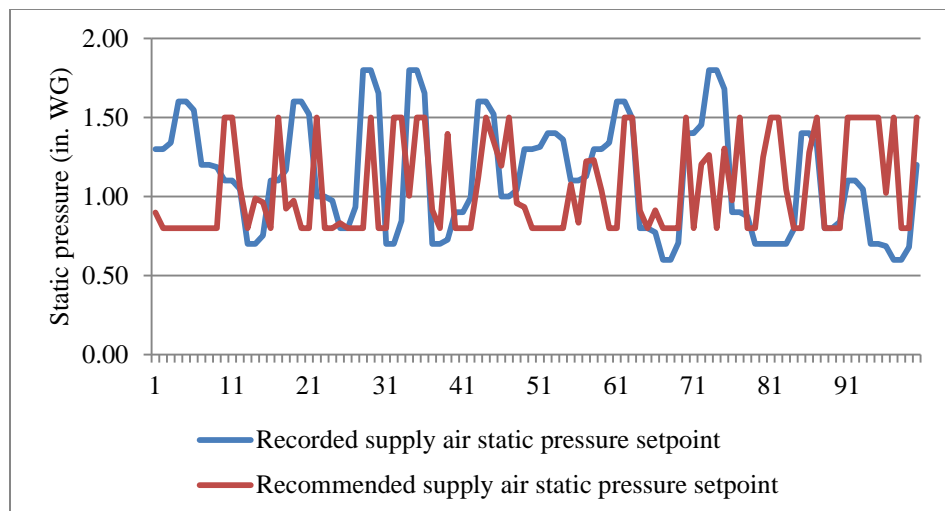


Figure 4.8 The recorded and recommended supply air static pressure setpoint settings in Experiment 1.

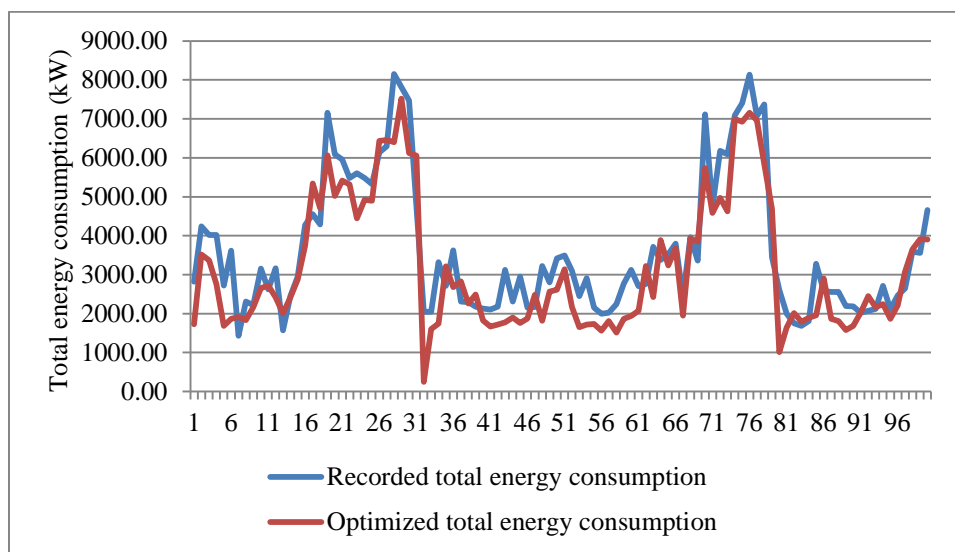


Figure 4.9 The recorded and optimized total energy consumption in Experiment 2

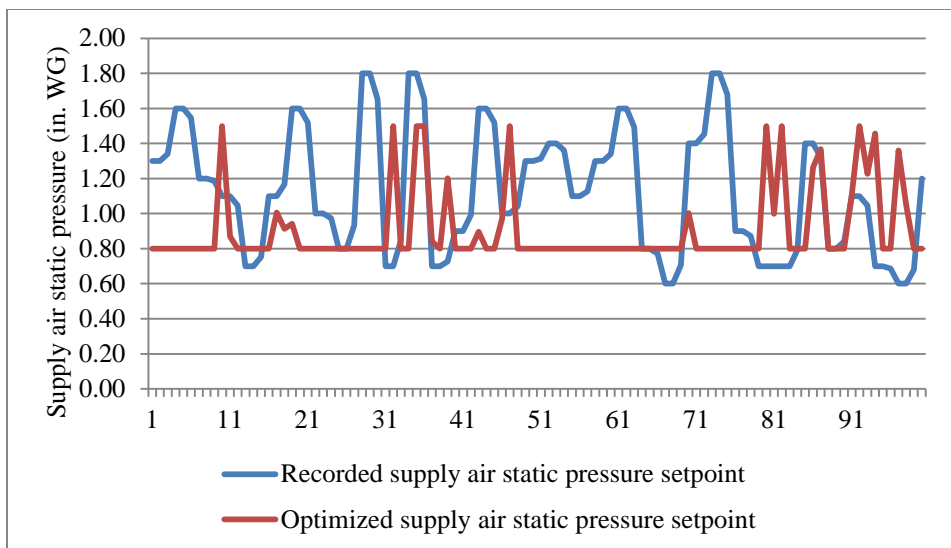


Figure 4.10 The recorded and recommended supply air static pressure setpoint settings in Experiment 2

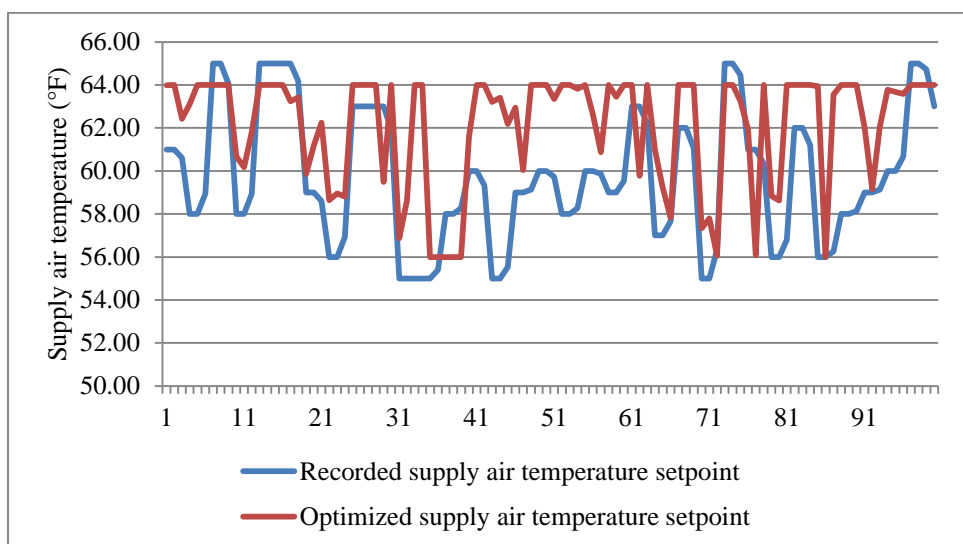


Figure 4.11 The recorded and recommended supply air temperature setpoint settings in Experiment 2

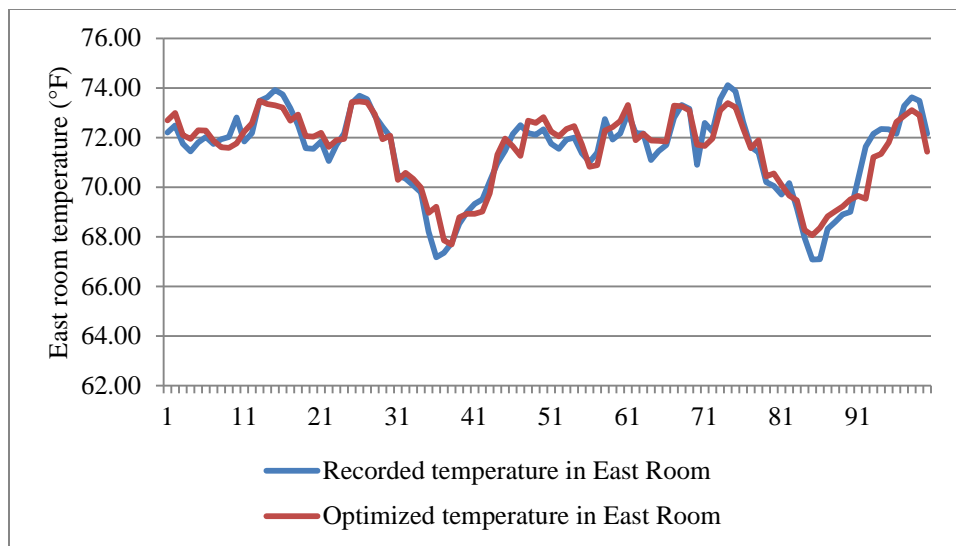


Figure 4.12 The recorded and optimized temperature of East Room in Experiment 1

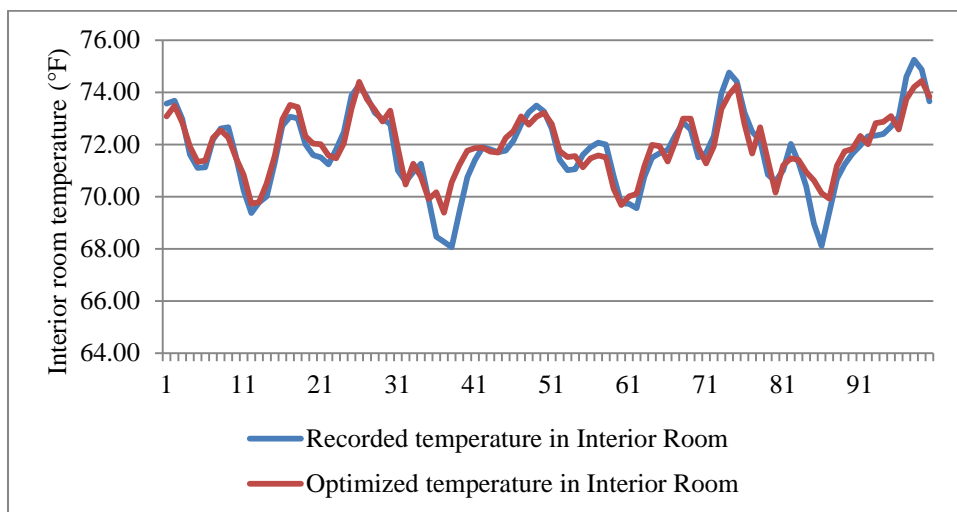


Figure 4.13 The recorded and optimized temperature of Interior Room in Experiment 1

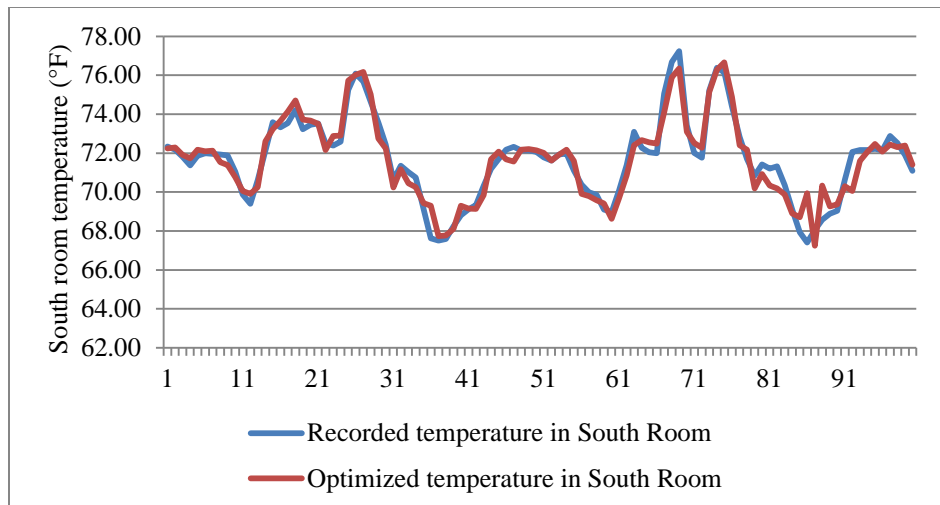


Figure 4.14 The recorded and optimized temperature of South Room in Experiment 1

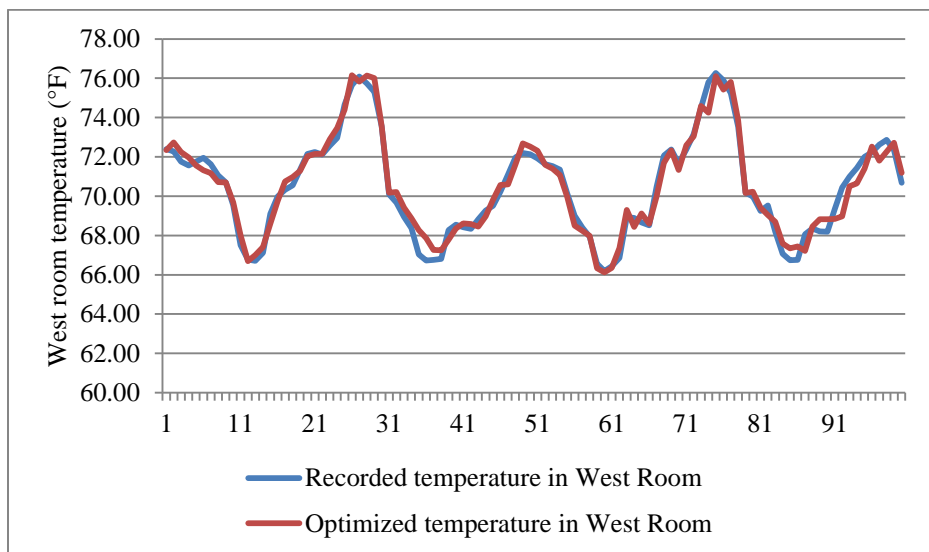


Figure 4.15 The recorded and optimized temperature of West Room in Experiment 1

4.5. Summary

This research presents a data mining approach to model a multi-zone HVAC system. Predictive models of the energy consumption and the thermal comfort of each zone, measured by room temperature, are built by a multilayer-perceptron neural network algorithm. An energy

optimization model is established by combining the predictive models and related constraints. After solving the optimization model by the firefly algorithm, two controllable parameters, namely the supply air temperature setpoint and the supply air static pressure setpoint, are optimized. The optimal settings constitute the best control strategies for the HVAC system. Two experiments with different constraints on the controlled temperature deviations are conducted to verify the proposed approach. Computational results show that more than 6% and 12% energy savings are respectively observed. The room temperatures are under control at the same time.

Modeling multi-zone HVAC system is complex. There are rooms for improving the accuracy of the energy consumption model built in this research. More accurate model will lead to more credible optimization result. Meanwhile, thermal comfort measured by better criteria or by considering more metrics, like the humidity, should to be investigated further.

CHAPTER 5

HVAC SYSTEM OPTIMIZATION VIA DATA MINING AND COMPUTATIONAL INTELLIGENCE: AN IMPLEMENTATION

5.1. Introduction

Heating, ventilation, and air conditioning (HVAC) systems are high energy consumers. Energy savings in HVAC systems could be obtained by utilizing intelligent control strategies. In our research, data-mining and computational intelligence are intensively applied to model and optimize HVAC systems with the objectives of energy savings and thermal comfort. Investigations show that data mining approach can successfully extract the underlying patterns in the system, and thus build accurate predictive models. These data-driven models are integrated in optimization models. Optimal control strategies, typically settings of setpoints, are generated by solving energy optimization models. Computational results in our previous research show that energy consumption of the HVAC system could be significantly reduced by our proposed modeling and optimization approaches.

A practical implementation with two objectives, focusing on the methodology validation and practical implementation, is conducted to demonstrate the applicability of the proposed approaches. At the methodology side, though theoretical studies demonstrate huge potential of energy savings by this promising approach, the reliability and accuracy of the predictive data-driven models are to be validated in this real case. At the implementation side, through this case, we aim to establish a unified framework of how data mining and computational intelligence are implemented in real-world HVAC systems. The interactions of different systems are tested and verified, the complete steps, from room selection to data collection, and to final implementation are discussed.

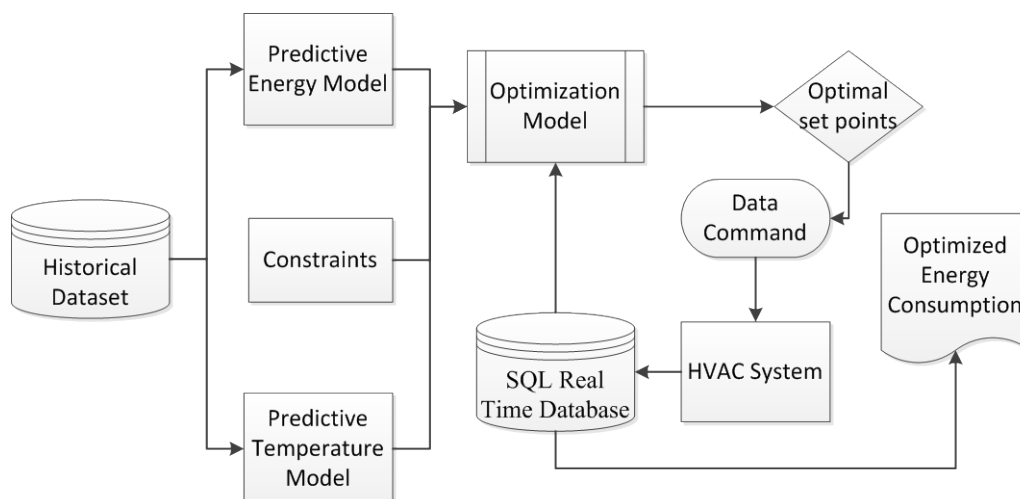


Figure 5.1 Framework of the real time online implementation

In this implementation, two setpoints, namely the supply air static pressure set point and the discharge air temperature set point are investigated. Optimal control strategy is the best settings of the two set points which control the system to achieve minimum energy consumption while maintaining the acceptable thermal comfort of the building. The main process of the real time online optimization for this implementation is illustrated by Figure 5.1. A data collection experiment is first conducted to collect data to build predictive energy consumption model and temperature models, which describe the relationship between the two setpoints and the output, energy consumption and temperature. Then by combining related thermal comfort constraints, which is temperature constraints in this study, and range constraints of set points, the energy optimization model is established. At time t , the optimal settings of the set points for time $t+1$ time are generated by intelligent algorithm and thus written to the real system. The system runs under the settings, and new real time data are extracted at time $t+1$, the optimization iterates for the next time interval.

5.2. Building and System

The commercial building investigated in this implementation is the University Services Building (USB) at the University of Iowa. The building was built in 1999, and is located at 1 West, Prentiss, Iowa city. The gross floor area is 71,123 square feet. The building has four floors, and provides offices, meeting rooms, and recreation areas for different departments of the university.



Figure 5.2 The University Services Building

The HVAC system in the building includes a single air handling unit (AHU), a chiller plant, boilers, pumps, fans, and serving zones. The system is controlled by Jonson Control system, the real time data are stored in a SQL server, shown in Figures 5.3-5.4. A software called Data Command (Figure 5.5) is used to connect the real physic system and the software control system. The values of the set points are read by the Data Command software, and then written to the real components of the HVAC system. In the real implementation, a csv file is created to store the values of the two setpoints first. Then each time the values are modified by the optimization program, Data Command software will notice that by scanning the csv file very one minute. After knowing the modification, Data Command will read the values and write them to the HVAC system automatically.

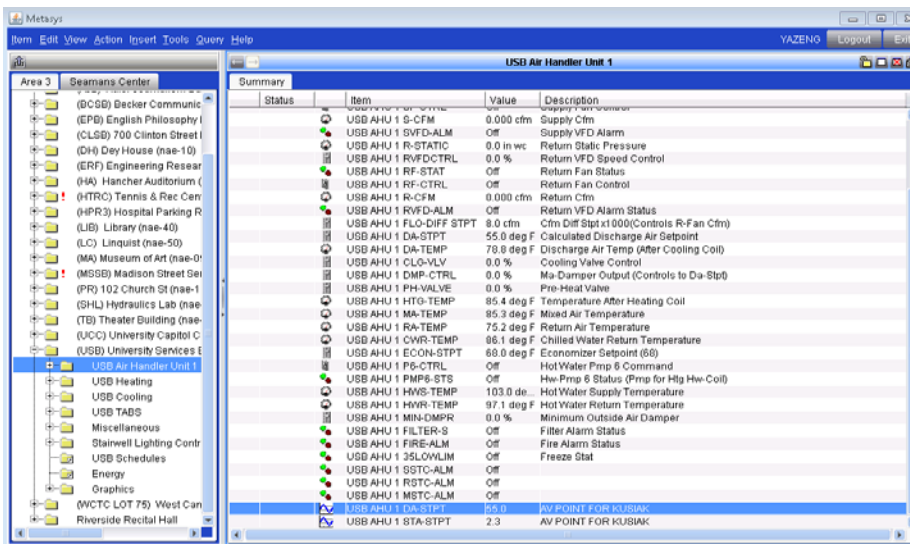


Figure 5.3 Johnson control system – parameters in the USB air handling unit

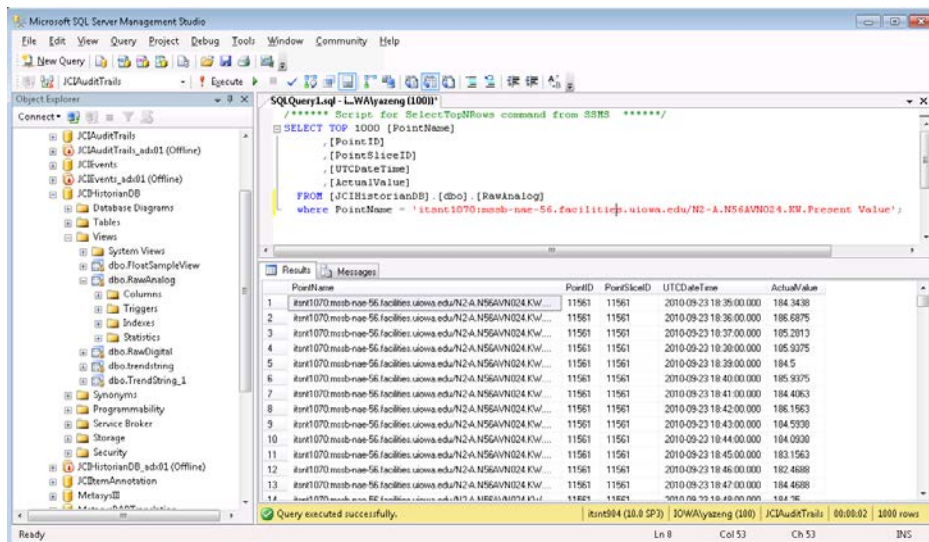


Figure 5.4 SQL server – store real time data

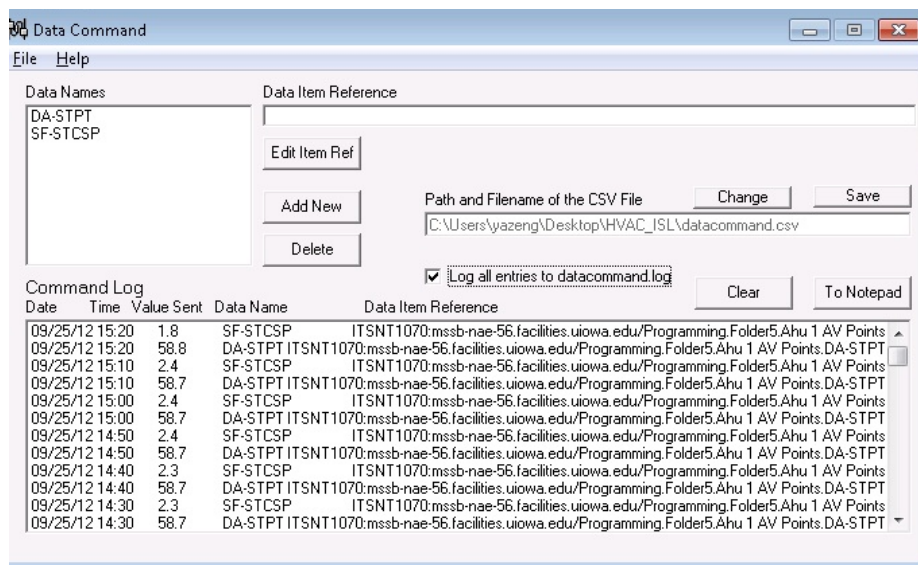


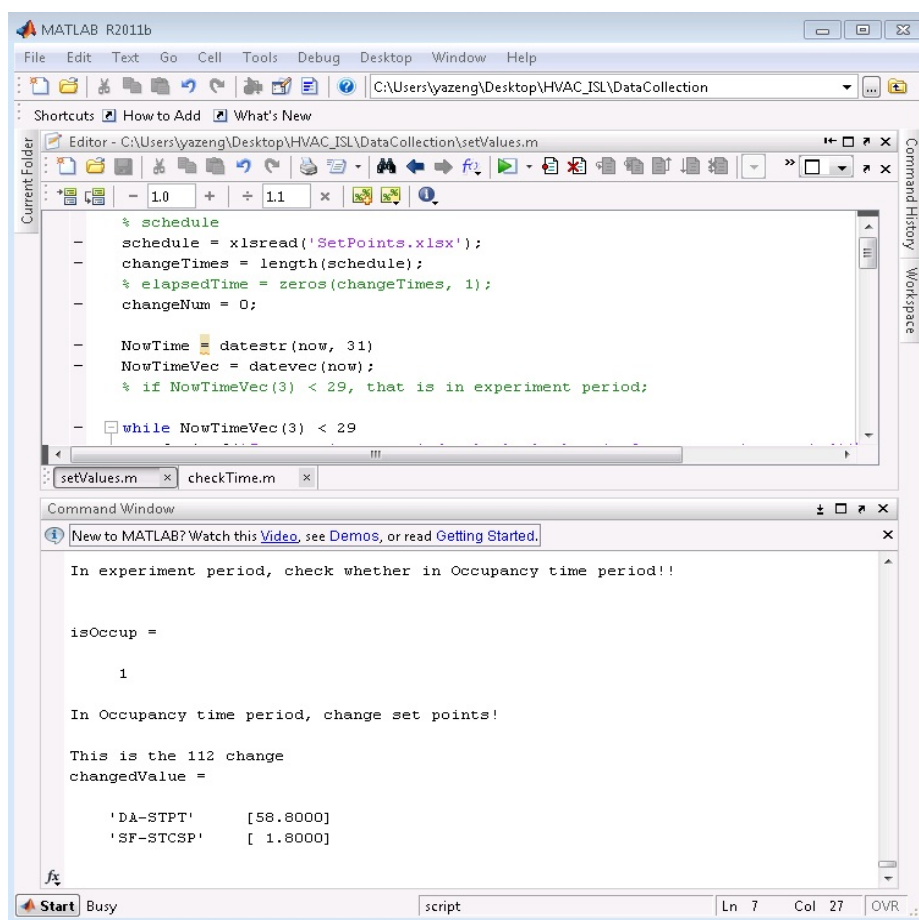
Figure 5.5 Data Command interface

5.3. Data Collection Experiment

In this implementation, two set points, the supply air static pressure set point and the discharge air temperature set point, are investigated. By optimally setting these two set points, the energy savings are expected to be captured. However, in practice, the values of the two set points are respectively fixed at 2.3 in. WG and 55°F in the system. In order to build the relationship between the two set points and the system outputs, like energy consumption and room temperature, the system should be running under changing settings of the two set points to collect enough data for model building. The data collection experiment is thus conducted to achieve this goal.

The occupancy period for the system is defined every 8:00 A.M. to 5:00 P.M., Monday to Friday. The data collection experiment was designed from 6:00 A.M., Sep. 10, 2012 to 6:30 P.M., Sep. 28, 2012. Two weekends (Sep. 15, 16, and Sep. 22, 23) were excluded. The two set points were changed every 30 mins. The schedules of the two set points are as follows. The discharge air temperature setpoint was changed from 55°F to 60°F with 0.1°F increment. The supply air static pressure setpoint was varied from 1.8 in. WG to 2.4 in. WG. with 0.1 in. WG increment. Ideally there should be 360 data points, 15 days with 24 records each day.

The data collection process was implemented by MATLAB. Figure 5.6 illustrates changing values of the set points in MATLAB. Figure 5.7 shows the data collection experiment in which the MATLAB program was running on a virtual machine at the Energy Control Center, which is located at the third floor of the University Services Building. The program ran all the time during the experiment period. It should be noted that there was a time limit, which is not quite clear, for Data Command software connecting with the corresponding server. That means if the Data Command could not read new data for a certain period of time, it will lose connection. To avoid this problem, the Matlab program wrote the old values of two set points every 10 mins. After 30 mins, the new values would be written (See Figure 5.5).



```

MATLAB R2011b
File Edit Text Go Cell Tools Debug Desktop Window Help
C:\Users\yazeng\Desktop\HVAC_ISL\DataCollection
Shortcuts How to Add What's New
Editor - C:\Users\yazeng\Desktop\HVAC_ISL\DataCollection\setValues.m
% schedule
- schedule = xlsread('SetPoints.xlsx');
- changeTimes = length(schedule);
- % elapsedTime = zeros(changeTimes, 1);
- changeNum = 0;

- NowTime = datestr(now, 31)
- NowTimeVec = datevec(now);
- % if NowTimeVec(3) < 29, that is in experiment period;

- while NowTimeVec(3) < 29

Command Window
New to MATLAB? Watch this Video, see Demos, or read Getting Started.

In experiment period, check whether in Occupancy time period!!

isOccup =

    1

In Occupancy time period, change set points!

This is the 112 change
changedValue =

    'DA-STPT'    [ 58.8000]
    'SF-STCSP'    [  1.8000]

Start Busy script Ln 7 Col 27 OVR

```

Figure 5.6 MATLAB for data collection

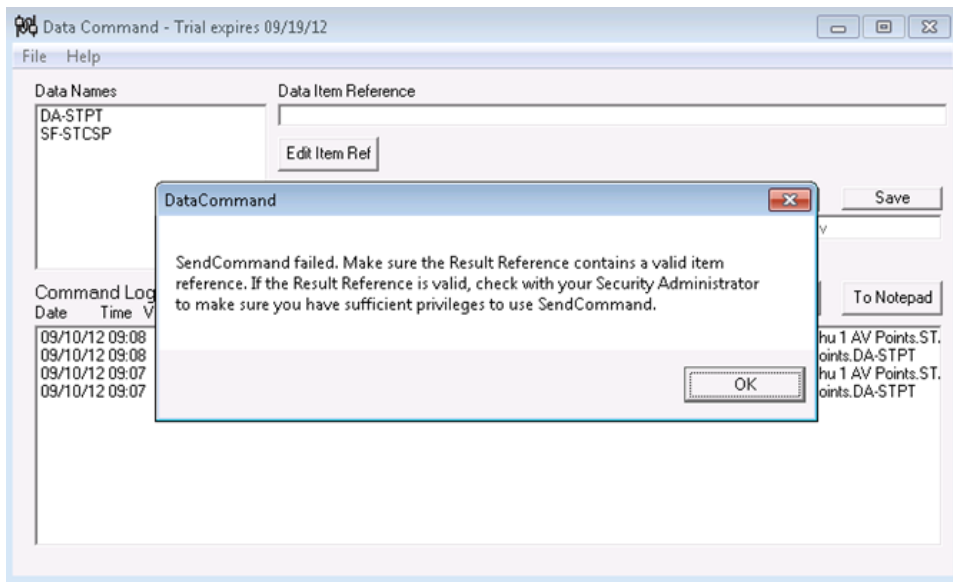


Figure 5.8 The first type of error during the data collection experiment

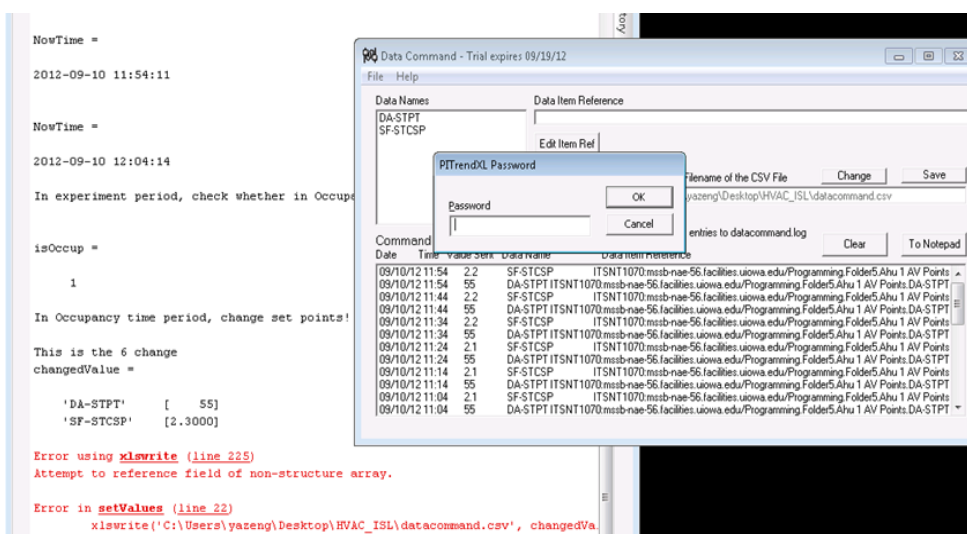


Figure 5.9 The second type of error during the data collection experiment

The second type of errors occurred around 12:00 pm, Sep. 10, 2012, shown in Figure 5.9. It involved the Excel Reading issue. Another error occurred during the process was that the virtual machine was forced shut down on Sep. 17, 2012 due to the system update on the virtual machine. This led that the whole day’s data was void. Additionally, during the experiment, a

problem occurred on the chiller and the chiller was taken out of service for a period of time. This made the discharge air temperature reach above 65°F, which was regarded abnormal. Thus, data points with a discharge air temperature above 65°F were also excluded from the data set.

5.4. Room Selection

To validate the data mining approach for HVAC optimization, evaluating whether the building is under control is of importance. Since the University Services Building has nearly a hundred of rooms and general zones controlled by the single air handling unit, it is impractical to monitor the system by taking all the zones into account.

Selecting representative rooms for monitoring is finished to better measure the controllability of the building. In this study, several factors, like the floor, the orientation, the type, are considered for the room selection. Critical rooms, which are defined as those with general usage and have typical characteristics shared by many others, are selected as representative zones to be monitored during this implementation. Usually meeting rooms have a very high cooling load when there is a meeting, but are not necessary to be controlled where they are unoccupied. These kinds of rooms are idle for very long time and couldn't be critical rooms.

The building is claimed under control if the selected critical rooms are under control, *i.e.*, the temperature in each critical room is within the range defined by the actual heating setpoint and actual cooling setpoint. For this study, the critical rooms should be those are already well under control by the original control strategy.

Eight rooms are initially picked for consideration. Data used for evaluating the rooms are collected from 5:15 P.M., July 30, 2012 to 5:00 P.M. August 30, 2012. Taking Room 4 as an instance, Figure 5.10 illustrates the comparison of the actual room temperature and the corresponding heating and cooling set points. Table 5.1 summarizes the information of the rooms. The control ratios are computed based on the occupancy period of the rooms. They basically mean that for how long the rooms are under control during the occupancy period. The table shows that only Room 4 are controlled well by the original control strategy. This is mainly

because that the actual cooling and heating setpoints are set tight and strict, making it hard for the room temperature to fall into the range. Figure 5.11 and Figure 5.12 intuitively demonstrate the situations in Room 7 and Room 8, in which the actual room temperatures vary beyond the predefined actual cooling and heating setpoints.

Considering the representativeness as well as the control ratio of the rooms, Room 2, 4, 7, and 8 are finally selected as critical rooms for this implementation, after changing the actual cooling and heating setpoints in Room 7 and Room 8. Table 5.2 presents the information of the final rooms.

Table 5.1 The room selected and the original control ratio

Room No.	Location	Rooms	Actual Cooling Setpoint	Actual Heating Setpoint	Control Ratio
1	First floor, North	ROOM 102A	74.98	73.98	0.085427
2	First floor, South	ROOM 121-31,32&33	75.5	74.5	0.440882
3	Second floor, West	ROOM 201	75.3	74.3	0.47806
4	Second floor, North	ROOM 220-5,6,7,8	77.38	76.38	0.804396
5	Second floor, Interior	ROOM 224	73.86	72.86	0.510158
6	Third floor, East	ROOM 341	67.63	66.63	0
7	Third floor, Interior	ROOM 320-5	69.5	68.5	0.118421
8	Third floor, South	ROOM 321-33	68.7	67.7	0

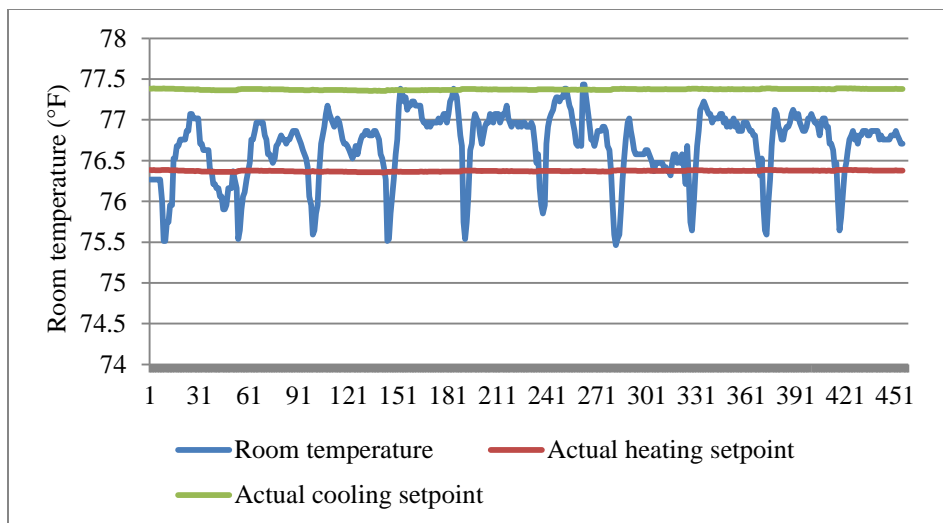


Figure 5.10 The comparison of the actual room temperature and setpoints in Room 4

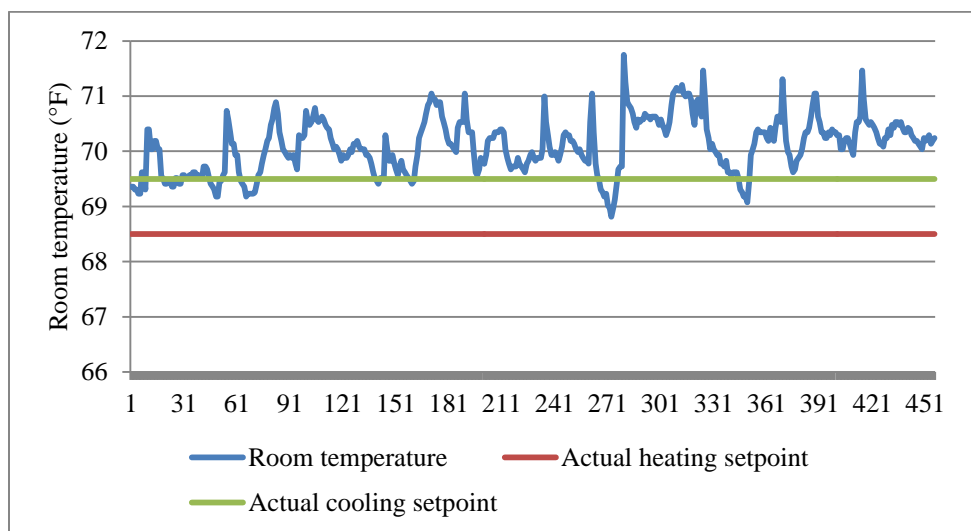


Figure 5.11 The comparison of the actual room temperature and setpoints in Room 7

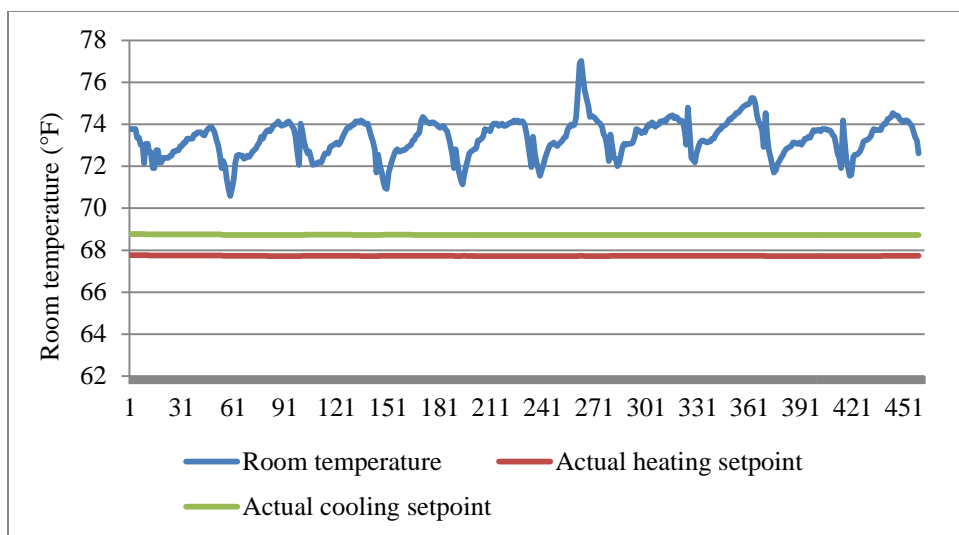


Figure 5.12 The comparison of the actual room temperature and setpoints in Room 8

Table 5.2 The critical rooms selected for the implementation

Room No.	Location	Rooms	Actual Cooling Setpoint	Actual Heating Setpoint	Control Ratio
2	First floor, South	ROOM 121-31,32&33	75.5	74.5	0.440882
4	Second floor, North	ROOM 220-5,6,7,8	77.38	76.38	0.804396
7	Third floor, Interior	ROOM 320-5	70	71	0.535087
8	Third floor, South	ROOM 321-33	73	74	0.440087

5.5. Data Mining Modeling

Parameters measuring the functioning of the air handling unit and thermal comfort of different zones were recorded every 1 minute. The time stamp is transformed into 30 minutes by averaging the original data points. After preprocessing, there are 300 data points in the final dataset. 85% are used to build the data mining models, and the remaining are for testing the accuracy and stability of the models.

The parameters selected for the energy consumption model are summarized in Table 5.3. Table 5.4 presents the parameters selected for building the temperature model in Room 8. The parameters used for temperature models in other rooms are the same with those in Table 5.4.

Table 5.3 Parameters selected for building energy consumption model

Point name	Rank	Importance	Description	Unit
CW-R-T	100	1.000000	Chilled water return temperature	°F
CW-S-T	87	0.871468	Chilled water supply temperature	°F
CL-VLV	77	0.765106	Cooling valve control	% Open
OA-TEMP	73	0.725706	Outside air temperature	°F
MA-TEMP	68	0.679566	Mixed air temperature	°F
DA-TEMP	66	0.655022	Discharged air temperature	°F
RA-TEMP	63	0.625273	Return air temperature	°F
DA-STPT	53	0.526073	Discharged air temperature setpoint	°F
RA-SP	46	0.455347	Return static pressure	In. WG
SA-SP	45	0.451086	Supply static pressure	In. WG
SA-CFM	43	0.426814	Supply air CFM	CFM
RA-CFM	42	0.420577	Return air CFM	CFM
RA-VFD	40	0.403371	Return VFD speed control	% Speed
CHWR-TEMP	40	0.402218	Chilled water return temperature	% Speed
SA-VFD	35	0.347783	Supply VFD Speed control	% Speed
STA-STSP	26	0.262965	Supply air static pressure setpoint	In. WG

Table 5.4 Parameters selected for building temperature model in Room 8

Point name	Rank	Importance	Description	Unit
DA-TEMP	100	1.000000	Discharged Air Temperature	°F
DA-STPT	97	0.969816	Discharged Air Temperature Setpoint	°F
CW-R-T	92	0.920689	Chilled water return temperature	°F
CW-S-T	87	0.873606	Chilled water supply temperature	c
MA-TEMP	84	0.837691	Air temperature after heating coil	°F
MA-TEMP	83	0.827385	Mixed air temperature	°F
OA-TEMP	77	0.766247	Outside air temperature	°F
CHWR-TEMP	73	0.730635	Chilled water return temperature	°F
RA-VFD	63	0.628827	Return VFD speed control	% Speed
SA-CFM	62	0.624080	Supply CFM	CFM
CL-VLV	58	0.584872	Cooling valve control	% Open
SA-VFD	58	0.581926	Supply VFD speed	% Speed
STA-STSP	49	0.492345	Supply air static pressure setpoint	In. WG

The multi-layer perceptron (MLP) neural network is employed to establish the models. To evaluate performance of the predictive models, four metrics are used: the mean absolute percentage error (*MAPE*), the standard deviation of absolute percentage error (*Sd_{PE}*), the mean absolute error (*MAE*), the standard deviation of absolute error (*Sd_{AE}*).

$$MAPE = \frac{1}{n} \sum_{i=1}^n \left| \frac{y_i - \hat{y}_i}{y_i} \right| \times 100\%$$

$$Sd_APE = \sqrt{\frac{\sum_{i=1}^n \left(\left| \frac{y_i - \hat{y}_i}{y_i} \right| - MAPE \right)^2}{n-1}}$$

$$MAE = \frac{1}{n} \sum_{i=1}^n |y_i - \hat{y}_i|$$

$$Sd_AE = \sqrt{\frac{\sum_{i=1}^n (|y_i - \hat{y}_i| - MAE)^2}{n-1}}$$

where y_i is the observed value, \hat{y}_i is the predicted value, and n is the size of the training or test data set.

Table 5.5 summaries information of the five neural network models. Table 5.6 presents the accuracy measured by the four metrics. Figure 5.13 shows the comparison between the observed and predicted energy consumption.

Table 5.5 Information about the neural network models

Model Output	No. of Hidden Units	Training Algorithm	Hidden Layer Activation Function	Output Activation Function
Energy consumption	8	BFGS 56	Tanh	Tanh
Temp-Room 2	9	BFGS 67	Logistic	Identity
Temp-Room 4	25	BFGS 66	Tanh	Logistic
Temp-Room 7	12	BFGS 66	Tanh	Exponential
Temp-Room 8	7	BFGS 147	Tanh	Exponential

Table 5.6 Prediction accuracy of the data-mining models

Model	MAPE	Sd_PE	MAE	Sd_AE
Total energy consumption	0.169039	0.413404	8.611003	9.217378
Temp-Room 2	0.003714	0.0029148	0.281503	0.221067
Temp-Room 4	0.00235	0.001874	0.18081	0.144214
Temp-Room 7	0.00313	0.00266	0.219767	0.186923
Temp- Room 8	0.003941	0.003561	0.292917	0.264546

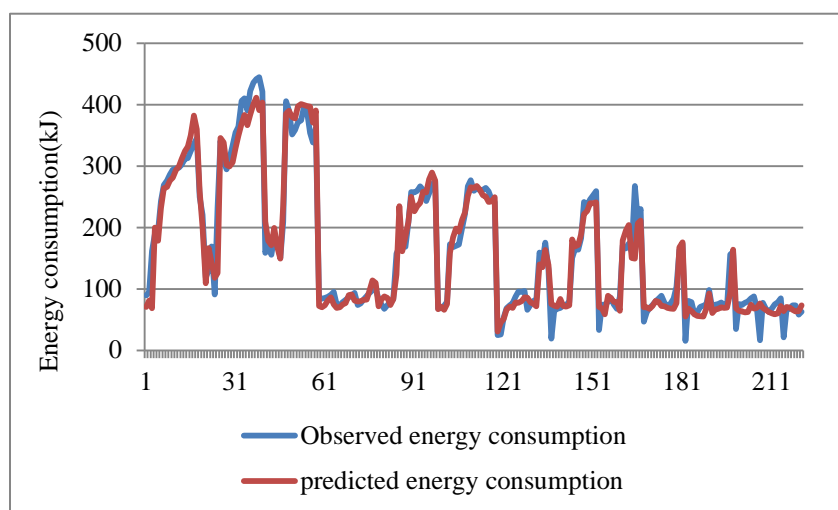


Figure 5.13 Comparison between the observed and predicted energy consumption

5.6. Implementation

The implementation is conducted through Oct. 11 to Oct. 19, 2012, despite of weekends. If the outside air temperature is below 60 °F, the HVAC system in the University Services Building will switch to heating mode, in which the chiller would be shut down. Since the optimization on the two setpoints is based on energy consumption model built for cooling mode, it makes no sense to conduct optimization on the real system if the chiller is shut down. Because of the relatively low outside air temperature during experiment period, there seems not so much room for optimization and the potential energy savings.

The software wrote for this implementation would first check whether the current time is in occupancy period, which is defined from 9 A.M. to 5 P.M., Monday to Friday. If so, the

software then pools out real time data for the models, and check whether the outside air temperature is below 60 °F. If the outside air temperature is below 60 °F, the software would set the default values for the two setpoints, which are respectively 55 °F and 2.3 in. WG. If the outside air temperature is above 60 °F, the optimization procedure is conducted to generate optimal settings of the two setpoints and write the optimal value to the system. Figure 5.14 and Figure 5.15 illustrate the output of the software in different scenarios.

A network problem occurred on the virtual machine for the experiment Oct. 16, 2012, which stopped the software from pooling data from the SQL server. Figure 5.16 depicts the problem.

```

*****In Implementation period, check whether in occupancy time period!*****
fsoccup =
  1
*****In occupancy time period, check whether the outside air temperature is lower than 60 !*****
outsideTemp =
  55.5812
outside air temperature lower than 60, the chiller does not run. Set as default values, 55 & 2.3. hold on for 30 mins !

NowTime =
  2012-10-15 11:31:22

changedValue =
  'DA-STPT' [ 55]
  'SF-STCSP' [2.3000]

NowTime =
  2012-10-15 11:41:23

changedValue =
  'DA-STPT' [ 55]
  'SF-STCSP' [2.3000]

NowTime =
  2012-10-15 11:51:24

changedValue =
  'DA-STPT' [ 55]
  'SF-STCSP' [2.3000]

```

Figure 5.14 Software output for scenario where outside air temperature is below 60 °F

```

*****This is the 7 change.*****

NowTime =
2012-10-15 16:02:51

changedValue =
    'DA-STPT'    [56.4113]
    'SF-STCSP'    [ 2.4000]

NowTime =
2012-10-15 16:12:52

changedValue =
    'DA-STPT'    [56.4113]
    'SF-STCSP'    [ 2.4000]

NowTime =
2012-10-15 16:22:54

changedValue =
    'DA-STPT'    [56.4113]
    'SF-STCSP'    [ 2.4000]
|
NowTime =
2012-10-15 16:32:55

ahuInput =
    columns 1 through 15
    2.2988  55.0000  51.7687  43.7188  68.2500  47.2188  56.0562  73.6750  75.9625  71.8375  0.7100  94.4
    Column 16
    59.1141

roomInput =
    2.2988  55.0000  51.7687  68.2500  47.2188  56.0562  72.5375  73.6750  75.9625  94.4500  93.8875  42.4

```

Figure 5.15 Software output for scenario where outside air temperature is above 60 °F

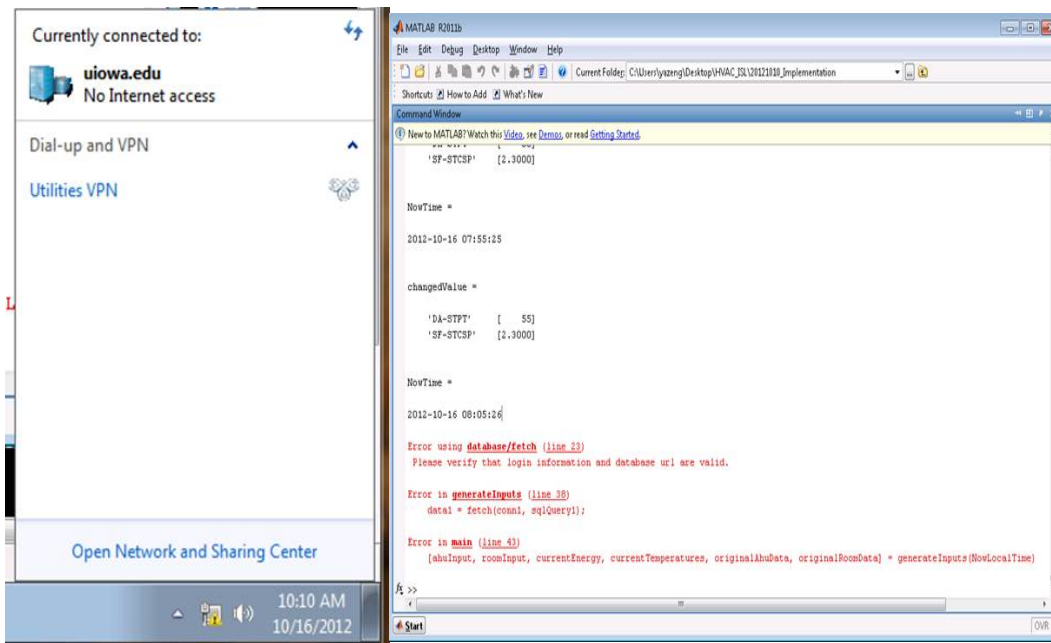


Figure 5.16 Network error forced the software to stop

The network problem is solved after the implementation period. As stated before, practical implementation involves a lot of work to deal with the security of the database, the network, the control system, the safe operation of the HVAC system, and the interactions of different software. Any error could interrupt the real time implementation. For this implementation, however, the goal of building a unified framework of applying data mining and computational intelligence to HVAC system optimization is achieved.

5.6. Summary

In this chapter, a real-time implementation was conducted with two objectives, to validate the data mining approaches, and to build a unified framework of applying data mining and computational intelligence to HVAC system optimization. A commercial building called the University Services Building at the University of Iowa was used for the experiment.

A data collection experiment was conducted to collect data for building data mining models. Critical rooms were selected to measure whether the system is under control during implementation. Different kinds of errors which occur because of system security and other issues were tackled. The HVAC system and the interactions of related software used in the implementation were successfully tested. The whole implementation process was verified.

To get accurate data mining models, enough data points are required. Therefore, a longer time period (at least one month) should be used for the data collection in future experiment. And a long time implementation is also needed to draw strong conclusion on the energy saving result.

CHAPTER 6

CONCLUSION

This thesis proposes data mining and computation intelligence to the system modeling and optimization. Two industrial systems, the HVAC system and the wastewater pumping system are considered to test the effectiveness of the proposed approach. Chapter 1 introduces current approaches of modeling and optimizing the two systems in literature, and reviews the data mining and computational intelligence in modeling and optimization.

In the first part (Chapter 2), a pumping system in a wastewater treatment plant is first examined. The performance of the pumping system evaluated by the energy consumption and the outflow rate are modeled by a data mining approach. A mixed-integer nonlinear programming (MINLP) model with regard to minimizing energy consumption was established and solved by a designed greedy electromagnetism-like (GEM) algorithm. The computational experiments demonstrated that significant energy savings can be achieved.

The second part (Chapter 3 – Chapter 5) mainly focuses on modeling and optimization of HVAC systems. In Chapter 3, energy consumption of different components in an air handling unit system was separately modeled. A non-linear optimization model was developed to minimize the total energy consumption of the air-handling unit while maintaining the supply air temperature and static pressure in a predetermined range. A dynamic penalty-based electromagnetism-like algorithm was employed. Energy consumption of the AHU system was reduced by almost 23% in the computational experiment.

Chapter 4 presents a multi-layer perceptron neural network to model the energy consumption and the thermal comfort of each zone, measured by room temperature, in a multi-zone HVAC system. The firefly algorithm is utilized to solve the energy optimization model. More than 6% and 12% energy savings are respectively observed in two computational experiments.

In Chapter 5, a real-time practical implementation was conducted to validate the data mining approach in HVAC system modeling. A unified framework of applying data mining and computational intelligence in HVAC system modeling and optimization is established. The real system and interactions of related used software are successfully tested and verified. Further implementation with longer time for data collection as well as real time implementation is needed.

Future research should focus on the improvement of the accuracy of data mining models while avoiding over-fitting and on the validation of the data mining approach by practical implementations in different systems. Comparison of and evaluation on the effectiveness of different intelligent algorithms are also to be considered.

REFERENCES

- [1] T.E. Mull, "HVAC Principles and Applications Manual," McGraw-Hill, New York, 1998.
- [2] F.W. Payne, "Energy Management Control System Handbook". Fairmont Press, Atlanta, 1984.
- [3] Clean energy opportunities in water & wastewater treatment facilities background and resources, EPA's clean energy-environment tech forum, http://epa.gov/statelocalclimate/documents/pdf/background_paper_wastewater_1-15-2009.pdf.
- [4] Wastewater management fact sheet, United States Environmental Protection Agency, July, 2006.
- [5] Goldstein, R., and Smith, W., Water & sustainability (Vol. 4): U.S. electricity consumption for water supply & treatment—The next half century. Technical Rep., Electric Power Research Institute (EPRI), Palo Alto, CA, 2002.
- [6] L. Lu, W. Cai, Y.C. and Soh, L. Xie, "Global optimization for overall HVAC systems—Part I problem formulation and analysis," Energy Conversion and Management, Vol. 46 No. 7, pp. 999-1014, 2005.
- [7] L. Lu, W. Cai, Y.C. and Soh, L. Xie, "Global optimization for overall HVAC systems—Part II problem solution and simulations," Energy Conversion and Management Vol. 46 No. 7, pp. 1015-1028, 2005.
- [8] Y. W. Wang, W. J. Cai, Y. C. Soh, S. J. Li, L. Lu, and L. Xie, "A simplified modeling of cooling coils for control and optimization of HVAC systems," Energy Conversion and Management, Vol. 45, No. 18-19, pp. 2915-2930, 2004.
- [9] Y. Zhang, and V. I. Hanby, "Model-based control of renewable energy systems in buildings," HVAC&R Research, Vol. 12, No. 3, pp. 739-760, 2006.
- [10] F. Engdahl, and D. Johansson, "Optimal supply air temperature with respect to energy use in a variable air volume system," Energy and Buildings, Vol. 36 No. 3, pp.205-218, 2004.
- [11] Y. Yao, Z. Lian, W. Liu, Z. Hou, and M. Wu, "Evaluation program for the energy-saving of variable-air-volume systems," Applied Thermal Engineering, Vol. 24, No. 7, pp. 1037-1050, 2004.
- [12] B. Yu, and A.H.C. van Paassen, "Simulink and bond graph modeling of an air-conditioned room," Simulation Modeling Practice and Theory, Vol. 12, No. 1, pp. 61-76, 2004.
- [13] S. Wang, and Z. Ma, "Supervisory and optimal control of building HVAC systems: A review," HVAC&R Research, Vol. 14, No. 1, pp. 3-32, 2008.
- [14] TRNSYS: A transient system simulation program, Volume 1 (reference manual), Solar Energy Laboratory, University of Wisconsin-Madison, WI, 1996.

- [15] D. R. Clark, "HVACSIM+ Building System and Equipment Simulation Program Reference Manual: NBSIR 84-2996," Gaithersburg, MA: National Institute of Standard Technology, 1985.
- [16] SIMBAD: Building and HVAC Toolbox. Center Scientifique et Technique du Batiment, 1999.
- [17] Y. P. Zhou, J. Y. Wu, R. Z. Wang, S. Shiochi, and Y. M. Li, "Simulation and experimental validation of the variable-refrigerant-volume (VRV) air-conditioning system in EnergyPlus," *Energy and Buildings*, Vol. 40, No. 6, pp. 1041-1047, 2008.
- [18] D. B. Crawley, J. W. Hand, M. Kummert, and B. T. Griffith, "Contrasting the capabilities of building energy performance simulation programs," *Building and Environment*, Vol. 43, No. 4, pp. 661-673, 2008.
- [19] L.E. Ormsbee, and K.E. Lansey, "Optimal control of water supply pumping systems," *Journal of Water Resources Planning and Management*, Vol. 120, No. 2, pp. 237-252, 1994.
- [20] S.P. Beckwith, and K.P. Wong, "A genetic algorithm approach for electric pump scheduling in water supply systems," 1995 IEEE International Conference on Evolutionary Computation, 1, pp. 21-26, Dec 1996.
- [21] B. Barán, C. von Lüken, and A. Sotelo, "Multi-objective pump scheduling optimisation using evolutionary strategies," *Advances in Engineering Software*, Vol. 36, Nov. 1, pp. 39-47, 2005.
- [22] Z. Yang, and H. Børsting, "Optimal Scheduling and Control of a Multi-Pump Boosting System," 2010 IEEE International Conference on Control Applications, pp. 2071-2076, Sept. 2010.
- [23] J.Y. Wang, T.P. Chang, and J.S. Chen, "An enhanced genetic algorithm for bi-objective pump scheduling in water supply," *Expert Systems with Applications*, Vol. 36, No. 7, pp. 10249-10258, 2009.
- [24] K. Lansey, and K. Awumah, "Optimal pump operations considering pump switches," *Journal of Water Resources Planning and Management*, Vol. 120, No. 1, pp. 17-35, 1994.
- [25] L. Magatão, L.V.R. Arruda, and F. Neves, "A mixed integer programming approach for scheduling commodities in a pipeline," *Computers & Chemical Engineering*, Vol. 28, No. 1-2, pp. 171-185, 2004.
- [26] R. Farmani, G. Walters, and D. Savic, "Evolutionary multi-objective optimization of the design and operation of water distribution network: total cost vs. reliability vs. water quality," *Journal of Hydroinformatics*, Vol. 8, No. 3, pp. 165-179, 2006.
- [27] C. Rygielski, J.C. Wang, and D.C. Yen, "Data mining techniques for customer relationship management," *Technology in Society*, Vol. 24, No. 4, pp. 483-502, 2002.
- [28] J. A. Harding, M. Shahbaz, S. Srinivas, and A. Kusiak, "Data mining in manufacturing: A review," *J. Manuf. Sci. Eng.*, Vol. 128, No. 4, pp.969-976, 2006.
- [29] Z. Zhang, and A. Kusiak, "Monitoring wind turbine vibration based on SCADA data," *Journal of Solar Energy Engineering*, Vol. 134, No. 2, pp. 021004-1-021004-12, 2012.

- [30] A. Kusiak, G. Xu, and F. Tang, "Optimization of an HVAC system with a strength multi-objective particle-swarm algorithm," *Energy*, Vol. 36, No. 5, pp. 184-192, 2011.
- [31] A. Kusiak, and Z. Zhang, "Adaptive control of a wind turbine with data mining and swarm intelligence," *Sustainable Energy*, Vol. 2, No. 1, pp. 28-36, 2011.
- [32] A. Verma, and A. Kusiak, "Fault Monitoring Wind Turbine Generator Brushes: A Data Mining Approach," *Journal of Solar Energy Engineering*, Vol. 134, No. 2, pp. 021001-1-021001-9, 2012,
- [33] A. Kusiak, W.Y. Li, "Short-term prediction of wind power with a clustering approach," *Renewable Energy*, Vol. 35, No. 10, pp. 2362-2369, 2010.
- [34] A. Kusiak, and M. Li, "Cooling output optimization of an air handling unit," *Applied Energy*, Vol. 87, No. 3, pp. 901-909, 2010.
- [35] A. Kusiak, M. Li, and F. Tang, "Modeling and optimization of HVAC energy consumption," *Applied Energy*, Vol. 87, No. 10, pp. 3092-3102, 2010.
- [36] M. J. A. Berry, and G. S. Linoff, "Data mining techniques: For marketing, sales, and customer relationship management," 2nd Ed., Wiley, New York, 2004.
- [37] S. Shah, A. Kusiak, and M. O'Donnell, "Patient-recognition data mining model for BCG-plus interferon immunotherapy bladder cancer treatment," *Comput. Biol. Med.*, Vol. 36, No. 6, pp. 634-655, 2006.
- [38] A.G. Parlos, K.T. Chong, and A.F. Atiya, "Application of the recurrent multilayer perceptron in modeling complex process dynamics," *IEEE Transactions on Neural Networks*, Vol. 5, No. 2, pp. 255-266, 1994.
- [39] J. C. Bezdek, "On the relationship between neural network, pattern recognition and intelligence," *The International Journal of Approximate Reasoning*, Vol. 6, pp. 85-107, 1992
- [40] M. Li, "Application of computational intelligence in modeling and optimization of HVAC systems." thesis, University of Iowa, 2009.
- [41] F. Rosenblatt, "Principles of Neurodynamics: Perceptrons and the Theory of Brain Mechanism," Spartan Press, Washington, 1961.
- [42] M. Minsky, and S. Pappert, "Perceptrons: An Introduction to Computational Geometry," MIT Press, Cambridge, MA, 1969.
- [43] J. H. Holland, "Adaptation in Natural and Artificial Systems," University of Michigan Press, Ann Arbor, MI, 1975.
- [44] L. J. Fogel, A. J. Owens, and M. J. Walsh, "Artificial Intelligence through Simulated Evolution," J. Wiley, Chichester, 1966.
- [45] J. Kennedy, and R.C. Eberhart, "Particle swarm optimization," *Proceedings of International Conference on Neural Networks*, pp. 1942-1948, IV (Perth, Australia), Piscataway, NJ, IEEE, Service Center (1995).

- [46] L. A. Zadeh, "Outline of a new approach to the analysis of complex systems and decision processes," *IEEE Transaction on Systems, Man, and Cybernetics*, Vol. 2, pp. 28-44, 1973.
- [47] A. P. Engelbrecht, "Computational Intelligence: An Introduction," NJ: John Wiley & Sons Inc, 2007.
- [48] X. Shi, "Design optimization of insulation usage and space conditioning load using energy simulation and genetic algorithm," *Energy*, Vol. 36, No. 3, pp. 1659-1667, 2011.
- [49] W.S. Lee, Y.T. Chen, and T.H. Wu, "Optimization for ice-storage air-conditioning system using particle swarm algorithm," *Applied Energy*, Vol. 86, No. 9, pp. 1589-1595, 2009.
- [50] Y.C. Chang, "An innovative approach for demand side management—optimal chiller loading by simulated annealing," *Energy*, Vol. 31, No. 12, pp. 1883-1896, 2006.
- [51] M.A. Abido, "A novel approach to conventional power system stabilizer design using tabu search," *International Journal of Electrical Power and Energy Systems*, Vol. 21, No. 6, pp. 443-454, 1999.
- [52] Z.W. Geem, J.H. Kim, and G.V. Loganathan, "A new heuristic optimization algorithm: harmony search," *Simulation*, Vol. 76, No. 2, pp. 60-68, 2001.
- [53] X.S. Yang, "Nature-Inspired metaheuristic algorithms," Luniver Press, 2008.
- [54] X.S. Yang, and A.H. Gandomi, "Bat algorithm: a novel approach for global engineering optimization," *Engineering Computations*, Vol. 29, No. 5, pp. 464 – 483, 2012.
- [55] A.G. Parlos, B. Fernandez, A.F. Atiya, J. Muthusami, and W.K. Tsai, "An accelerated learning algorithm for multilayer perceptron networks," *IEEE Computational Intelligence Society*, Vol. 5, No. 3, pp. 493-497, 1994.
- [56] B. B. Chaudhuri, and U. Bhattacharya, "Efficient training and improved performance of multilayer perceptron in pattern classification," *Neurocomputing*, Vol. 34, No. 1-4, pp. 11-27, 2000.
- [57] S.S. Haykin, "Neural networks: a comprehensive foundation," NJ: Prentice Hall, 2nd Ed, 1999.
- [58] Ş.İ. Birbil, and S.C. Fang, "An electromagnetism-like mechanism for global optimization," *Journal of Global Optimization*, Vol. 25, No. 3, pp. 263-282, 2003.
- [59] A. Rocha, and E. Fernandes, "Feasibility and dominance rules in the electromagnetism-like algorithm for constrained global optimization," *Computational Science and Its Applications—ICCSA 2008*, pp. 768-783, 2008.
- [60] P. Wu, W.H. Yang, and N.C. Wei, "An electromagnetism algorithm of neural network analysis—An application to textile retail operation," *Journal of the Chinese Institute of Industrial Engineers*, Vol. 21, No. 1, pp. 59-67, 2004.
- [61] B. Naderi, R. Tavakkoli-Moghaddam, and M. Khalili, "Electromagnetism-like mechanism and simulated annealing algorithms for flowshop scheduling problems minimizing the total weighted tardiness and makespan," *Knowledge-Based Systems*, Vol. 23, No. 2, pp. 77-85, 2003.

- [62] A. Yurtkuran, and E. Emel, "A new hybrid electromagnetism-like algorithm for capacitated vehicle routing problems," *Expert Systems with Applications*, Vol. 37, No. 4, pp. 3427-3433, 2010.
- [63] C.T. Su, H.C. Lin, "Applying electromagnetism-like mechanism for feature selection," *Information Sciences*, Vol. 181, No. 5, pp. 972-986, 2011.
- [64] R.W. Haines, C.L. Wilson, "HVAC systems design handbook," second ed., McGraw-Hill, New York, 1994.
- [65] J. Wang, "Data mining: opportunities and challenges," Idea Group Inc., Hershey, PA, 2003.
- [66] R. Kohavi, and G.H. John, "Wrappers for feature subset selection," *Artificial Intelligence*, Vol. 97, No. 1-2, pp. 273-324, 1997.
- [67] J.H. Friedman, "Greedy function approximation: a gradient boosting machine," *Annals of Statistics*, Vol. 29, No. 5, pp. 1189-1232, 2001.
- [68] J.H. Friedman, "Stochastic gradient boosting," *Computational Statistics & Data Analysis*, Vol. 38, No. 4, pp. 367-378, 2002.
- [69] K. Bailly, and M. Milgram, "Boosting feature selection for neural network based regression," *Neural Networks*, Vol. 22, No. 5, pp. 748-756, 2000.
- [70] T. Hill, and P. Lewicki, "Statistics: methods and applications: a comprehensive reference for science, industry, and data mining," StatSoft Inc., Tulsa, OK, 2006.
- [71] Y. Yao, Z. Lian, W. Liu, Z. Hou, and M. Wu, "Evaluation program for the energy-saving of variable-air-volume systems," *Energy and Buildings*, Vol. 39, No. 5, pp. 558-568, 2007.
- [72] L. Breiman, "Random forests," *Machine Learning*, Vol. 45, No. 1, pp. 5-32, 2001.
- [73] B. Schölkopf, C.J.C. Burges, and A.J. Smola, "Advances in kernel methods: support vector learning," The MIT Press, Cambridge, MA, 1999.
- [74] L. Breiman, J.H. Friedman, R.A. Olshen, and C.J. Stone, "Classification and regression trees," Wadsworth, Monterey, CA, 1984.
- [75] X. Yu, and M. Gen, "Introduction to evolutionary algorithms," Springer, New York, 2007.